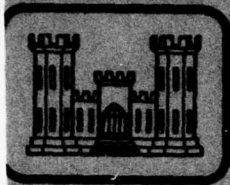


AD A062843



**LEVEL** *IV*

*12*



TECHNICAL REPORT S-78-15

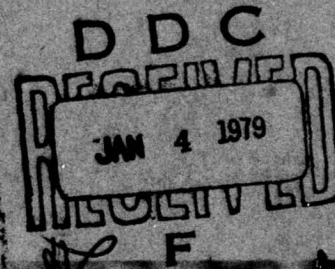
**GYRATORY SHEAR APPARATUS  
DESIGN, TESTING PROCEDURES, AND  
TEST RESULTS ON UNDRAINED SAND**

by

Arthur Casagrande and Franklin Rendon  
Pierce Hall  
Harvard University  
Cambridge, Massachusetts 02138  
Harvard Soil Mechanics Series No. 89

October 1978  
Final Report

Approved For Public Release; Distribution Unlimited



DDC FILE COPY

**THIS DOCUMENT IS BEST QUALITY FROM  
THE COPY FURNISHED TO DDC CONTAINING  
SIGNIFICANT NUMBER OF PAGES WHICH DO  
NOT REPRODUCE LEGIBLY.**

Prepared for Office, Chief of Engineers, U. S. Army  
Washington, D. C. 20314

Under Contract No. DACW39-74-C-0026

Monitored by Geotechnical Laboratory  
U. S. Army Engineer Waterways Experiment Station  
P. O. Box 631, Vicksburg, Miss. 39180

79 01 02 008

**Destroy this report when no longer needed. Do not  
it to the originator.**

## **DISCLAIMER NOTICE**

**THIS DOCUMENT IS BEST QUALITY  
PRACTICABLE. THE COPY FURNISHED  
TO DDC CONTAINED A SIGNIFICANT  
NUMBER OF PAGES WHICH DO NOT  
REPRODUCE LEGIBLY.**

18 WES

Unclassified

SECURITY CLASSIFICATION OF THIS PAGE (When Data Entered)

REPORT DOCUMENTATION PAGE		READ INSTRUCTIONS BEFORE COMPLETING FORM
1. REPORT NUMBER Technical Report S-78-15	2. GOVT ACCESSION NO.	3. RECIPIENT'S CATALOG NUMBER
4. TITLE (and Subtitle) GYRATORY SHEAR APPARATUS; DESIGN, TESTING PROCEDURES, AND TEST RESULTS ON UNDRAINED SAND	5. TYPE OF REPORT & PERIOD COVERED Final report	
6. AUTHOR(s) Arthur Casagrande Franklin Rendon	7. PERFORMING ORGANIZATION REPORT NUMBER	
8. PERFORMING ORGANIZATION NAME AND ADDRESS Pierce Hall, Harvard University Cambridge, Mass. 02138	9. CONTRACT OR GRANT NUMBER (if any) Contract No. DACW39-74-C-0026	
10. CONTROLLING OFFICE NAME AND ADDRESS Office, Chief of Engineers, U. S. Army Washington, D. C. 20314	11. PROGRAM ELEMENT, PROJECT, TASK AREA & WORK UNIT NUMBERS CWIS Work Unit 31145	
12. MONITORING AGENCY NAME & ADDRESS (if different from Controlling Office) U. S. Army Engineer Waterways Experiment Station Geotechnical Laboratory P. O. Box 631, Vicksburg, Miss. 39180	13. REPORT DATE October 1978	
14. DISTRIBUTION STATEMENT (of this Report) Approved for public release; distribution unlimited.	15. NUMBER OF PAGES 99	
15. SECURITY CLASS. (of this report) Unclassified	16. SECURITY CLASS. (of this report) Unclassified	
16. DISTRIBUTION STATEMENT (of the abstract entered in Block 20, if different from Report)	17. SECURITY CLASS. (of this report) Unclassified	
17. SUPPLEMENTARY NOTES This is No. 89 of the Harvard Soil Mechanics Series.	18. SECURITY CLASS. (of this report) Unclassified	
18. KEY WORDS (Continue on reverse side if necessary and identify by block number) Cyclic load tests Gyratory testing machines Sands Undrained shear tests	19. SECURITY CLASS. (of this report) Unclassified	
19. ABSTRACT (Continue on reverse side if necessary and identify by block number) When a saturated mass of undrained sand in situ is subjected to cyclic loading, the stresses within any small element remain uniform, although changing cyclically. However, in cyclic laboratory tests the stresses on rigid boundaries are nonuniform and their cumulative effect during cyclic loading causes progressive redistribution of water content and density within specimen. The purpose of this investigation was to measure such redistribution in sand subjected to (1) cyclic simple shear (X) tests and (2) gyratory shear	20. SECURITY CLASS. (of this report) Unclassified	

DD FORM 1 JAN 73 1473

EDITION OF 1 NOV 65 IS OBSOLETE

Unclassified

SECURITY CLASSIFICATION OF THIS PAGE (When Data Entered)

326400  
79 01 02 008

Cont →

## 20. ABSTRACT (Continued).

CONT' → (Y) tests, using a gyratory apparatus designed to perform both types of tests. Negator springs mounted on a gyratory arm apply a constant horizontal force which for X tests is transformed into a reciprocating shear force, and for Y tests produces a constant, rotating shear force. The cylindrical test specimen is enclosed in a rubber membrane, which is supported on the outside by a flat coil spring whose leaves are slightly separated at start of test. At end of test the specimen is frozen (permitting expanding water to discharge into a burette) and cut into 64 elements for determination of distribution of water content and relative density. The report includes (1) description of apparatus and appurtenant test equipment, with shop drawings, (2) description of test procedures, (3) typical test results, and (4) discussion. Measured redistribution of density shows clearly that loose and medium dense specimens are compacted in zones adjacent to the rigid top and bottom boundaries and are loosened in zones along midplane and adjacent to membrane. With increasing number of cycles, redistribution and softening in loose and medium-dense specimens continue until steady-state deflections develop. In terms of relative density of elements, redistribution can be expressed by standard deviation, which is from 2.0 to 2.5 percent for specimens of all densities as placed, and which increases to a maximum of about 10 percent for loose specimens when cycled to steady-state displacements. Significant cyclic softening also develops in dense specimens, although determination of redistribution by freezing and cutting is too crude for measuring magnitude. When steady displacements are reached in X tests, each time the shear stress cycles through zero, the cyclic peak pore pressure increases with a sharp peak almost equal to the effective vertical stress at start of test. In Y tests, the pore pressure rises to a maximum that is about two-thirds of effective vertical stress at start of test. When a specimen softens during a cyclic test, the displacements change from a pattern which indicates that the sand responds with a constant shearing resistance to an entirely different pattern with an almost sudden and great drop in shear strength followed by an equally sudden increase. This pattern reflects alternate development of liquefaction and dilation within one or more zones of specimen. Urgently needed are more precise measurements of redistribution during first stage of cyclic tests, while cyclic peak pore pressure rises to its maximum. Necessary accuracy could probably be achieved with cyclic triaxial tests and by freezing and cutting specimens into horizontal slices.

THE CONTENTS OF THIS REPORT ARE NOT TO BE  
USED FOR ADVERTISING, PUBLICATION, OR  
PROMOTIONAL PURPOSES. CITATION OF TRADE  
NAMES DOES NOT CONSTITUTE AN OFFICIAL EN-  
DORSEMENT OR APPROVAL OF THE USE OF SUCH  
COMMERCIAL PRODUCTS.

ACCESSION NO.	
NTIS	<input checked="" type="checkbox"/>
DDI	<input type="checkbox"/>
DISSEMINATED	<input type="checkbox"/>
J.S. 100-127	
DISSEMINATION/AVAILABILITY OF INFO	
	CIVIL
A 23 1978	

## PREFACE

This investigation was conducted and this report was prepared by Professor Arthur Casagrande and Mr. Franklin Rendon under Contract No. DACW39-74-C-0026 as part of the ongoing work at the U. S. Army Engineer Waterways Experiment Station (WES) under CWIS Work Unit 31145, "Liquefaction of Dams and Foundations During Earthquakes."

The study was initiated at the request of Mr. Ralph W. Beene, who monitored the work for the Office, Chief of Engineers, U. S. Army. The WES Contracting Officer's Representative was Dr. W. F. Marcuson, III, Research Civil Engineer, Earthquake Engineering and Vibrations Division, Geotechnical Laboratory (GL). General guidance and direction were provided by Mr. S. J. Johnson, Special Assistant (now retired), GL, and Mr. J. P. Sale, Chief, GL.

Directors of the WES during this investigation were COL G. H. Hilt, CE, and COL J. L. Cannon, CE. Technical Director was Mr. F. R. Brown.

## CONTENTS

	<u>Page</u>
PREFACE . . . . .	ii
LIST OF FIGURES . . . . .	v
NOTATION . . . . .	vii
DEFINITIONS . . . . .	xi
CHAPTER 1 INTRODUCTION . . . . .	1
1.1 Purpose and Scope . . . . .	1
1.2 History of Gyrotory Apparatus and of Investi- gations Performed . . . . .	1
1.3 Acknowledgments . . . . .	2
CHAPTER 2 MECHANICS AND PRINCIPAL FEATURES OF GYRATORY APPARATUS FOR PERFORMING CYCLIC RECIPROCATING (X) TESTS AND GYRATORY (Y) TESTS . . . . .	4
CHAPTER 3 ASSEMBLY OF APPARATUS, TEST PROCEDURES, AND USE OF APPURTENANT EQUIPMENT . . . . .	8
3.1 Apparatus Support Assembly and Gyrotory Arm Assembly . .	8
3.2 Membrane and Slinky (Flat Coil Spring) . . . . .	8
3.3 Preparation of Test Specimen and Assembly of Confining Elements . . . . .	8
3.4 Assembly of Apparatus . . . . .	10
3.5 Saturation of Specimen . . . . .	11
3.6 Consolidation of Specimen Under Desired Effective Stress . . . . .	12
3.7 Application of Back Pressure . . . . .	12
3.8 Application of Shear Force in X and Y Tests . . . . .	13
3.9 Recording Pore Pressures and Deflections . . . . .	14
3.10 Slippage in Transmission . . . . .	14
3.11 Freezing of Test Specimen . . . . .	15
3.12 Disassembly of Equipment, Removal and Cutting of Frozen Specimen, and Determination of Distribution of Water Content . . . . .	16
CHAPTER 4 GENERAL INFORMATION ON TESTS PERFORMED AND TYPICAL TEST RESULTS . . . . .	19
4.1 Description of Sand Used in Tests . . . . .	19
4.2 Definitions of W, X, and Y Tests, and Number of Tests Performed . . . . .	19
4.3 Distribution of Relative Density in W Tests . . . . .	20
4.4 Statistical Parameters for Analyzing Redistribution of Relative Density in X and Y Tests . . . . .	21
4.5 Review of Three Typical Reciprocating (X) Tests . . . . .	22
4.6 Review of Three Typical Gyrotory (Y) Tests . . . . .	27

	<u>Page</u>
CHAPTER 5 THE MECHANICS OF PORE PRESSURE RESPONSE AND OF CYCLIC DISPLACEMENTS IN X AND Y TESTS . . . . .	30
5.1 General Comments on Liquefaction . . . . .	30
5.2 Analysis of Typical Cycles Without and With Liquefaction/Dilation Response in Reciprocating (X) Tests . . . . .	33
5.3 Analysis of Typical Cycles Without and With Liquefaction/Dilation Response in Gyratory (Y) Tests . . . . .	39
5.4 Comparison of Response of Saturated Sand in X and Y Tests . . . . .	42
CHAPTER 6 DISCUSSION, CONCLUSIONS, AND RECOMMENDATIONS . . . . .	44
6.1 Development, Capabilities, and Limitations of the Gyratory Shear Apparatus . . . . .	44
6.2 Recommendation to Investigate Redistribution in Cyclic Triaxial Tests . . . . .	44
6.3 Discussion of Test Results . . . . .	45
REFERENCES . . . . .	50
APPENDIX A DETAILED DESCRIPTION OF GYRATORY APPARATUS AND SHOP DRAWINGS . . . . .	83
A.1 Lateral Confinement of Specimen by Slinky (Flat Coil Spring) and Rubber Membrane . . . . .	83
A.2 Slinky Guide Columns . . . . .	84
A.3 Base, Cap, and Valves . . . . .	84
A.4 Application of Vertical Load . . . . .	85
A.5 Equipment for Saturation and Application of Back Pressure . . . . .	86
A.6 Application of Horizontal Force . . . . .	86
A.7 Gyratory Sliding Plate and Gyratory Test Starting Plate . . . . .	87
A.8 Reciprocating Sliding Plate . . . . .	88
A.9 Measurement of Horizontal Displacements . . . . .	88
A.10 Measurement of Vertical Displacements . . . . .	90
A.11 Pore Pressure Measurements . . . . .	90
A.12 Auxiliary Devices for Placement and Compaction of Specimens . . . . .	91

## LIST OF FIGURES

No.	Title
1	Mechanics of (a) reciprocating and (b) gyratory shear as applied to a perfectly elastic specimen
2	Operation of gyratory apparatus
3	Assembled gyratory shear apparatus with Negator springs attached to gyratory arm and before removing centering screws
4	Front view and section of gyratory shear apparatus
5	Diagram of gyratory shear apparatus and appurtenant equipment, except items used for setting up a specimen and freezing it at end of test
6	Specimen set up in apparatus, with slinky spreaders inserted and guide columns mounted
7	Standard deviation versus redistribution index for reciprocating shear (X) tests
8	Standard deviation versus redistribution index for gyratory shear (Y) tests
9	Distribution of relative density in specimen as prepared (test W3)
10	Reciprocating test No. X13
11	Reciprocating test No. X22
12	Reciprocating test No. X12
13	Gyratory test No. Y21
14	Gyratory test No. Y25
15	Gyratory test No. Y18
16	Redistribution index versus relative density for reciprocating shear (X) tests
17	X tests--shear strain versus relative density during steady state
18	Displacements and shear stresses during 12th cycle of reciprocating test X12
19	Pore pressures, shear stresses, and displacements during 21st cycle of reciprocating test X22
20	Mobilized shear stresses versus displacements during 21st cycle of reciprocating test X22
21	Path of displacement vector $\bar{d}$ during 2nd to 6th cycles in gyratory test Y25
22	Displacements during 10th cycle of gyratory test Y21
23	Path of displacement vector $\bar{d}$ during 10th cycle of gyratory test Y21

<u>No.</u>	<u>Title</u>
A1	Slinky guide columns, O-ring expander, and slinky coil spreader
A2	Base (brass)
A3	Cap (brass)
A4	Gyratory sliding plate and piston bushing
A5	Assembly of gyratory sliding plate, gyratory bearings, and piston bushing
A6	Gyratory bearing
A7	Apparatus support column
A8	Assembly of Negator springs
A9	Gyratory arm (steel)
A10	Test starting plate
A11	Apparatus chamber, base plate for chamber, and guide rings
A12	Guide ring spacers and horizontal screws to center cap
A13	Arrangement for measuring displacements in gyratory shear tests
A14	Assembly of reciprocating sliding plate, lateral guide bearings, and piston bushing
A15	Arrangement for measuring displacements in reciprocating shear tests
A16	Devices for placement and compaction of test specimens
A17	Supporting frame for (1) dial extensometers and (2) displacement transducers when used

## NOTATION

a	mm	(For X tests) total amplitude of movement of top of specimen during one cycle = $(d\downarrow + d\uparrow)$
d	mm	(For X tests) displacement of top of specimen
$d\downarrow$	mm	(For X tests) extreme displacement of top of specimen in forward direction
$d\uparrow$	mm	(For X tests) extreme displacement of top of specimen in backward direction
$d_1$	mm	(For Y tests) displacement of top of specimen in plane of gyratory arm
$d_2$	mm	(For Y tests) displacement of top of specimen normal to gyratory arm
$\bar{d}$	mm	(For Y tests) displacement vector of top of specimen = $\sqrt{d_1^2 + d_2^2}$
$\bar{d}_{\max}$	mm	(For Y tests) the greatest displacement vector in one cycle
$\bar{d}_{\min}$	mm	(For Y tests) the smallest displacement vector in one cycle
$D_r$	percent	Relative density = $100(e_{\max} - e)/(e_{\max} - e_{\min})$
$D_{rc}$	percent	Relative density of entire specimen after consolidation under normal stress $\bar{\sigma}_c$
$D_{rf}$	percent	Relative density of entire specimen at end of cycling, computed using $w_f$
$D'_{rf}$	percent	Relative density of an element at end of cycling, computed using $w'_f$
e		Void ratio
$e_c$		Void ratio of specimen after consolidation under normal stress $\bar{\sigma}_c$
$e_f$		Void ratio of specimen at end of cycling, computed using $w_f$
$e_{\max}$		Void ratio in loosest state

$e_{min}$		Void ratio in densest state
f	cps	Frequency
$H_c$	mm	Height of specimen after consolidation under normal stress $\bar{\sigma}_c$
n		Number of frozen elements; normally $n = 64$
$N_f$		Number of cycles to end of test
$N_s$		Number of cycles to start of steady pattern of displacements
P	kg	Constant force applied by Negator springs
$s_s$		Specific gravity of sand
$S_\alpha$	kg	(For X tests) shear force $P \cdot \sin \alpha$ , corresponding to angle of rotation $\alpha$
$S_{max}$	kg	(For X tests) maximum shear force $+P$ for $\alpha = 90$ deg and $\alpha = 270$ deg
u	kg/cm <sup>2</sup>	Pore pressure induced in X and Y tests
$u_c$	kg/cm <sup>2</sup>	Back pressure = 1.0 kg/cm <sup>2</sup> , applied after consolidation
w	percent	Water content
$w_c$	percent	Water content of entire specimen after consolidation under normal stress $\bar{\sigma}_c$
$w_f$	percent	Water content of entire specimen at end of cycling, computed from $w'_f$ of all elements
$w'_f$	percent	Computed water content of an element at end of cycling = 1.09 $w'_z$
$w'_z$	percent	Measured water content of a frozen element (weighed with accuracy of $\pm 0.001$ g)
$\alpha$	deg	(For X and Y tests) the angle which defines the direction of the force P applied by the Negator springs, measured counterclockwise from the X-direction; see Fig. 2(b) and 2(c). The fulcrum of rotation of the gyratory arm is fixed and its angle of rotation $\omega$ is recorded during a test. The fulcrum of rotation of the direction of force P is the deflected center of

the top of the specimen and it is a function of  $\omega$  and the deflection. The deviation ( $\alpha - \omega$ ) ranges up to a maximum of 5 deg for the greatest deflections observed in this investigation, but for most tests it was much smaller. For the purposes of investigation, it was found acceptable to use the known angle  $\omega$  in lieu of the unknown angle  $\alpha$  which can be determined only by a cumbersome computation

$\beta$	deg	(For Y tests) angle of displacement vector, measured counterclockwise, using $\omega = 0$ deg as reference
$\gamma$	percent	(For X tests) shear strain computed with average of extreme displacements during one cycle, i.e., $100(d_{\uparrow} + d_{\downarrow})/2H_c = 100 a/2H_c$  (For Y tests) shear strain during one cycle = $100(\bar{d}_{\max} + \bar{d}_{\min})/2H_c$
$\gamma_s$	percent	(For X and Y tests) shear strain during phase with steady pattern of displacements
$\delta$	deg	(For X tests) lag angle, also called phase difference, defined as the angle which the arm has advanced after passing through $\omega = 0$ deg or $\omega = 180$ deg, to the moment when the specimen deflects through the point of zero displacement
$\lambda$	deg	(For Y tests) lag angle, defined as the difference ( $\omega - \beta$ ) between the direction of the arm $\omega$ and the direction of the displacement vector $\beta$
$\rho_i$	percent	(For X and Y tests) redistribution index = the difference between the average relative density of the four densest elements and the average relative density of the four loosest elements, when the specimen is cut into 64 elements
$\sigma$	percent	Standard deviation of distribution of relative density when the specimen is cut into 64 elements
$\bar{\sigma}$	kg/cm <sup>2</sup>	Effective normal stress
$\bar{\sigma}_c$	kg/cm <sup>2</sup>	Effective normal stress at end of consolidation
$\bar{\sigma}_f$	kg/cm <sup>2</sup>	Effective normal stress at end of test
$\tau$	kg/cm <sup>2</sup>	Average applied shear stress = shear force divided by the area of specimen

$\tau_f$	kg/cm <sup>2</sup>	(For X tests) average shear stress at end of test
$\tau_m$	kg/cm <sup>2</sup>	(For X tests) average shear stress mobilized in specimen
$\tau_{max}$	kg/cm <sup>2</sup>	(For X tests) the maximum average shear stress during each cycle
$\bar{\phi}$	deg	Effective friction angle of sand in a loose state
$\phi_m$	deg	Friction angle mobilized in specimen
$\omega$	deg	(For X and Y tests) the angle of rotation of the arm, measured counterclockwise from 0 to 360 deg, and using for each cycle $\omega = 0$ deg when the arm moves through the position at start of test, which is the X-direction, i.e., the direction to the left of the operator as shown in Fig. 2(b) and (c)

## DEFINITIONS

Important discoveries or results of research almost inevitably produce a need for new terms and definitions. As further investigations and experience lead to a clearer understanding of the phenomena involved, one may find that some of the new terms and definitions are deficient or misleading. Nevertheless, the new terminology may be so well entrenched that there is a strong tendency to continue its use in spite of the recognized shortcomings. To fill the need to convey more correctly the new concepts and to protect readers from misunderstandings, other terms are tried. Eventually, by compromise agreement, or by a process of "survival of the fittest," more realistic definitions, terms, and symbols evolve.

Such a sequence of developments has occurred since Seed and Lee (Ref. 1) and Lee and Seed (Ref. 2) developed the cyclic triaxial test for investigating the response of saturated sand to cyclic loading. In these publications they began using the term "liquefaction" for the response of the test specimen when the peak pore pressure rose momentarily in each cycle to the confining pressure. To prevent confusion with the prior use of the term liquefaction, the senior author initiated efforts in 1969 that are briefly described by Gonzalo Castro in Refs. 3 and 4; and further efforts are discussed by H. B. Seed in Ref. 5 and by the senior author in Ref. 6. Response to all these efforts convinced the senior author that satisfactory clarity has not yet been achieved. Therefore, he proposes to use in this report the following terms and definitions:

Contractive response is the tendency of sand to decrease its volume and/or increase the pore pressure when subjected to an increase in shear stress.

Dilative response is the tendency of sand to increase its volume and/or decrease the pore pressure when subjected to an increase in shear stress.

Note: The contractive and dilative responses are functions of the type of sand, its relative density, its stress-strain history, and confining pressure, the stress ratio  $\tau/\bar{\sigma}$ , and the rate of straining.

Liquefaction is the transformation of the normal structure of loose

sand into a "flow state" in which the grains are highly mobile and keep turning in relation to their neighbors so as to maintain a minimum frictional resistance. In the flow state, the movement of a saturated mass of sand resembles the flow of a liquid. Transformation from the solid phase to the liquid phase is accompanied by a great increase in pore pressure and corresponding decrease in strength of the sand. Transformation into a flow state can be generated by a shock, by monotonic strain, or by cyclic loading and is maintained while the mass is deforming or flowing. When deformation stops, the sand grains rearrange themselves again into a normal structure of loose sand.

Note: In his paper presented at the 5th Panamerican Conference on Soil Mechanics and Foundation Engineering in Buenos Aires, November 1975 (Ref. 6), the senior author used the terms "flow structure," "actual liquefaction," and "cyclic liquefaction," which led to misunderstandings by readers. Therefore, he decided to use instead in this paper the terms "flow state," "liquefaction" (without an adjective, i.e., in agreement with the meaning as originally used in literature), and "cyclic straining," respectively.

Liquefaction-dilation (L/D) response is the alternate development of liquefaction and dilation within one or more zones of a saturated sand specimen subjected to an undrained cyclic test. When liquefaction develops in zones of a reciprocating shear (X) test, two major L/D responses are repeated in each cycle. However, when liquefaction develops in a gyratory (Y) test, it usually consists of many L/D responses of small and varying magnitude within each cycle.

Cyclic straining is a general term to describe all types of responses of a test specimen, or of an element of sand in situ, to cyclic loading. The L/D response is one type of cyclic straining.

Note: In laboratory tests, redistribution of water content and relative density causes an increase in pore pressure and cyclic straining as compared with a homogeneous element in situ in which stress distribution during cyclic loading remains homogeneous. Currently, the magnitude of this increase is a highly controversial subject that urgently requires major research efforts. The senior author believes that laboratory tests as now used grossly overestimate the magnitude of in situ straining of sands, except for very loose sands which have a potential for liquefaction.

Steady pattern of displacements is that phase in a cyclic test during which, for practical purposes, the pattern of displacements remains reasonably steady. During that phase the pore pressure fluctuations usually display also a reasonably steady pattern. (Note: In a few cyclic shear tests a sufficient number of cycles were not applied to develop a clearly defined steady pattern of displacements.)

W test is a test in which the distribution of water content and relative density is determined on a test specimen as prepared for a cyclic shear test, but not subjected to shear.

X test = reciprocating shear test is a type of simple shear test in

which a reciprocating, sinusoidal shear force is applied by load control.

Y test = gyrotory shear test is a type of simple shear test in which the test specimen is subjected to a constant shear force which rotates monotonically.

GYRATORY SHEAR APPARATUS  
DESIGN, TESTING PROCEDURES, AND  
TEST RESULTS ON UNDRAINED SAND

CHAPTER 1  
INTRODUCTION

1.1 Purpose and Scope

The purpose and scope of this report can be described by quoting from Article 1 of Contract No. DACW39-74-C-0026 with the U. S. Army Engineer Waterways Experiment Station (WES): "The Contractor shall furnish....a report on an investigation of the utility of a gyratory shear and reciprocating shear apparatus for liquefaction studies. The report will include results and interpretation of tests and a sketch of the apparatus sufficient such that the apparatus can be reproduced by others."

1.2 History of Gyratory Apparatus and of Investigations Performed

In 1968, the senior author suggested to Gonzalo Castro to supplement his doctoral research by a pilot investigation of the redistribution of the water content in sand specimens subjected to cyclic  $\bar{R}$  (consolidated-undrained) triaxial tests and then freezing the specimens. These tests, which are included in Castro's dissertation (Ref. 3), demonstrated the importance of redistribution of the water content within a test specimen subjected to cyclic loading. Later it occurred to the senior author that redistribution might be studied better in direct shear tests using wire-reinforced membranes of the type developed by the Norwegian Geotechnical Institute. Then he realized that it would not be practicable to cut such membranes after freezing the test specimen in order to measure the redistribution of the water content. Later it occurred to him to support a conventional rubber membrane laterally by means of a flat coil spring of the type known as "slinky." This feature was incorporated in the design of a "gyratory apparatus" which permitted performance of "reciprocating direct shear" as well as "gyratory shear" tests.

In the first model of the gyratory apparatus, which the senior author designed with Castro's assistance, a polished steel sliding plate moved between Teflon guide rings. A number of pilot tests, performed by the junior author, showed that this sliding plate developed excessive friction which is created chiefly by the overturning moment of the shear force that is applied to the piston well above the elevation of the top of the specimen. To lower the plane of this force to the level of the specimen cap would have required designing and building a completely new and more complex apparatus. Harald D. Robinson, specialist in design and construction of scientific instruments, developed a satisfactory solution by means of roller-supported sliding plates.

In this report are included the following topics:

- (1) Brief description of gyratory apparatus for performing reciprocating and gyratory shear tests.
- (2) Test procedures.
- (3) Typical test results.
- (4) Discussion, conclusions, and recommendations.
- (5) Shop drawings with detailed description of all parts of the apparatus and of appurtenant equipment (in Appendix A).

The results of all tests performed with this apparatus will be included in the junior author's doctoral thesis.

### 1.3 Acknowledgments

The early development of the gyratory apparatus was in part supported by the National Science Foundation Grant No. GK-2565 to Harvard University titled "Research on Liquefaction of Sands." The senior author's final report to the National Science Foundation, dated 9 June 1971, includes a summary of Gonzalo Castro's research by means of triaxial tests and a description of the first design of the gyratory apparatus.

Since 1971, contributions from the following sources have supported the further developments of the gyratory apparatus and the performance of tests:

The Harvard Soil Mechanics Research Fund

The U. S. Army Engineer Waterways Experiment Station,  
Contract No. DACW39-74-C-0026  
The Institute of Engineering, National University of Mexico

In addition, the junior author was granted financial support from the following sources:

Consejo Nacional de Ciencia y Tecnologia, Mexico  
Organization of American States  
Universidad Veracruzana, Mexico  
Harvard Soil Mechanics Research Fund  
Direccion General de Asentamientos Humanos y Obras Publicas,  
Gobierno del Estado de Veracruz, Mexico

Ingenious solutions of difficult problems we owe to Harald D. Robinson. He designed and constructed the roller-supported sliding plates and other improvements of the apparatus and also suggested changes in the techniques of testing which increased the accuracy of the results.

Charles C. Osgood assisted in the development of the technique for determining the redistribution of water content by freezing specimens and cutting them into elements.

The Institute of Engineering, National University of Mexico, temporarily assigned Alberto Jaime-Paredes to assist the junior author in the performance of tests. For a similar assignment, the WES temporarily loaned Paul A. Gilbert to the Harvard Soil Mechanics Laboratory.

We are indebted to Stanley D. Wilson, Raul J. Marsal, and Gonzalo Castro for valuable suggestions concerning the design of the gyratory apparatus, the interpretation of the test results, and for comments on the draft of this report.

CHAPTER 2  
MECHANICS AND PRINCIPAL FEATURES OF GYRATORY APPARATUS  
FOR PERFORMING CYCLIC RECIPROCATING (X)  
TESTS AND GYRATORY (Y) TESTS

To simplify explanation of the operation of the gyratory apparatus for reciprocating (X) tests and for gyratory (Y) tests, the mechanism of the motions is illustrated in Fig. 1 for tests performed on a perfectly elastic specimen for which the displacements are directly proportional to the applied shear force. Negator springs which are attached to a rotating arm, the gyratory arm, apply a constant radial force  $P$  to a horizontal sliding plate. When the motion of this plate is restricted by guide rollers to a forward and backward movement (X test), the component of the rotating horizontal force of the Negator springs in the direction of movement is a cyclic shear force applied to the top of the specimen. This force varies sinusoidally between plus and minus the rotating force  $P$ , as shown in Fig. 1(a). When the sliding plate is free to move laterally in any direction (Y test), the springs apply a constant shear force  $P$ , which rotates monotonically, as shown in Fig. 1(b).

When testing a material that has internal friction, such as sand, the deflection of the top of the specimen lags behind the applied shear force. This lag is expressed for X tests by the lag angle  $\delta$ , also designated the "phase difference," and for Y tests by the lag angle  $\lambda$ . These lag angles will be explained in Chapter 5.

A schematic drawing of the gyratory shear apparatus is shown in Fig. 2. A photograph of the assembled apparatus is shown in Fig. 3, and a drawing, to scale, in Fig. 4. Figures 2(a) and 4 show the following:

- (1) The test specimen is enclosed in a rubber membrane which is sealed against cap and base with O-rings and hose clamps. The membrane is retained by a flat-coil spring, the "slinky." Before the specimen is consolidated, the coils are separated slightly by inserting "spreaders" (Fig. A-1, Appendix A), which are removed before a cyclic shear test is started to eliminate friction between the coils. A straight-sided lateral deflection of the slinky is enforced by means of

three columns with universal joints at top and bottom, designated the "slinky guide columns" (Fig. A-1).

- (2) The base on which the specimen rests and the baseplate of the apparatus chamber are attached with screws to the apparatus support column (Fig. A-7).
- (3) From the porous plate in the base, tubing leads to a valve block which is attached to two burettes (Fig. 5). In the valve block is mounted a pore pressure transducer.
- (4) A second pore pressure transducer is installed in the cap, and a second tube leads from the porous plate in the cap to the same valve block.
- (5) The valve block and the two burettes (Fig. 5) are used before the test to saturate the specimen and after the test to permit drainage of water that is displaced while the specimen is being frozen from the bottom up.
- (6) Two guide rings, mounted on top of the chamber, guide the movement of the sliding plate. Different sliding plates and bearings are used for gyratory and reciprocating shear tests. In Fig. 4, only the gyratory sliding plate is shown.
- (7) Through the piston, the vertical load is transmitted to the cap and the specimen. The piston moves through a ball bushing. To the piston bushing is attached the appropriate sliding plate.
- (8) A constant horizontal force  $P$  is applied radially to the piston bushing by means of a pair of Negator springs that are attached to the gyratory arm and to a bearing that rotates around the piston bushing.
- (9) The gyratory arm rotates around the apparatus support by means of a ball bearing. Rotation is effected by a variable transmission and a belt which runs around a pulley below the bearing.

The motion of the gyratory sliding plate is illustrated in Fig. 2(b). This plate moves between gyratory ball bearings. Hard vinyl plastic balls are used in these bearings to prevent damage to the sliding plate and the guide rings.

The motion of the reciprocating sliding plate is shown in Fig. 2(c). This plate rolls between the upper and lower guide rings by means of vertical guide bearings, and it is restrained laterally by lateral guide bearings.

The vertical load is applied to the piston by means of a loading yoke, a hanger, and dead weights, as shown in Fig. 5. A damping device

controls oscillations of the hanger.

Vertical displacements in X and Y tests are measured by a dial extensometer between the upper beam of the loading yoke and the apparatus support, as illustrated in Figs. 3 and 5.

For gyratory shear tests, two displacement transducers measure horizontal displacements in two directions normal to each other (Fig. 2(b)). Transducer No. 1 is mounted to the top of the gyratory arm (Figs. 2(a) and 4), and transducer No. 2 is mounted on a bracket that is attached to the top of the gyratory arm, advanced at a 90-degree angle to the gyratory arm in direction of its rotation (Fig. A-13). The probes of both transducers are screwed into a ball bearing that rotates around the piston (Figs. 2(a), 3, and 4). The wires from both transducers lead to spring contacts which in turn transfer the signals to slip rings surrounding the support of the apparatus (Fig. 4), and from there wires lead to the power supply and the recorder.

For reciprocating shear tests, the two displacement transducers are removed from the gyratory arm and are mounted to measure horizontal and vertical displacements, respectively, as follows: (1) between the bearing on the piston and a fixed reference, to measure horizontal displacements; (2) between the platform attached to the loading piston (item No. 40 in Fig. 4; see also Fig. A-17) and the support of the apparatus, to measure vertical displacements.

For calibration tests and for checking the performance of the apparatus, silicone rubber specimens were prepared with the same dimensions as the sand specimens. When such a rubber specimen is subjected to a gyratory shear test, the direction of the deflection of the top of the specimen coincides with the direction of the gyratory arm. However, when sand specimens are tested, the direction of the deflection vector lags behind the direction of the arm by the "lag angle  $\lambda$ ," as shown in Fig. 2(b).

This apparatus permits performance of tests within the following ranges:

Dimensions of the Test Specimen: height = 2.7 to 3.2 cm;  
diameter = 6.8 cm

Allowable horizontal displacement: up to 1.3 cm for X tests; up to 1.5 cm for Y tests

Maximum applied normal stress: up to 4.0 kg/sq cm

Back pressure: 1.0 kg/sq cm

Maximum developed pore pressure: up to 2.0 kg/sq cm

Maximum cyclic shear stress: up to 1.0 kg/sq cm

Frequency: 0.05 to 2.5 cycles/sec

A detailed description of the apparatus and all appurtenant equipment, with shop drawings, is presented in Appendix A.

CHAPTER 3  
ASSEMBLY OF APPARATUS, TEST PROCEDURES, AND USE  
OF APPURTENANT EQUIPMENT

The apparatus and appurtenant equipment required for performing gyratory and reciprocating shear tests, excepting items used for setting up a test specimen and freezing it at the end of the test, are illustrated schematically in Fig. 5. They are briefly described in the following account, in the order in which they are used in a test. (A detailed description of the test procedures will be included in the junior author's doctoral thesis.)

3.1 Apparatus Support Assembly and Gyratory Arm Assembly

Items 1 through 13, in Fig. 4, which form the apparatus support assembly and the gyratory arm assembly, normally remain permanently assembled and are carefully levelled on an appropriate supporting platform. Items 1 through 4 form the apparatus support column (Fig. A-7).

3.2 Membrane and Slinky (Flat Coil Spring)

The membrane and slinky are assembled as follows:

- (1) Slide the membrane over the base.
- (2) With the help of an O-ring expander, place two O-rings over the membrane around the base.
- (3) Slide the slinky downward, to rest on the upper O-ring of the base.
- (4) Stretch the top of the membrane by gently pulling it with the fingers and fold it over the upper end of the slinky.
- (5) Insert the three rigid columns (for the temporary support of the slinky) into the base column holders and then screw these column holders tightly to the base (Fig. A-1).

3.3 Preparation of Test Specimen and Assembly of Confining Elements

Dry sand for the test specimen is placed inside the membrane, in layers with a thickness of about 3 mm, by means of a device called the "sand placer." An essential part of this device is a rotating vane which levels the surface and controls the thickness of each layer, as described in Appendix A and illustrated in Fig. A-16. For relative densities up to 75 percent, compaction is achieved by gentle tamping

with the sand placer; and for greater densities, a lightweight tamping weight is dropped with controlled height of fall onto an anvil, Fig. A-16, which is placed on the surface of each layer. To produce uniform compaction throughout the specimen, the number of tamps is increased with each layer using an empirical relationship.

When it is desired to examine visually, and to photograph, the distortions within a specimen, alternating layers of uncolored and colored sand are used.

After the cap is placed on top of the test specimen, the membrane is sealed to the cap by means of two O-rings. Then the valve in the cap is closed, and vacuum is applied through the base by opening valves 1, 4, 5, and 7 while valves 2, 3, and 6 remain closed, Fig. 5, to effect connection through burette B-1 to the vacuum pump. The vacuum imparts rigidity to the specimen and permits execution of the following steps:

- (1) Remove the three rigid columns. This requires loosening the screws that attach the guide column holders to the base (which will be tightened again in step 6).
- (2) Stretch the slinky slightly by raising its upper end, and then measure with a vernier caliper (with jaws of sufficient length) the diameter of the specimen at several levels between the coils of the slinky.
- (3) With the depth gage extension of a vernier caliper, measure carefully the vertical distance from the edge of the cap to the surface of the chamber baseplate (items 16 and 10 in Fig. 4) at three locations approximately 120 deg apart. The height of the specimen is then computed by subtracting the thickness of the specimen base and cap (items 11 and 16 in Fig. 4) from the average of the three measurements.
- (4) Place the hose clamps over the O-rings, tighten the hose clamp over the O-rings around the base, but only very slightly around the cap. (Note: The hose clamp around the cap is not tightened, to allow vertical movement of the cap during the consolidation phase. Otherwise vertical load would be transmitted to the slinky during consolidation.)
- (5) Insert the coil spreaders between the coils of the slinky, midway between the base column holders, to create the desired separation of the coils; see Fig. 6.
- (6) Attach loosely to the cap an upper column holder, slip into the holder a slinky guide column, and insert the column into

the base column holder. After all three slinky guide columns are so placed, tighten the screws of the base column holders to the base. (Note: At this stage do not tighten the top column holders because it would cause a portion of the vertical load to be transmitted to the slinky during consolidation of the specimen.) Figure 6 shows this stage of the assembly.

### 3.4 Assembly of Apparatus

To prevent disturbance to the specimen, the vacuum in the specimen is maintained while the entire apparatus is assembled as follows:

- (1) Screw the apparatus chamber, to which is attached the lower guide ring, down onto its base plate (items 26 and 10 in Fig. 4).
- (2) Center the cap by means of the three horizontal centering screws (Figs. 3 and A-12).
- (3) Insert the loading piston into the cap (item 25 in Fig. 4).
- (4) For a gyratory shear test, place the lower gyratory bearing on the top flange of the chamber which serves as lower guide ring (items 28 and 27 in Fig. 4). This step is eliminated for reciprocating shear tests.
- (5) Gently lower the piston bushing, with the appropriate sliding plate attached, over the piston (items 31, 29, and 25 in Fig. 4).
- (6) For a gyratory shear test, place the upper gyratory bearing on top of the sliding plate (items 28 and 29a in Fig. 4). For a reciprocating shear test, attach the lateral guide bearings to the lower guide ring (Fig. A-14).
- (7) Insert the appropriate spacer columns and then attach the upper guide ring (items 34 and 30 in Fig. 4).
- (8) For a gyratory shear test, slide the "test starting plate" over the piston bushing in the Y-axis; then mount two lateral guide bearings to the left of the plate on the upper guide ring (Fig. A-10). (Note: These guide bearings are one pair of the four required for the reciprocating sliding plates; Fig. A-14, Details A and B.)
- (9) For a reciprocating shear test, place the spacer ring over the bushing (items 33 and 31, Fig. 4).
- (10) Attach the free ends of the Negator springs to the shear force ball bearing and slide the ball bearing over the piston bushing (items 36, 35, and 31 in Fig. 4).
- (11) Slide the transducer ball bearing over the piston (items 39 and 25 in Fig. 4).
- (12) If vertical displacements are to be measured with a

displacement transducer, attach a small platform near the top of the piston for the transducer probe to rest against (items 40 and 41 in Fig. 4). This transducer must be mounted after completion of the next step.

- (13) Move the accurately counterweighted loading yoke over the piston and center it. Then apply a 100-g seating load on the yoke hanger. The bottom of the hanger is held sideways by springs which dampen lateral oscillations, as shown in Fig. 5. (Comments: The large mass of this entire arrangement has the disadvantage that it requires the use of slow cycles to reduce the inertia forces to a tolerable magnitude. Tests have shown that for practical purposes, a period of 10 sec per cycle reduces the inertia forces to a negligible magnitude. The magnitude of these inertia forces could be substantially reduced by a rather complicated redesign of the loading arrangement.)
- (14) Mount the instrument support frame, which is shown in Fig. A-17, in the Y-axis direction to a fixed overhead beam. Center the stem of the vertical dial extensometer to rest against the top of the upper loading yoke beam. If used, mount the vertical displacement transducer and adjust the probe to rest against the platform attached to the top of the piston. For reciprocating shear tests, mount the horizontal displacement transducer on the instrument support frame; then screw the end of the transducer probe into the transducer ball bearing.
- (15) For gyratory shear tests, attach the housing of the horizontal displacement transducer to the top of the gyratory arm; then screw the other end of the transducer probe into the transducer ball bearing.
- (16) Make initial readings of the vertical dial extensometer and of the horizontal and vertical (if used) displacement transducers.

### 3.5 Saturation of Specimen (Fig. 5)

While the vacuum is maintained, the cap valve and valves 6 and 8 are opened. Then the source of de-aired water is connected by means of hose H-2 to the top of burette B-2, with pinchcock P closed. Valve 3 is then opened to evacuate the burette and the hose to pinchcock P. Valve 5 is then closed and pinchcock P is opened to permit de-aired water to flow through the specimen and through burette B-1 and hose H-1 as far as the water trap that protects the vacuum pump. Flow is continued until no more air bubbles are observed to rise in burette B-1. Then valves 1 and 3 are closed, and hoses H-1 and H-2 are

disconnected from both burettes. A 2-kg weight is applied to the hanger to prevent lifting of the cap by accidental application of excessive water pressure. Now valve 1 is opened to establish atmospheric pressure within the specimen. This causes a slight expansion of the specimen and thereby several cubic centimetres of water to flow into the specimen from burette B-1.

### 3.6 Consolidation of Specimen Under Desired Effective Stress, (Fig. 5)

Before application of the vertical load, the water level in burette B-1 (which is open to the atmosphere) is adjusted approximately to the lower third point, as follows: If the level is too high, water is drained by opening valve 2 slightly; if the level is too low, de-aired water is allowed to flow into the burette by opening valves 3 and 5 slightly. Then the vertical load is applied to the hanger, in several increments, to produce the desired effective stress  $\bar{\sigma}_c$ . Each increment is allowed to rest for about 5 min, and then burette B-1 and the vertical dial extensometer are read before the next increment is applied.

### 3.7 Application of Back Pressure

The principal purpose of application of back pressure is to maintain a high degree of saturation during the cyclic shear test. In addition, the back pressure permits checking the entire system for leakage. According to Fig. 5, the following steps are used to check for leakage and to apply the back pressure:

- (1) Tighten the hose clamp over the O-rings of the cap and screw the upper guide column holders firmly to the cap.
- (2) Close valves 1 and 6 and the valve in the cap.
- (3) Connect tube T-1 to burette B-2.
- (4) Open valve 3 to connect burette B-2 to the bottom of the specimen.
- (5) Adjust the air pressure regulator to increase the pore pressure in increments of about  $0.1\bar{\sigma}_c$ , in 1-min intervals, until the pore pressure reaches about  $0.9\bar{\sigma}_c$ , as read on gage G-1. After each increment, read and record the reading on (a) the dial extensometer, (b) burette B-2, and (c) gage G-1.

- (6) To reduce the pore pressure to atmospheric pressure, adjust the air pressure regulator in decrements of similar magnitude as the increments applied in step 5; and finally open valve 10 to connect to the atmosphere. After each decrement, read and record the readings on (a) the dial extensometer, (b) burette B-2, and (c) gage G-1.
- (7) Close valve 10 and then increase the pore pressure to the desired back pressure  $u_c$  in similar increments as in step 5. Read and record the readings on (a) the dial extensometer, (b) burette B-2, and (c) gage G-1.
- (8) Increase the dead load on the hanger to achieve again the desired effective stress  $\bar{\sigma}_c$ . Read and record the readings on (a) the dial extensometer, (b) burette B-2, and (c) gage G-1.

### 3.8 Application of Shear Force in X and Y Tests

The steps in applying the shear force in X and Y tests are as follows:

- (1) Rotate the gyratory arm in the X-direction which is shown in Fig. 2(c). Attach the Negator springs to the shear force ball bearing (item 35 in Fig. 4). For springs with a capacity of less than 10 kg, stretch the springs by hand and attach the spool holder to the gyratory arm with the screws (Fig. 4). It is recommended that springs with a capacity greater than 10 kg be stretched by means of the threaded rod and wing nut shown in Fig. A-9.
- (2) Pull out the coil spreaders through the large windows of the chamber and remove the horizontal centering screws (Fig. A-11).
- (3) Start the pore pressure and displacement recorders.
- (4) Close valve 3 (Fig. 5) when the pressure transducer in the valve block is used. However, when the pressure transducer in the cap is used, close the valve in the base. (Note: The valve in the cap was closed already when applying the back pressure.)
- (5) For X tests, the starting position of the rotating arm is as in step 1 above. For Y tests, rotate the gyratory arm by hand 90 deg counterclockwise to the Y-direction, i.e., toward the operator, as shown in Fig. 2(c), and remove the two lateral guide bearings. The gyratory plate will then be free to move in any direction.
- (6) Start the Zero-Max motor and engage the transmission such that the gyratory arm will move counterclockwise. (Note: The counterclockwise rotation was arbitrarily adopted and used for all X and Y tests.)

- (7) Apply the desired number of cycles; then disengage the Zero-Max transmission and stop the motor. An X test should be stopped when the gyratory arm moves through the Y-direction, i.e., when the specimen has reached the maximum deflection pointing toward the operator. (Note: If the test is stopped in the moment of zero deflection, i.e., when the pore pressure passes through its cyclic maximum, the liquefied zones of the specimen consolidate under their own weight and expel water to the top surface of the specimen where, after freezing, it becomes incorporated in the top elements and causes erroneously high water contents and low relative densities of these elements.) A Y test should be stopped when the arm has moved beyond the Y-direction by about 45 deg.

### 3.9 Recording Pore Pressures and Deflections

For most tests one pore pressure transducer and one or two displacement transducers were used for recording the response of the specimen. For X tests, normally one 2-channel recorder was used to record the output from the pore pressure transducer and from the horizontal displacement transducer. For Y tests, two 2-channel recorders were used: one for recording the output from the pore pressure transducer and from the displacement transducer that measured the displacements in the plane of the arm; and one channel of the second recorder for recording the output of the displacement transducer that measured the displacement normal to the rotating arm. For further details, see Appendix A. In addition to the output signals from the transducers, a signal was transmitted into the markers of the recorders to mark the time required for each rotation of the arm, i.e., the period. Because the chart moves at a constant speed, one can readily determine from the record the period for each cycle and the position of the gyratory arm at any time.

### 3.10 Slippage in Transmission

After completion of the testing program it was discovered that the speed of rotation of the arm gradually decreased during a test, for some tests only very slightly and for others substantially. A review of the test results disclosed that the increase in the period is caused chiefly by inertia forces created during liquefaction-dilation (L/D) responses of the specimen. Because the type of variable transmission used in this investigation causes slippage when sudden changes in the

magnitude of forces are transmitted into the transmission, the worst slippage developed in those tests in which the greatest L/D responses developed. This is illustrated by a comparison of the following two tests.

In reciprocating test X12 (Fig. 12) on a very dense specimen (relative density of 90.9 percent), the magnitude of the horizontal deflections and the inertia forces caused by L/D responses were small; and there was practically no change in the period during 100 cycles.

In reciprocating test X13 (Fig. 10), on a loose specimen (relative density of 39.8 percent), the large horizontal deflections that occurred in each cycle almost suddenly and then were stopped almost suddenly by dilatancy created inertia forces which caused a progressive and substantial increase in the period from 8.5 sec in the 2nd cycle to 12.0 sec in the 7th cycle, i.e., an increase of about 40 percent in five cycles.

This comparison, as well as similar ones that can be made with other tests, demonstrate that it would have been better to use a type of transmission which ensures a constant period. Fortunately, even such large variations as illustrated in the preceding test did not affect the basic results and conclusions of this investigation.

### 3.11 Freezing of Test Specimen

Before the specimen is frozen, it is necessary to establish in burette B-2 (Fig. 5) the same pressure as that in the specimen at the end of the test, which is shown on the record of the pore pressure transducer. Then the fluid lines from the cap and the base are connected to the valve block and valves 6 and 7 are opened (Fig. 5).

An elbow-shaped standpipe is screwed into the side-outlet hole of the apparatus chamber (Fig. A-11), and adjusted such that its outlet elevation is at the same level as the bottom of the sample. Then a freezing mixture of ground dry ice and ethyl alcohol, with a temperature of about minus 70°C, is poured into the apparatus chamber through one of the large windows, and the chamber is filled to the level of the bottom of the specimen. As freezing progresses from the bottom to the top of the specimen, the volume expansion of the freezing water causes upward flow of pore water through the still unfrozen portion of

the test specimen. The expelled water raises the water level in burette B-2 (Fig. 5) where it is measured. The time for freezing the specimen averages 25 min. Freezing and upward flow of water progress so slowly that the structure of the sand remains undisturbed. (Note: By experimentation, a layout of drainage grooves in the cap was developed which ensures that no displaced water will be blocked prematurely by freezing the outlet from the cap to the burette, Fig. A-3.) When the theoretical volume of water that should flow into the burette when freezing the water in base + specimen + cap was compared (i.e., the approximately nine percent increase in the total volume of water upon freezing) with the volume of water as measured in the burette, good agreement was found. For specimens that have not been subjected to cyclic shear, the agreement is within less than plus/minus 1 percent of the expelled volume of water, or plus/minus 0.1 percent of the total volume of water. When this comparison is made after cyclic shear tests, the two quantities will agree within plus/minus 3 percent of the expelled volume of water or less than plus/minus of 0.3 percent of the total volume of water.

### 3.12 Disassembly of Equipment, Removal and Cutting of Frozen Specimen, and Determination of Distribution of Water Content

Dismount the equipment in the following order: (1) Negator springs from gyratory arm; (2) load from hanger; (3) displacement transducers; (4) dial extensometer; (5) loading yoke; (6) drain freezing mixture from chamber through the hole in the sidewall of the chamber by turning the standpipe downward; (7) upper guide ring, sliding plate, and chamber; (8) guide columns, hose clamps, and cap O-rings.

Removal and cutting of the frozen specimen is then carried out as follows:

- (1) Loosen slinky from membrane by slightly twisting top of slinky clockwise.
- (2) Cut membrane along edges of cap and base, i.e., along the top and the bottom of the specimen.
- (3) With a screwdriver through the coils of the slinky, wedge apart cap and base from specimen using very light blows with a hammer.

- (4) Remove cap and slinky.
- (5) Immediately place frozen specimen in a plastic sandwich bag and close it with a twist-tie; then place into a second sandwich bag and close again with a twist-tie; and finally place into a precooled aluminum can which is immediately transferred into a Styrofoam container, together with a small amount of dry ice to maintain the specimen in a frozen state.

Two men working together can perform steps 1 through 5 in less than 30 sec.

For determining the water content distribution, the specimen was usually cut into 64 elements, in the following sequence: (a) the five vertical slices in the direction of the deflection of the specimen; (b) the four outside slices into four parallel columns each (the middle slice being used for examining and photographing the distortions); and finally (c) each column into four elements horizontally.

The cutting operations were performed inside a cabinet constructed of transparent plastic sides and top. The cabinet is 40 cm high and has 40 by 100-cm horizontal dimensions. One of the sidewalls has two openings to which are attached two rubber sleeves that permit the operator to work with his hands inside the cabinet. On the opposite sidewall there is a flap door, normally sealed with masking tape, through which a second operator can quickly place or remove a tray with small aluminum cans for water content determinations. The cabinet is placed over a jigsaw which stands on a table, with the jigsaw on one side of the cabinet. A block of dry ice is placed on a platform that hangs 10 cm below the ceiling in the middle of the cabinet. Below the block of dry ice, an aluminum tray with calcium chloride rests directly on the table and maintains low humidity to prevent condensation of water vapor on the surfaces of the frozen elements. The bottom edges of the cabinet are sealed to the table with masking tape.

When cutting and handling the frozen elements, the operator must wear vinyl gloves. The elements are placed in aluminum cans with covers and then on an aluminum tray which rests on the table inside the cabinet opposite to the jigsaw. While a vertical slice is cut into elements, the remaining slices should be kept sealed in plastic bags

and placed in the Styrofoam container. After a slice is cut into its 16 elements, the tray is removed by the second operator and both operators weigh the cans as fast as possible on two analytical balances with digital readout, with an accuracy of  $\pm 0.001$  g. It required not more than 2 min to cut one slice into its 16 elements, and about 6 min for both operators to weigh the 16 aluminum cans.

From the measured water content of an element,  $w'_z$ , the water content that existed in this element before freezing,  $w'_f$ , is computed as follows:  $w'_f = 1.09w'_z$ . This water content  $w'_f$  is then used to compute the relative density of the element before freezing as follows:

$$D'_{rf} = \frac{e_{\max} - s_s w'_f}{e_{\max} - e_{\min}} \cdot 100$$

Careful attention to all details and speed of operations were found necessary in order to keep condensation of water on the surfaces of the frozen elements within a tolerable magnitude. Before this technique was fully developed, and particularly during summer months when the indoor humidity was high, condensation caused the computed total water content of a test specimen after freezing to be up to two percent greater than the actual water content of the specimen. However, such a testing error affects all elements approximately to the same degree and, therefore, does not affect the magnitude of the redistribution of the water content or relative density which is produced within the specimen in reciprocating and gyratory tests.

CHAPTER 4  
GENERAL INFORMATION ON TESTS PERFORMED AND  
TYPICAL TEST RESULTS

Note: A detailed presentation of all tests performed and their analysis will be included in the junior author's doctoral thesis.

4.1 Description of Sand Used in Tests

Sand with the trade name "Banding Sand," obtained from the Ottawa Silica Co., Ottawa, Illinois, was used in this investigation. Although it is the same type of sand that Gonzalo Castro (Ref. 3) used in his doctoral research, the shipment received for this investigation was slightly coarser. It is a uniform, clean, fine quartz sand with sub-rounded to subangular grains, a specific gravity of 2.65,  $D_{60} = 0.24$  mm,  $D_{10} = 0.140$  mm, and a coefficient of uniformity of 1.7. On the basis of a number of measurements of the loosest and densest states, the following void ratios were adopted for computing all relative densities in this investigation:  $e_{\max} = 0.821$ ;  $e_{\min} = 0.487$ .

4.2 Definitions of W, X, and Y Tests, and Number of Tests Performed

The distribution of water content and relative density in test specimens was investigated in three types of tests:

- (1) W test. The specimen is placed at a desired relative density, saturated, and consolidated under a desired effective normal stress; then it is frozen and the water content and relative density distributions are determined to establish the pattern of typical distribution that can be expected in test specimens as prepared. Five W tests were performed.
- (2) X test. The specimen is placed at a desired relative density, saturated, consolidated under a desired effective normal stress, and then subjected to a reciprocating (X) test using a desired shear stress. The specimen is then frozen, and the distribution of water content and relative density is determined. Thirty-five X tests were performed.
- (3) Y test. The specimen is placed at a desired relative density, saturated, consolidated under a desired effective normal stress, and then subjected to a gyratory (Y) test using a desired shear stress. The specimen is then frozen, and the distribution of water content and relative density is determined. Twenty-six Y tests were performed.

#### 4.3 Distribution of Relative Density in W Tests

Typical results of the distribution of the relative density of a specimen as placed and consolidated, but not subjected to cyclic shear, are summarized in Fig. 9. The average water content of the specimen before freezing was  $w_c = 23.3$  percent and at the end of the test (after correction for water expelled by freezing)  $w_f = 23.3$  percent. (Note: This was one of the rare tests in which the two water contents agreed perfectly.) The water contents  $w'_f$  of the 64 individual elements, i.e., computed for the state before freezing, ranged between 22.6 percent and 23.9 percent, and the corresponding relative densities ranged from 66.5 percent to 56.3 percent. The 1.3 percent maximum difference in the water contents of the elements is chiefly due to the range of testing errors in measuring the water contents of such small elements which are subjected to different lengths of time of exposure to absorption of moisture by condensation while being cut in the cabinet. Only a portion of the measured range is caused by variation in the density of the specimen as placed. It should be emphasized that the small range of 1.3 percent in water content corresponds to the large 10.2 percent range in terms of relative density. The histogram of the relative densities of the 64 elements of the specimen in Fig. 9 has the shape of a normal distribution. A total of five W tests, performed over a range of relative densities between 48 percent and 90 percent, yielded similar histograms.

Note: To assist in visualizing deviations from a uniform distribution of relative density in the distribution diagrams of the vertical slices, in Figs. 9-15, zones with a range of relative density less than plus/minus five percent from the average relative density  $D_{rf}$ , as determined at the end of the test, are shown by dotted areas; zones with lower relative densities by blank areas; and zones with greater relative densities by hatched areas. The range of plus/minus five percent from the average relative density is the "normal" range of variation found in specimens as prepared. Therefore, any substantial deviation from such range, caused by redistribution of water content during testing, can be brought out more clearly in the distribution diagrams of the vertical slices.

#### 4.4 Statistical Parameters for Analyzing Redistribution of Relative Density in X and Y Tests

During X and Y tests on loose to medium-dense specimens, the water content and relative density develop substantial redistribution, as can be seen by comparing the histograms of X and Y tests in Figs. 10, 11, 13, and 14 with the histogram in Fig. 9 for a specimen as placed but not subjected to shear. For dense test specimens, Figs. 12 and 15, the redistribution is small. To investigate the variables that affect redistribution and the deviations from normal distribution, two statistical parameters were used: (1) the standard deviation of relative density,  $\sigma$  percent; and (2) the "redistribution index,"  $\rho_i$  percent, which the senior author defined for the purpose of this investigation as the difference between the average relative densities of the four densest elements and of the four loosest elements, when the specimen is cut into 64 elements. In contrast to the standard deviation, this redistribution index is quickly computed. For a normal distribution curve, the relationship between these two parameters for 64 equal elements can be computed and is  $\rho_i = 3.94\sigma$ , or approximately  $\rho_i = 4\sigma$ . This relationship was computed by the following formula for the distance  $z_c$  of the center of gravity of a tail-end area of a normal distribution area from the center line:

$$z_c = \frac{y_t}{A_t}$$

where

$y_t$  = ordinate at point where the tail-end area starts

$A_t$  = tail-end area, one side only, expressed as dimensionless fraction of total area

(Note: This formula is valid only in conjunction with the normal distribution curve for which the pertinent (dimensionless) quantities can be found in books on statistics, e.g., Tables A-3 and A-4 in Ref. 7.) The ratio of both tail-end areas to the total area of normal distribution is  $zA_t = (1-A) = 8/64 = 0.125$ . For this value the corresponding coordinates  $z = 1.533$  and  $y_t = 0.123$  were obtained by plotting

pertinent points from above-referenced tables. Hence,  $z_c = 0.123/0.0625 = 1.97$  and  $\rho_i = 2z_c = 3.94\sigma$ . This relationship between the standard deviation  $\sigma$  and the redistribution index  $\rho_i$  for normal distribution is plotted in Figs. 7 and 8 as a full-drawn line. In Fig. 7 is also plotted a dashed line which is the relationship  $\rho_i = 3.23\sigma$  for rectangular distribution of 64 equal elements that may be considered to represent an extreme case of "thickening" of the ends as compared with normal distribution.

#### 4.5 Review of Three Typical Reciprocating (X) Tests

The results of three typical X tests on a loose, a medium-dense, and a dense specimen are summarized in Figs. 10, 11 and 12, respectively. In the upper left of these figures are reproduced the pore pressure transducer and the horizontal displacement transducer records; and in the lower left is shown the distribution of relative density in the 64 elements obtained after the test. In the upper right is shown the distribution histogram; and in the lower right are summarized all pertinent quantities: (1) at start of test, (2) at end of test, and (3) after freezing.

It can be seen in Figs. 10(a), 11(a) and 12(a) that the pore pressures increase cyclically until they reach a maximum cyclic peak, and that then a fairly steady pattern continues during all additional cycles. Whenever the top of the specimen moves through zero displacement during the steady pattern, the pore pressure rises momentarily to its cyclic peak, which is almost equal to the confining pressure, and it drops to a cyclic minimum when the displacements are at their cyclic maximum. The pattern of pore pressures and displacements indicates that even in the loose specimen X13, Fig. 10(a), a dilative response developed within portions of the specimen. The denser the specimen, the greater is the number of cycles required to reach the maximum peak pore pressure and the steady pattern of pore pressure response.

The distribution diagrams in Figs. 10(b) and 11(b) show typical patterns of compaction in zones adjacent to the cap and the base, i.e., adjacent to those boundaries where confining friction forces develop, but volume expansion in the vertical end slices A and D and also

within a horizontal zone in the middle of the specimen, i.e., in the zones that are left blank in these plots. However, the dense specimen, Fig. 12(b), developed practically no redistribution of relative density. There seems little doubt that some redistribution is also responsible for the softening of dense specimens, but that the zones in which the water content has increased are too narrow to permit clear definition by measuring the water contents of relatively large elements. It is not difficult to visualize the geometry of narrow zones of loosened sand through the midplane and along the cylindrical surface, which can impart to the specimen the observed mobility, while major zones of densified sand adjacent to the top and bottom of the specimen remain practically immobile during cycling when a steady pattern of deflections has developed.

The displacements of the top of the specimen increase much more slowly than the pore pressures, and they reach a steady pattern after a much greater number of cycles than the pore pressures. Figures 11(a) and 12(a) show that in medium-dense and dense specimens the cyclic displacements start with a sinusoidal shape which gradually changes into a rectangular pattern. However, Fig. 10(a) shows that in a loose specimen a rectangular shape of cyclic displacements develops already during the second half of the first cycle and before the maximum peak pore pressure has developed. The sinusoidal cyclic displacements indicate that normal frictional resistance is mobilized within the entire specimen. The parallel sides of rectangular cyclic displacements indicate sudden displacements caused by liquefaction in portions of the specimen followed by dilation. The liquefaction-dilation response will be further discussed in Chapter 5.

The actual pattern of density distribution in loose and medium-dense specimens, after a steady pattern of deflections has developed, is probably not constant but is in a state of flux. Even within the same cycle one would probably observe large variations in the shape of the loosened zones in which liquefaction-dilation responses develop, if it were possible to observe continuously the density distribution. However, the shape of the compacted zones probably changes little,

although they may undergo slight additional compaction.

The histograms in Figs. 10(c), 11(c) and 12(c) are distinctly different. The histogram for the loose specimen, Fig. 10(c), shows a very wide and unsymmetrical redistribution of relative density; for the medium-dense specimen, Fig. 11(c), also an unsymmetrical but somewhat narrower redistribution; and for the dense specimen, Fig. 12(c), almost the same as for the W tests, i.e., for specimens as prepared but not sheared.

To facilitate comparison of the results of these three X tests, the following tabulation summarizes: (1) the average water content at start of test, (2) the average water content at end of test computed from the frozen elements, (3) the corresponding relative densities, and (4) the redistribution parameters  $\sigma$  and  $\rho_i$ .

Fig. and Test Numbers		Fig. 10-X13	Fig. 11-X22	Fig. 12-X12
Description of Density		loose	medium-dense	dense
Average Water Content, %	at start of test	26.0	23.7	19.5
	at end of test	26.7*	24.0	19.8
Average Relative Density, %	at start of test	39.8	58.1	90.9
	at end of test	33.7	55.3	88.9
Standard Deviation, $\sigma\%$		9.8	8.5	2.6
Redistribution Index, $\rho_i\%$		35.2	31.0	10.8

\* In test X13, the ambient humidity was not properly controlled when the frozen specimen was cut into elements. This caused the excessive, apparent increase of the water content from 26.0% to 26.7% and the corresponding decrease in relative density from 39.8% to 33.7%.

In Fig. 7 are plotted all X tests which were performed with the same shear stress ratio  $\tau_{\max}/\bar{\sigma}_c$  and with approximately equal cyclic frequency  $f$ , as listed in that figure. It can be seen that all tests with  $\rho_i \leq 26$  percent lie close to the normal distribution line  $\rho_i = 3.94\sigma$ . However, the tests with  $\rho_i > 26$  percent stray chiefly above that line.

By comparing in Fig. 7 the tests performed at approximately the same relative density, one can see that the redistribution index increases with increasing number of cycles. However, above a certain number of cycles, when the pattern of displacements becomes steady, further increase in redistribution seems to be only slight. For example, points 8 and 13 in Fig. 7 are tests on specimens with relative densities of 39 percent and 40 percent, respectively; the first one with 2 cycles resulted in  $\rho_i = 14$  percent, and the second test with 7 cycles produced  $\rho_i = 35$  percent. When comparing points 12 and 19, which are tests on very dense specimens, we see that point 12, with 100 cycles, resulted in only  $\rho_i = 11$  percent, i.e., still within the range of samples as placed but not subjected to shear, and point 19, with 200 cycles, produced  $\rho_i = 19$  percent.

The normal distribution curves, which are plotted in the left upper diagram in Fig. 7, convey a visual picture of the range of redistribution that developed in these tests for: (1) the standard deviation,  $\sigma = 2$  percent, which corresponds to the lower limit of distribution of samples as placed; and (2) the upper limit of redistribution,  $\sigma = 10$  percent, which was observed in this investigation. However, as already stated, the actual shapes of redistribution may deviate considerably from the shape of normal distribution; and this is reflected in Fig. 7 by tests located above the normal distribution line.

From Fig. 7, it is concluded that either of the two parameters  $\sigma$  and  $\rho_i$  would be sufficient to indicate the magnitude of redistribution, but with  $\rho_i$  being much simpler to compute. Neither parameter alone will indicate whether and to what extent the distribution deviates from normal distribution. However, this information is reflected by using both parameters  $\sigma$  and  $\rho_i$  and plotting the results, as in Fig. 7, and more clearly by the histograms.

The results of all X tests which were performed with test parameters other than those listed in Fig. 7, if plotted in this figure, would show the same pattern in relation to the normal distribution line as the points actually plotted.

A plot of redistribution index  $\rho_i$  versus relative density, Fig. 16,

permits identifying the role of the number of cycles as a variable. In Fig. 16, the number next to each point is the number of cycles at the end of the test,  $N_f$ . The open circles are tests which were not carried to a steady pattern of strains, whereas the  $N_f$  values for the full circles were large enough to clearly define the number of cycles  $N_s$  when a steady pattern of displacements started. In this plot,  $N_s$  values are combined for groups of tests by encircled ranges; and from this can be concluded that after a steady pattern of displacements is reached, additional cycles do not cause a further increase in redistribution. Also shown in Fig. 16, by two horizontal dashed lines, is the range of distribution of "specimens as prepared," i.e., the inevitable deviation from perfect uniformity, which in part is due to the method of placement but probably chiefly due to errors produced by condensation of water on the surfaces of the frozen elements. With allowance for scatter of results, the full-drawn  $N_s$  line represents approximately the relationship between  $\rho_i$  and  $D_{rc}$  when a steady pattern of displacements is reached.

In Fig. 17 are plotted the shear strains during the steady pattern of displacements or at end of test, as function of the relative density and number of cycles. For the purpose of this investigation, shear strain  $\gamma$  in X tests is defined as one half of the total amplitude of maximum displacements in one cycle divided by the thickness of the specimen, expressed in percent.

By combining the information in Figs. 16 and 17, it is possible to summarize for X tests the relationships between the variables affecting redistribution when a steady pattern of displacements is reached, by the following averages:

Relative Density After Consolidation	No. of Cycles to Reach Steady Pattern of Displacements	Redistribution Index	Shear Strain
$D_{rc}$ percent	$N_s$	$\rho_i$ percent	$\gamma_s$ percent
50	10	35	40
70	30	26	25
90	50	15	9

#### 4.6 Review of Three Typical Gyrotory (Y) Tests

The results of three typical Y tests on a medium-loose, a medium-dense, and a dense specimen are summarized in Figs. 13, 14, and 15, respectively.

From a comparison of all X and Y tests performed, it is concluded that the pore pressure response in the Y tests shows two significant differences from those observed in X tests:

- (1) In Y tests, the pore pressure rises to its maximum peak on an average in one-third the number of cycles required in X tests.
- (2) After the pore pressure cycles reach a steady pattern, the peak pore pressures in Y tests are only about two-thirds the initial effective normal stress, and they fluctuate much less than in X tests. Also, in contrast to X tests, the pore pressures in Y tests never approach, even momentarily, the initial effective confining pressure. In fact, the greatest pore pressures in Y tests do not rise higher than the minimum cyclic pore pressures during the phase of steady displacements in X tests.

In spite of such radical differences in pore pressure response, the redistribution of the water content and of the corresponding relative density in Y tests is fairly similar to that observed in the X tests. In the medium-loose and in the medium-dense specimens, Figs. 13(b) and 14(b), we observe compaction of the sand adjacent to the upper and lower specimen boundaries.

The direction of the maximum horizontal displacement, i.e., the displacement vector, which is measured with two displacement transducers mounted at right angles to each other (Fig. 2(b) and Fig. A-13), lags substantially behind the direction of the applied shear force. This phenomenon will be reviewed in detail in Chapter 5. (Note: For future tests, it is suggested to move the transducer which is mounted at right angle to the gyrotory arm (Fig. A-13) onto the opposite side of the arm so that both transducers will register outward deflections.)

To facilitate comparison of the results of these three Y tests, the following tabulation lists: (1) the average water content at start of test, (2) the average water content at end of test computed from the

frozen elements, (3) the corresponding relative densities, and (4) the redistribution parameters  $\sigma$  and  $\rho_i$ .

Fig. and Test Numbers		Fig. 13-Y21	Fig. 14-Y25	Fig. 15-Y18
Description of Density		medium-loose	medium-dense	dense
Average Water Content, %	at start of test	24.7	23.3	19.8
	at end of test	25.0	23.5	20.1
Average Relative Density, %	at start of test	50.1	61.7	88.6
	at end of test	47.4	59.2	86.1
Standard Deviation, $\sigma\%$		7.7	6.2	3.6
Redistribution Index, $\rho_i\%$		28.4	27.0	12.6

In Fig. 8 are plotted all Y tests which were performed with the same stress ratio  $\tau/\bar{\sigma}_c$  and with approximately equal cyclic frequency  $f$ , as listed in that figure. The full-drawn line is again the relationship  $\rho_i = 3.94\sigma$  for normal distribution. As can be seen, this line represents a good average line of all tests plotted in this graph. Computation of a linear regression, with the restraint requirement that the line should pass through the origin, yielded  $\rho_i = 3.87\sigma$ , i.e., a line very close to the line of normal distributions. For  $\rho_i$  values up to about 25 percent, we see again that the test results lie close to the normal distribution line. The test results for greater redistributions scatter more widely about that line.

By comparing the results of tests for approximately equal relative densities, but with different number of cycles, one can see that the redistribution increases with increasing number of cycles. For example, points 5, 17, 3, and 10 are for tests with  $D_{rc} = 61$  percent; and for 1, 8, 11, and 14 cycles, respectively, for these four tests, with increasing number of cycles,  $\rho_i$  increases from 14 percent to 26 percent.

For the tests on dense specimens, points 19, 18, and 1, with 10, 25, and 100 cycles, respectively,  $\rho_i$  increases from about 10 percent to 21 percent.

The results of two additional Y tests, but with other test

parameters than those listed in Fig. 8, are located practically on the normal distribution line.

For the Y tests, a plot of  $\rho_i$  versus  $D_{rc}$  shows a trend similar to the X tests in Fig. 16, although not so well defined because of the smaller number of Y tests performed.

CHAPTER 5  
THE MECHANICS OF PORE PRESSURE RESPONSE AND OF  
CYCLIC DISPLACEMENTS IN X AND Y TESTS

5.1 General Comments on Liquefaction

In this report, the term "liquefaction" is used to define the phenomenon that occurs when the structure of loose, saturated sand is transformed into a "flow state" in which the grains keep turning in relation to their neighbors so as to maintain a minimum frictional resistance. In the flow state, sand has not the characteristics of a solid, but its movement resembles the flow of a liquid. From Castro's investigations (Ref. 3), it is concluded that a high rate of straining facilitates development of a flow state. When the rate of straining is reduced below a critical value, the sand grains lose the ability to maintain themselves in the flow state, friction builds up, the sand mass reverts to a normal structure of loose sand, and the conflict between the grains creates dilatancy.

The transformation from a solid structure to the flow state at constant volume and the reverse transformation are functions of (1) relative density, (2) confining pressure, (3) principal stress ratio at the moment when the sand is subjected to increasing shear strains, and (4) whether the sand is subjected to an increase in shear stresses by strain control or load control. (Note: When using load control in laboratory tests, the rate of straining, which develops during liquefaction, can reach magnitudes several orders greater than with conventional strain control methods. Therefore, investigations of susceptibility to liquefaction by means of strain control tests are liable to yield results that are well on the unsafe side.)

In nature, liquefaction will normally start in a lens of particularly loose sand; and from such a nucleus it may spread also into somewhat denser sand layers. The driving mechanism is usually by gravity. Flow continues until the driving forces are reduced to the small shearing resistance of the sand in its flow state; then dilation will cause the liquefied mass to "freeze" again into a solid structure,

accompanied by a great reduction in pore pressures; and the mass then stops flowing.

In cyclic laboratory tests, only those portions of a specimen which have expanded into a loose state by redistribution of density can change from a solid structure to a flow state and, by dilation, revert again to a solid structure. The transformation of sand in portions of a specimen from a normal structure of sand to a flow state and then again to a solid structure, and the corresponding almost sudden changes in shearing resistance from high to low and again to high, will be referred to as the "liquefaction-dilation (L/D) response." During this transformation, the compacted zones contribute to the L/D response. In the moment when the pore pressures pass through their cyclic maximum and minimum, the compacted sand zones develop contractive and dilative responses, respectively. This probably makes a significant contribution to the sharp, momentary spikes in the pore pressure response. Thus, the compacted zones not only contribute the volume of water for the loosened zones but also accentuate the response after a steady pattern of cyclic pore pressures and deflections has developed.

The patterns of L/D response are quite different in X and Y tests. In X tests, it is easy to judge from the shape of the cyclic deflections whether an L/D response has developed within a test specimen. Without liquefaction-dilation, the cyclic deflections have sinusoidal shape which indicates that during the entire cycle the sand has maintained a solid structure. When redistribution has developed to the extent that portions of the specimen have become so loose that they are susceptible to liquefaction, or when the specimen is initially in a loose state, two sudden deflections develop in each cycle, which can be seen clearly in the transducer records in form of vertical lines that appear as a quasi-rectangular pattern, differing distinctly from a sinusoidal pattern. It can be seen in Fig. 10(a) that a loose specimen can develop an L/D response pattern already during the first cycle. However, the medium-dense and dense specimens, Figs. 11(a) and 12(a), show during the first stage of these tests well-defined sinusoidal displacements which gradually increase in amplitude. Later their shape

changes gradually to a rectangular pattern with parallel sides which reflect very fast loss and recovery of shearing resistance, i.e., the typical L/D response when portions of the specimen liquefy and dilate in each cycle. Test X12 on a very dense specimen, Fig. 12(a), shows during the first 14 cycles sinusoidal displacement with increasing amplitude. In the 18th to 20th cycles, one can see the gradual development of an almost vertical tangent when the displacements pass through the point of zero applied shear force. Then, in the range of cycles Nos. 90 to 100 (note that cycles Nos. 26 to 90 are deleted in Fig. 12), one can see typical L/D responses that are created by redistribution of density, even in such a dense specimen. Considering that additional compaction in the densified zones of an initially dense specimen could not have yielded much water, it follows that the zones, which have loosened to the point that they can liquefy, must be narrow and therefore could not be easily detected by the procedure used for determining redistribution.

In Y tests, the displacement records in Figs. 13(a), 14(a), and 15(a) show entirely different displacement patterns from those in X tests. To convey a clear and complete picture of the deflections requires computation of the movement of the displacement vector from its components  $d_1$  and  $d_2$ , as will be shown in a later section. However, even without such detailed analysis, with some experience one can judge from the shape of the displacement components whether the specimen retained during a cycle its solid structure or developed L/D responses. In Y tests, L/D responses are usually numerous within one cycle, alternating with relatively slow displacements, as seen, e.g., in Fig. 13(a) by the zigzag pattern. On the other hand, test Y18, on a dense specimen, Fig. 15(a), shows the regular deflections that indicate no L/D responses. A similar Y test on a specimen with about the same density was carried to 100 cycles and also did not develop L/D responses. In contrast to X tests, in Y tests on dense specimens no L/D responses were observed.

In the next two sections, the displacements and other observations are analyzed in detail for typical cycles of X and Y tests without and

with liquefaction-dilation response.

## 5.2 Analysis of Typical Cycles Without and With Liquefaction/Dilation Response in Reciprocating (X) Tests

### 5.2.1 Cycles Without and With L/D Response in Dense Sand, Test X12

In Fig. 12(a), the transducer record of the displacements shows for the first 14 cycles typical sinusoidal shapes with increasing amplitude. In Fig. 18 are plotted, in the upper diagram, an enlargement of the transducer record of the cyclic displacements during the 12th cycle together with the applied shear stresses and, in the lower diagram, the stress-displacement loop. The displacement curve in the upper diagram is unsymmetrical, and therefore the lag angles  $\delta$  differ substantially between the forward and backward displacements. In both diagrams, there is no indication of the development of loss of shearing resistance due to liquefaction in any portion of the test specimen.

In Fig. 12(a), it can be seen that the cyclic pore pressure was still rising in the 12th cycle and reached its maximum cyclic peak in the 18th or 19th cycle when also the shape of the cyclic displacement is changing with the development of a vertical tangent in the moment the displacement passes through zero deflection. This vertical tangent is probably the first indication that a momentary loss of shearing resistance is developing in a small portion of the specimen. In subsequent cycles the vertical segments of the cyclic displacements keep increasing until the vertical sides modify the shape of the cyclic displacements into the typical rectangular pattern of L/D response in X tests, as can be seen well developed for the last ten cycles in Fig. 12(a). Because the magnitude of asymmetry of these displacements is unusually great, the more symmetrical shape of a cycle in test X22 was used for a detailed analysis, which is presented in the next section.

Note: The authors suspect that the cause of the excessive asymmetry in test X12 may have been inaccurate centering of the damping springs at the bottom of the load hanger (Fig. 5), which would produce an inclination of the vertical load and thus a horizontal component acting on the piston. Therefore, it is recommended to replace the

damping springs by a vertical cylinder which is attached rigidly to the bottom of the hanger and is immersed in a viscous fluid. A less likely explanation of such great asymmetrical deflections would be that they were generated by asymmetrical redistribution of density in the specimen.

#### 5.2.2 Cycles with L/D Response in Medium-Dense Sand, Test X22

The effects of redistribution on the development of (1) the pore pressures, (2) the mobilized effective normal and shear stresses, and (3) the displacements are analyzed for the 21st cycle, during the phase of steady displacements, of test X22 performed on medium-dense sand ( $D_{rc} = 58$  percent). In the transducer records of this test, Fig. 11(a), it can be seen that (1) the maximum pore pressure was reached for the first time during the 3rd cycle, (2) a steady pattern of pore pressures started with the 14th cycle, and (3) a pattern of steady displacements started with the 18th cycle.

The displacement and pore pressure observations during the 21st cycle are enlarged in Fig. 19, plotted as a function of the angle  $\omega$  which defines the position of the rotating arm. In the lower diagram is also plotted the sinusoidal shear stress  $\tau$  which is the component in the direction of the displacements of the force applied by the Negator springs, divided by the area of the specimen. It should be noted that as the average shear stress  $\tau$  decreased from  $\tau_{max}$  to zero during the last quadrant of the 20th cycle, the deflection of the specimen remained almost constant. Then, when the shear force increased from the negative to the positive direction during the first quadrant of the 21st cycle, the specimen developed first a small, gradually increasing displacement from A to B; and when the arm advanced by a lag angle  $\delta$  of about 65 deg from the zero-displacement axis, i.e., when the shear force had increased to about 0.20 kg/sq cm, almost to its maximum in the opposite direction, the specimen suddenly deflected from the negative to the positive side, from B to D, by almost 2 cm. (The lag angle  $\delta$  is the angle which the arm has advanced after passing through  $\omega = 0$  deg or  $\omega = 180$  deg to the moment when the specimen deflects through the point of zero displacement.)

Such a great and sudden displacement reflects a sudden and substantial decrease of the shear strength within the specimen and suggests that loosened zones in the specimen had liquefied. Then, near the end of this sudden displacement, the liquefied zones developed a dilative response and "froze," i.e., the sand in the liquefied zones changed from a flow state to a normal sand structure and thus mobilized the required shear strength to arrest the movement at point D. The additional small increase in shear stress to  $\tau_{\max}$  caused only the minor additional deflection from D to E. From E to F, while the average shear stress decreased from  $\tau_{\max}$  to zero, the deflection decreased by an insignificant amount. The applied shear force then increased in the opposite direction, and a gradual acceleration of deflection developed from F to G and then changed to a large, sudden displacement to J, i.e. another L/D response. This sudden displacement developed also at a shear stress of about 0.20 kg/sq cm. During the additional small increase in shear stress to  $\tau_{\max} = 0.22$  kg/sq cm, the sample deflected by a small amount from J to K. Finally, during the 4th quadrant of the 21st cycle, when the shear stress decreased from  $\tau_{\max}$  to zero, the deflection decreased only very slightly from K to L.

The essential feature of this pattern of deflections is that while the externally applied shear force reciprocates back and forth in a regular sinusoidal form, most of the deflection lags well behind the applied shear force and develops in two major jumps in that cycle. The specimen retains the shape which is deformed in one direction while the shear force keeps increasing in the opposite direction almost to its maximum; and then suddenly the specimen develops a major deflection in the direction of the shear force.

The pore pressures are plotted in the upper diagram of Fig. 19 with A', B', etc., to designate the points that correspond in the lower displacement diagram to A, B, etc. During the rapid acceleration and then the sudden displacement from B to D, the pore pressure rose in the form of a sharp spike from B' to C', reaching a maximum of 1.8 kg/sq cm (as compared with the constant vertical stress of 2.0 kg/sq cm); and then it dropped sharply to about 0.9 kg/sq cm, followed by an equally

sharp rise to about 1.2 kg/sq cm and oscillations that rapidly decayed. The oscillations were probably induced by the shock when the fast displacement was suddenly arrested by dilatancy. Then, when the shear stress decreased from  $\tau_{\max}$  to zero, the pore pressure rose only slightly from E' to F'. But when the shear stress then increased in opposite direction, the pore pressure rose at a faster rate to point G', increased sharply to its maximum at H', dropped suddenly to its minimum at J', and then recovered to K'; and after the oscillations attenuated, it remained almost constant to the end of the cycle, point L', where the shear stress again passed through zero.

Because the changes in pore pressures from B' to D' and the displacements from B to D developed very fast, it is not possible from the instrument records to conclude that the peak pore pressures at C' and H' correspond exactly to the moment when the displacements passed through zero at points C and H. By analogy with cyclic triaxial tests, in which the peak pore pressures always develop at the moment when the mobilized cyclic shear stresses in the specimen are a minimum, it is reasonable to assume that this holds true also for cyclic shear tests.

During the almost sudden displacement, when the pore pressure rose momentarily to its peak, a substantial portion of the applied shear force was used for accelerating the following parts of the apparatus: cap, piston, and reciprocating sliding plate with piston bushing and several bearings. Near the end of the sudden displacement, when the sample "froze" by dilatancy and the pore pressure dropped to D', these masses decelerated as additional frictional resistance was mobilized in the sand. Therefore, during the very fast acceleration and deceleration, the actually mobilized shearing resistance in the specimen was not equal to the shear force component applied by the Negator springs, except during a short transition when the velocity was constant.

During the rapid displacement, some loosened portions of the specimen had liquefied. Therefore, the actually mobilized shear stress  $\tau_m$  can be computed from the equation  $\tau_m = \bar{\sigma} \tan \bar{\phi}$ , where  $\bar{\phi}$  is the effective friction angle of the sand in a flow state, which is estimated to be about 30 deg on the basis of other investigations. In

the moment of the peak pore pressure  $u_{\max} = 1.8 \text{ kg/sq cm}$ , the effective normal stress was reduced to  $\bar{\sigma} = 0.2 \text{ kg/sq cm}$ . Therefore, the mobilized shear strength in the liquefied zones of the specimen in which the rapid deformation of the specimen developed dropped to only about  $\tau_m = 0.2 \tan 30 \text{ deg} = 0.12 \text{ kg/sq cm}$ . In Table 1 are summarized all pertinent data and computed mobilized friction angles and shear stresses for all points from A and A' to L and L'.

During the acceleration between B and C, the shear stresses mobilized within the specimen are smaller than the force applied externally by the Negator springs and energy is stored up in all moving parts; and during the deceleration from C to D, the shear force mobilized within the specimen is greater than the force applied externally by the Negator springs and the stored-up energy is used to stop the moving parts. Therefore, in the plot of mobilized shear stress versus displacement, Fig. 20, the areas below and above the shear stress  $\tau_m = \pm 0.20 \text{ kg/sq cm}$ , should be approximately equal. On the basis of these considerations, the relationship between the mobilized shear stress and the displacements was estimated as shown in Fig. 20. All points from A'' to L'' in Fig. 20 correspond to points from A and A' to L and L' in Fig. 19.

In Fig. 20, point C'' is plotted to coincide approximately with zero displacement. However, there is no physical reason why the transition from acceleration to deceleration should coincide with the point of zero displacement. A more important question concerning the accuracy of point C'' arises because the authors have developed doubts whether the writing pen of the recorder was able to record the extreme maxima and minima of the sharp spikes of the developed pore pressures during a fast liquefaction-dilation response. In fact, some of the pore pressure transducer records show beyond the well-defined end points of the spikes a series of faint dots in vertical extensions. This suggests the possibility that the pen had moved very fast, considerably beyond the recorded ends of the spikes, and was not able to record a continuous line. Therefore, the correct maxima and minima in the enlarged transducer record in Fig. 19 could be higher and lower,

Table 1  
Pore Pressures, Shear Stresses and Displacements  
During 21st Cycle of Reciprocating Test X22

1 Points in Fig. 18 and Fig. 19	2 Externally Applied Shear Stress $\tau$ kg/sq cm	3 Induced Pore Pressure $u$ kg/sq cm	4 Effective Stress $\bar{\sigma} = 2.0 - u$ kg/sq cm	5 Friction Angle Mobilized in Specimen $\phi_m^*$ deg	6 Shear Stress Mobilized in Specimen $\tau_m = \bar{\sigma} \tan \phi_m$ kg/sq cm	7 Displacement $d$ mm
A	zero	1.35	0.65	zero	zero	- 9.5
B	+0.19	1.47	0.53	20	+0.19	- 8.0
C	+0.20	1.80	0.20	30	+0.12	zero
D	+0.20	0.90	1.10	10	$\leq +0.64^{**}$	+11.5
E	+0.22	1.20	0.80	15	+0.22	+12.5
F	zero	1.30	0.70	zero	zero	+12.0
G	-0.19	1.50	0.50	21	-0.19	+10.0
H	-0.20	1.80	0.20	30	-0.12	zero
J	-0.20	0.90	1.10	10	-0.20	- 9.0
K	-0.22	1.25	0.75	16	-0.22	-10.0
L	zero	1.35	0.65	zero	zero	- 9.5

\*  $\tan \phi_m = \tau/\bar{\sigma}$  ; but  $\phi_m$  cannot exceed 30 deg.

\*\* Not exceeding the possible maximum for  $\bar{\sigma} = 1.10$  kg/sq cm .

respectively, than points C', H' and D', J'. This would move points C'' and H'' in Fig. 20 much closer to the zero shear-stress axis, and thus their positions would be more consistent with the low strength of sand in liquefied state. There is no doubt that when an accurate record of the pore pressures during a very fast L/D response is desired, a different type of recording instrument will be needed.

In Fig. 11(a), it can be seen that during the first few cycles of test X22, before redistribution caused the cyclic peak pore pressure to increase to the maximum, the applied shear force probably did not cause failure stresses to develop in a significant portion of the specimen. Only after redistribution caused some zones in the specimen to expand into a loose state and then rendered them potentially capable of liquefaction, should one expect sudden displacements to develop. Failure would then be controlled by the combination of (1) an effective friction angle of about 30 deg of this sand in a loose state, and (2) the acting effective vertical stress which is the total vertical stress reduced by the induced pore pressure.

Finally, it is pertinent to inquire whether the test records yield any indication concerning the size of the zones which are involved in the L/D responses. Considering the limited degree of accuracy with which the redistribution of density could be determined and the uncertainties concerning the maximum and minimum cyclic pore pressures during L/D cycles, it is probably not possible to derive any quantitative information on this question.

### 5.3 Analysis of Typical Cycles Without and With Liquefaction/Dilation Response in Gyrotory (Y) Tests

#### 5.3.1 Cycles Without L/D Response in Medium-Dense Sand, Test Y25

In Fig. 14(a), the displacement transducer record of test Y25, on a medium-dense specimen with a relative density of 62 percent, indicates no L/D response during the first six cycles. From an enlargement of the records of the two displacement components, points of the actual path of the displacement vector were derived for the arm in the position  $\omega = 0, 90, 180, \text{ and } 270$  deg and were plotted in Fig. 21. Next to each point is shown the cycle number, including fraction of cycle.

In addition, the lag angles  $\lambda$  are shown for the points with  $\omega = 0$  and  $180 \text{ deg}$ . It can be seen that the path of the displacement vector is a spiral which approaches a circle when a steady pattern of deflections is reached.

After the 6th cycle, the displacement vector  $d_1$  gradually developed, in each cycle, many alternating fast and slow movements which are typical for L/D response in Y tests. To analyze such a pattern, a more clearly defined cycle in test Y21 was selected and is described in the next section.

### 5.3.2 Cycles With L/D Response in Medium-Loose Sand, Test Y21

The transducer records of test Y21, on a medium-loose specimen with a relative density  $D_{rc} = 50 \text{ percent}$ , are reproduced in Fig. 13(a). (Note that in Fig. 13(a) the vertical scales for the displacement transducers No. 1 and No. 2 are different.) To an enlarged scale, the displacement components  $d_1$  and  $d_2$  are plotted in Fig. 22(a) and (b), for the 10th cycle, when a steady pattern of displacements had developed. In Fig. 22(c) are plotted the displacement vectors  $\bar{d}_A$  to  $\bar{d}_E$  and their reference angles  $\omega$ ,  $\beta$ , and  $\lambda$ , which are defined in that vector diagram and are tabulated next to that diagram. These displacement vectors correspond to points  $A_1$  and  $A_2$  to  $E_1$  and  $E_2$  in the plot of the displacement components  $d_1$  and  $d_2$  in the upper part of Fig. 22.

In order to understand clearly the deflection of the top of the specimen during one full cycle of the arm, the reader should keep in mind the meaning of the following details in the vector diagram:

(1) Point "0" represents the center of the base of the specimen and the center of rotation of the arm, which does not change during the test; and it is also the center of the top of the specimen at the start of the test. (2) A horizontal line through "0" represents the starting position of the arm in the direction to the left, from which the angles  $\omega$  and  $\beta$  are measured counterclockwise. The angle  $\omega$ , which defines the direction of the arm, is only approximately equal to the angle  $\alpha$ , which defines the direction in which the shear force is acting, because the center of the cap is not stationary. The angle  $\beta$  defines

the direction of the displacement vector. For example, when the end-point of the displacement vector is at point A, the displacement vector is  $\bar{d}_A$ , its direction defined by the angle  $\beta_A = 120$  deg; and the direction of the arm, and approximately of the shear force, is defined by the angle  $\omega_A = 231$  deg. Note that the direction of the displacement is lagging behind the direction of the arm by the lag angle  $\lambda_A = \omega_A - \beta_A = 111$  deg.

The gradual buildup and release of shear stress in combination with the changing lag angle  $\lambda$  causes the displacements to develop in alternating steps of slow and fast and occasionally almost sudden movements which are reflected by a zigzag pattern of the displacement  $d_1$  in the direction of the arm. The actual elapsed times for the zigzags between points A and E in Fig. 22 and the angular displacements of the gyratory arm and of the displacement vectors were as follows:

Displacement	Elapsed Time sec	Rotation, deg	
		Gyratory Arm	Displacement Vector
A to B	0.70	23	17
B to C	0.04	Almost zero	48
C to D	0.82	27	10
D to E	0.09	3	12

During the almost sudden displacement from B to C, the direction of the gyratory arm remained practically constant; and the displacement developed with a very fast acceleration during the first part and very fast deceleration during the last part of that movement, i.e., by a liquefaction-dilation response.

The component of the displacement normal to the arm,  $d_2$ , changes at a much smaller rate; therefore, there is usually no zigzag pattern in the record of  $d_2$ . For example, note that as the displacement vector rotates from A to B in Fig. 22(c), the component  $d_2$  remains practically constant. However, in the direction of the arm, the component  $d_1$  shows the displacement from  $A_1$  to  $B_1$ , Fig. 22(a). At B, the lag angle  $\lambda$  has increased to 117 deg. Then a sudden large

displacement developed from B to C. During this movement, the angle  $\omega$ , i.e., the direction of the arm, did not change and the magnitude of the displacement vector remained practically unchanged, as disclosed by the fact that points  $B_2$  and  $C_2$  coincide and points  $B_1$  and  $C_1$  lie practically on the same vertical. This great, sudden displacement, which is a typical liquefaction-dilation response in Y tests on medium-loose sand, caused the lag angle  $\lambda$  to decrease abruptly from 117 to 69 deg and the displacement  $d_1$  to change from a negative to a positive value. (Note: A lag angle  $\lambda = 90$  deg indicates that the displacement in the plane of the arm is zero. For  $\lambda < 90$  deg the displacement is positive, and for  $\lambda > 90$  deg it is negative.) During those movements in which the lag angle increases, the frictional resistance builds up within the specimen. However, sharp decreases in the lag angle during rapid movements indicate that liquefaction has developed in loosened zones of the specimen.

In Fig. 13, it can be seen that (1) the induced pore pressure in the 10th cycle of test Y21 decreased during the sudden displacement from a peak of about 1.60 kg/sq cm to a low point of about 1.25 kg/sq cm, followed by oscillations that rapidly attenuated; and (2) all transducer records of several preceding cycles are almost identical to those of the 10th cycle, each cycle displaying one major L/D response.

#### 5.4 Comparison of Response of Saturated Sand in X and Y Tests

From a comparison of the results of all X and Y tests performed with the same externally applied stresses and frequency, the following differences and similarities in the response of the test specimens were identified:

- (1) The number of cycles to reach the maximum peak pore pressure in X tests as compared with Y tests is about the same for loose specimens, about twice as great for medium-dense specimens, and up to four times as great for dense specimens.
- (2) The maximum pore pressures that are developed in Y tests are only about two thirds of the maximum in X tests, regardless of the density of the specimen.
- (3) The cyclic pore pressure fluctuations in Y tests are much smaller than in X tests, regardless of density.

- (4) The shear strains, when a steady pattern is reached, are somewhat smaller Y tests than in X tests at equal density.
- (5) A greater number of cycles are required to initiate L/D responses in Y tests than in X tests at equal density. In dense specimens, even at 100 cycles, no L/D response was observed in Y tests; whereas, in all X tests on dense specimens L/D responses developed.
- (6) The intensity of the L/D response in X tests is substantially greater than in Y tests.
- (7) The L/D responses in X and Y tests are entirely different. In one cycle of an X tests they consist of two well-defined and strong events. However, in one cycle of a Y test they develop in form of a complex pattern of many weak L/D events of irregular magnitude.
- (8) The redistribution of density in Y tests, expressed by statistical parameters, is generally somewhat smaller than in X tests at equal density.
- (9) The patterns of redistribution in the zones adjacent to the cap and base, which develop compaction, are similar in both types of tests. The zones along the sides and through the midplane of the specimen, in which the sand is loosened, develop somewhat different patterns in X and Y tests.

Most of the differences in response are consistent with the important differences in the cyclic shear forces to which test specimens are subjected in X and Y tests. In X tests, the applied shear forces reciprocate between maxima and zero. In Y tests, the magnitude of the applied shear force is constant, but its direction rotates monotonically at a constant angular velocity.

The reciprocating action in X tests is more effective in developing the liquefaction-dilation response. On the other hand, the gyratory kneading action in Y tests is more effective during the first phase of a test, while the pore pressures are rising, and before any L/D responses have started. It is interesting that in spite of all differences between the mechanisms of X and Y tests, almost the same magnitude of redistribution of density is created in both types of tests at equal density, when cycling is continued into the range of a steady pattern of displacements.

## CHAPTER 6

### DISCUSSION, CONCLUSIONS, AND RECOMMENDATIONS

#### 6.1 Development, Capabilities, and Limitations of the Gyratory Shear Apparatus

Development of the gyratory apparatus was a much more difficult, time-consuming, and expensive undertaking than the senior author had envisioned when he initiated this research project. By a systematic investigation of the operation of the first model, and then changing the design to reduce testing errors to tolerable magnitudes, and by experimentation with various techniques of testing, particularly the procedure of freezing the specimen and cutting it into a large number of segments, we finally succeeded in measuring with reasonable accuracy the distribution of the water content and corresponding relative density in undrained sand specimens subjected to (1) reciprocating shear (X) tests and (2) gyratory shear (Y) tests. As designed, the apparatus was limited to narrow ranges of normal and shear stresses and to specimens of one size only. In spite of these limitations, it proved to be a useful research tool for investigating the redistribution of the relative density which is generated by boundary effects.

The principal purpose of this research project, investigation of redistribution produced by reciprocating and gyratory shear tests, was fulfilled. But inevitably, when an unexplored area is pioneered, for every question answered new questions arise and demand further investigations. In particular, we recognize that much greater accuracy in the determination of the redistribution is required for the purpose of investigating the progress of redistribution during the first stage of such tests when the pore pressure rises toward its maximum. For this purpose, it would be necessary to test much larger specimens and to develop refinements in the procedures of cutting the frozen specimen into elements and in measuring the water content distribution.

#### 6.2 Recommendation to Investigate Redistribution in Cyclic Triaxial Tests

Comparison with the few available tests on redistribution in cyclic

triaxial tests, which were carried out by Castro on small-diameter specimens (Ref. 3), convinced the senior author that the mechanism of redistribution in cyclic triaxial tests differs considerably from that in X and Y tests. Therefore, he recommended to WES the construction of a triaxial apparatus in which large-diameter specimens could be frozen in the apparatus at the end of a cyclic test; and he assisted in its design.

As compared with the complex three-dimensional redistribution of density in gyratory test specimens, the great advantage of triaxial tests is that the redistribution in the specimen is more nearly one-dimensional. Therefore, it would probably be sufficient to investigate the vertical redistribution by cutting a frozen specimen only into horizontal slices. This would greatly increase the size of the individual elements and the accuracy of the measurements and also decrease the amount of work as compared with the tests described in this report. For such triaxial tests there is no reason why one should adhere to the conventional height-diameter ratio of about 2.5. Besides, it would be desirable to investigate the effect of the height-diameter ratio as one of the variables that may influence redistribution.

It would be necessary to develop a reliable procedure for placing specimens with uniform density at the start of the tests, and this would require use of thin layers and a systematic investigation of the effects of all details of various placement procedures. The uniformity achieved should be determined by freezing specimens as prepared and saturated and cutting them into thin horizontal slices.

If water is used in the triaxial cell, it would have to be drained before start of freezing. Probably the use of silicone oil, which does not freeze, would ensure a reasonably uniform advance of the freezing front through the specimen while the freezing mixture is circulated within the base.

### 6.3 Discussion of Test Results

The following summary is based on the results of all 35 X tests and 26 Y tests performed. The results of all these tests will be included in the junior author's thesis.

Under the following subheadings, the results of X and Y tests are compared for tests performed with the same externally applied stresses and frequency and similar relative densities.

#### 6.3.1 Pore Pressure Development During X and Y Tests

In X tests, the pore pressure rises cyclically until the momentary peak in each cycle almost reaches the effective vertical stress at the start of the test; and the cyclic pore pressure fluctuations are great. The cyclic peak pore pressures always occur when the applied cyclic shear stress passes through zero.

In Y tests, the pore pressures do not rise higher than about two thirds of the initial effective vertical stress; and the cyclic fluctuations are small.

The number of cycles to reach the maximum peak pore pressure in X tests as compared with Y tests at equal density is about the same for loose specimens, about twice as great for medium-dense specimens, and up to four times as great for dense specimens.

#### 6.3.2 Redistribution of Water Content and Relative Density

The magnitude of redistribution of water content and relative density in X and Y tests is approximately the same, or somewhat smaller in Y tests than in X tests. Both types of tests produced in loose to medium-dense specimens a similar geometry of the zones adjacent to cap and base, in which the sand is being compacted, but somewhat different geometry of the zones along the sides and in the midplane, where the sand is being loosened. The progressive softening of the specimen develops in these loosened zones. The compacted zones do not contribute significantly to the progressive increase in cyclic strains.

The redistribution of relative density can be expressed conveniently by two statistical parameters: (1) the standard deviation,  $\sigma$  percent; and (2) the redistribution index,  $\rho_i$  percent, which is defined as the difference between the average relative densities (in percent) of the four densest and the four loosest elements when the specimen is cut into 64 elements of approximately the same size. For a normal distribution curve, the theoretical relationship between the two parameters is  $\rho_i = 3.94\sigma$  (or approximately  $\rho_i = 4\sigma$ ), which is

represented by the full-drawn straight line in Figs. 7 and 8. The deviation of the test results from this straight line is a measure of the deviation of the measured distribution from a normal distribution curve.

The inevitable testing errors in measuring the water contents of the small elements into which a frozen specimen is cut, and the variations in density within an "as prepared" specimen caused typical standard deviations of about 2.0 percent to 2.5 percent and redistribution indices of about 8 percent to 10 percent. The redistribution created during X and Y tests is reflected by an increase in the magnitude of these statistical parameters to a maximum of about four times the values at the start of a cyclic test. This range of increase is best visualized by comparing the normal distribution curves for  $\sigma = 2.5$  percent and 10 percent in the upper left diagrams in Figs. 7 and 8. The plotted results of X and Y tests in Figs. 7 and 8, respectively, show the wide range of redistribution, and its dependency on the relative density and the number of cycles applied.

A systematic investigation of redistribution between the start of cyclic loading and the moment when the induced pore pressure reaches for the first time its maximum is urgently needed, as recommended in Section 6.2. A hypothesis of the mechanics of redistribution, where it starts and how it propagates in cyclic laboratory tests, was discussed by the senior author in Chapter X of Ref. 6, with emphasis on the differences between the cyclic stresses induced in an element in situ and in laboratory test specimens.

### 6.3.3 Shear Displacements and Strains

After a steady pattern of displacements is reached in both X and Y tests, the shear displacements and strains decrease in both with increasing relative density such that for dense specimens the magnitude is about one fifth as compared with loose specimens. For example, for X tests performed with  $\tau_{\max}/\bar{\sigma}_c = 0.11$  and  $\bar{\sigma}_c = 2.0$  kg/sq cm, at a relative density of 40 percent the shear strain  $\gamma_s$  is about 50 percent, and at a relative density of 90 percent the shear strain  $\gamma_s$  is about 10 percent.

For Y tests, the following deficiencies did not permit

determination of a reasonably well-defined relationship between the magnitude of the shear strains and the relative density: (1) the smaller number of Y tests performed; (2) a majority of Y tests not carried out with a sufficient number of cycles; and (3) in about one half of the Y tests, the displacement component normal to the plane of the arm was not recorded. There is an indication that at equal test parameters the shear strains in Y tests are somewhat smaller than in X tests at similar relative densities.

#### 6.3.4 Cyclic Deflection Patterns Without and With L/D Responses

Analysis of the X and Y tests on sand led to recognition of characteristic patterns in the displacement records which permit differentiation between the pattern when, during an entire cycle, the specimen retains the structure of solid sand and the pattern when portions of the specimen develop liquefaction-dilation responses.

In an X test, a sinusoidal shape of the displacement transducer record indicates clearly that no portions of the specimen developed liquefaction. A "rectangular" pattern, i.e., with parallel sides, shows that two sudden displacements developed in each cycle during which the shearing resistance in portions of the specimen dropped radically and then recovered, i.e., that the specimen experienced two liquefaction-dilation events. The gradual change from a sinusoidal to a rectangular pattern reflects progressive redistribution of density within the specimen. The L/D responses will not develop until redistribution has loosened the sand in portions of the specimen to a degree which renders it susceptible to liquefaction. In a loose specimen, L/D responses may develop already during the first cycle and before the pore pressure reaches its maximum. In a dense specimen, a test may have to be continued many cycles beyond the point when the maximum pore pressure is reached for the first time to achieve well-developed L/D responses.

During the first phase of a Y test in which no liquefaction develops, the displacement vector rotates and grows cyclically in form of a smooth spiral. Then, when zones in the specimen become so loose by redistribution that they are susceptible to liquefaction, the

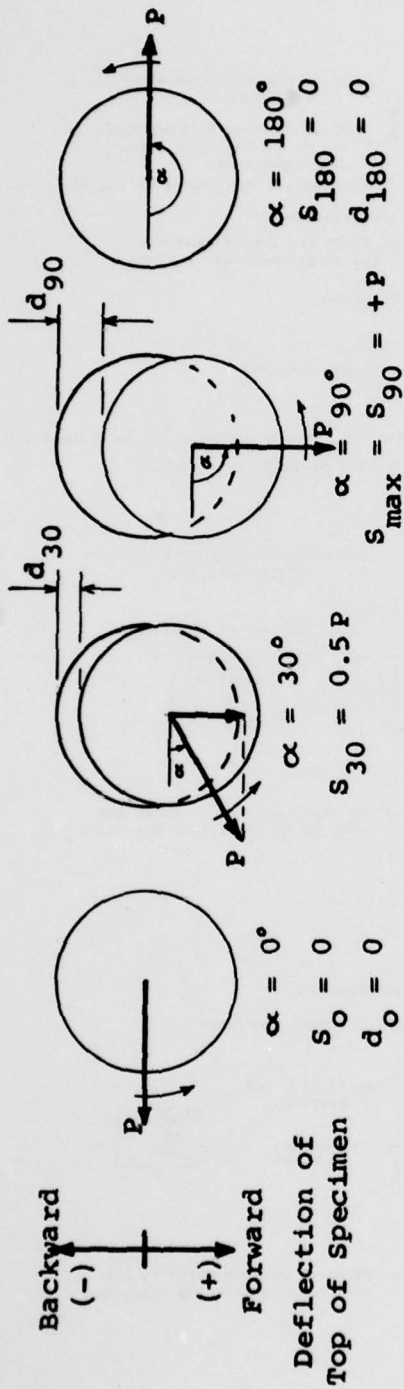
displacement vector rotates in form of many alternating slow and fast angular displacements within each cycle.

The type of liquefaction-dilation response in a Y test is quite different and much less intense than the two strong and well-developed L/D responses in X tests. The reason for this difference resides in the fundamentally different application of the cyclic shear force. In X tests, the shear force reciprocates between maxima and zero, whereas in Y tests the magnitude of the applied shear force remains constant, but its direction rotates monotonically.

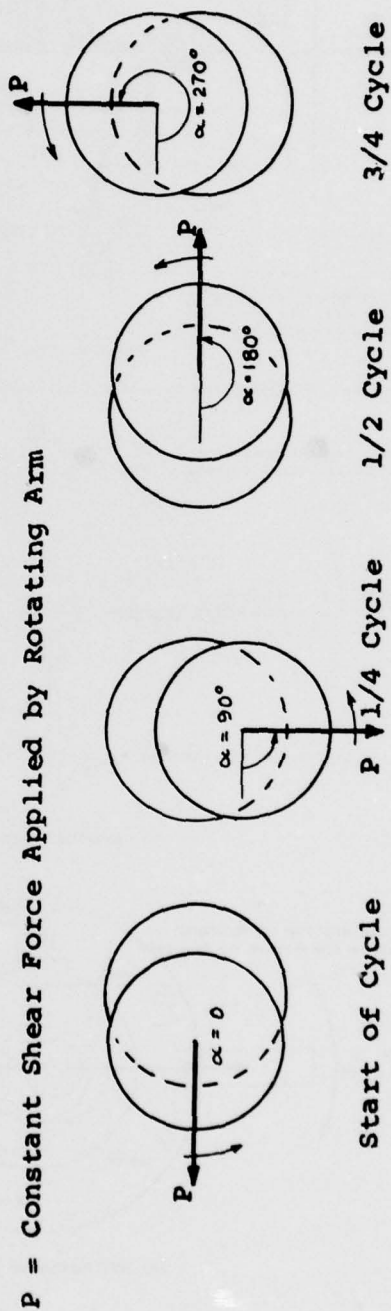
In contrast to X tests, in which the geometry of the displacement records conveys directly a clear picture of the type of response, the records of the two displacement components in Y tests become meaningful only after one has acquired some experience by analyzing in detail the movement of the displacement vector in typical cycles, such as presented in Section 5.3 and Figs. 21, 22, and 23.

#### REFERENCES

1. Seed, H. B. and Lee, K. L., "Liquefaction of Saturated Sands during Cyclic Loading," Journal of the Soil Mechanics and Foundations Division, ASCE, Vol 92, No. SM6, Nov 1966.
2. Lee, K. L. and Seed, H. B., "Cyclic Stress Conditions Causing Liquefaction of Sand," Journal of the Soil Mechanics and Foundations Division, ASCE, Vol 93, No. SML, Jan 1967.
3. Castro, G., "Liquefaction of Sands," Harvard Soil Mechanics Series No. 81, Jan 1969, Harvard University, Pierce Hall, Cambridge, Mass.
4. \_\_\_\_\_, "Liquefaction and Cyclic Mobility of Saturated Sands," Journal of the Geotechnical Engineering Division, ASCE, Vol 101, No. GT6, Jun 1975.
5. Seed, H. B., "Evaluation of Soil Liquefaction and Cyclic Mobility on Level Ground During Earthquakes," State-of-the-Art Report to the 1976 ASCE National Convention in Philadelphia; Preprint Volume titled "Liquefaction Problem in Geotechnical Engineering."
6. Casagrande, A., "Liquefaction and Cyclic Deformation of Sands - A Critical Review," Harvard Soil Mechanics Series No. 88, 1976, Harvard University, Pierce Hall, Cambridge, Mass., Presented at the Fifth Panamerican Conference on Soil Mechanics and Foundation Engineering, Buenos Aires, November 1975.
7. Dixon, W. J. and Massey, F. J., Introduction to Statistical Analysis, 3rd ed., McGraw-Hill, New York, 1969.

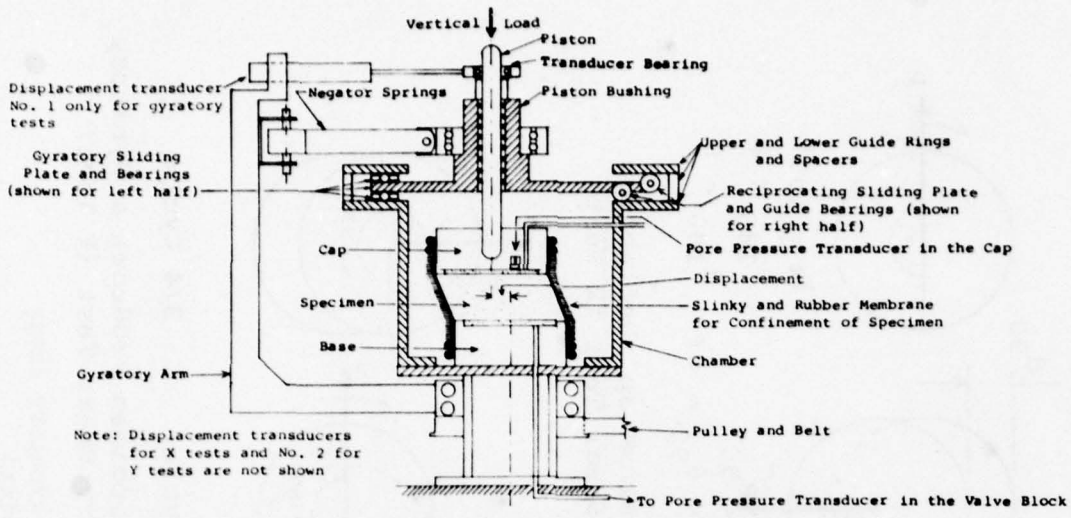


(a) Changing Magnitude of Shear Force  $S_\alpha = P \cdot \sin \alpha$  and Deflection of Top of Specimen During Reciprocating Shear Test (X Test)

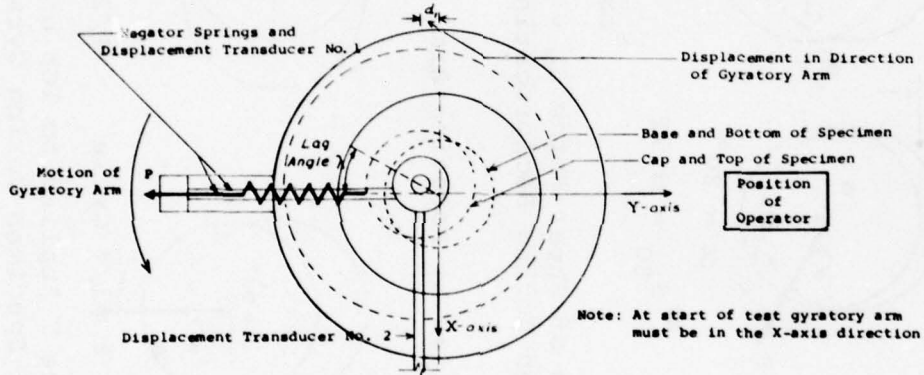


(b) A Constant Rotating Force P Applied to Top of Specimen Produces a Gyratory Deflection of Top of Specimen During Gyratory Shear Test (Y Test)

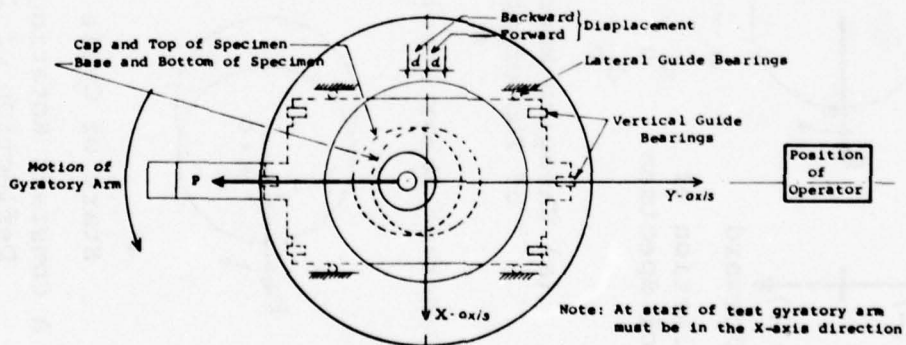
Fig. 1. Mechanics of (a) reciprocating and (b) gyratory shear as applied to a perfectly elastic specimen



(a) Section - Sliding Plate on Left for Gyrotary Tests, on Right for Reciprocating Tests



(b) GYRATORY SLIDING PLATE



(c) RECIPROCATING SLIDING PLATE

Fig. 2. Operation of gyrotary apparatus

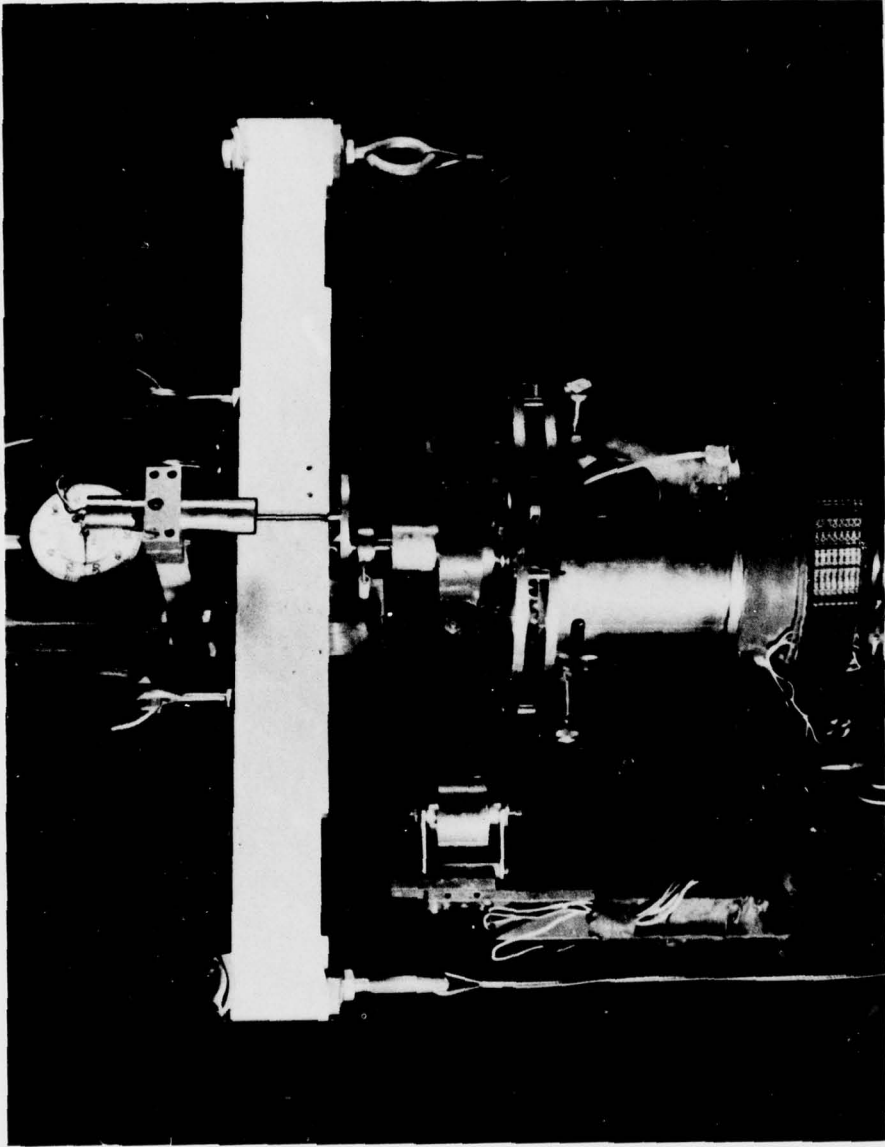
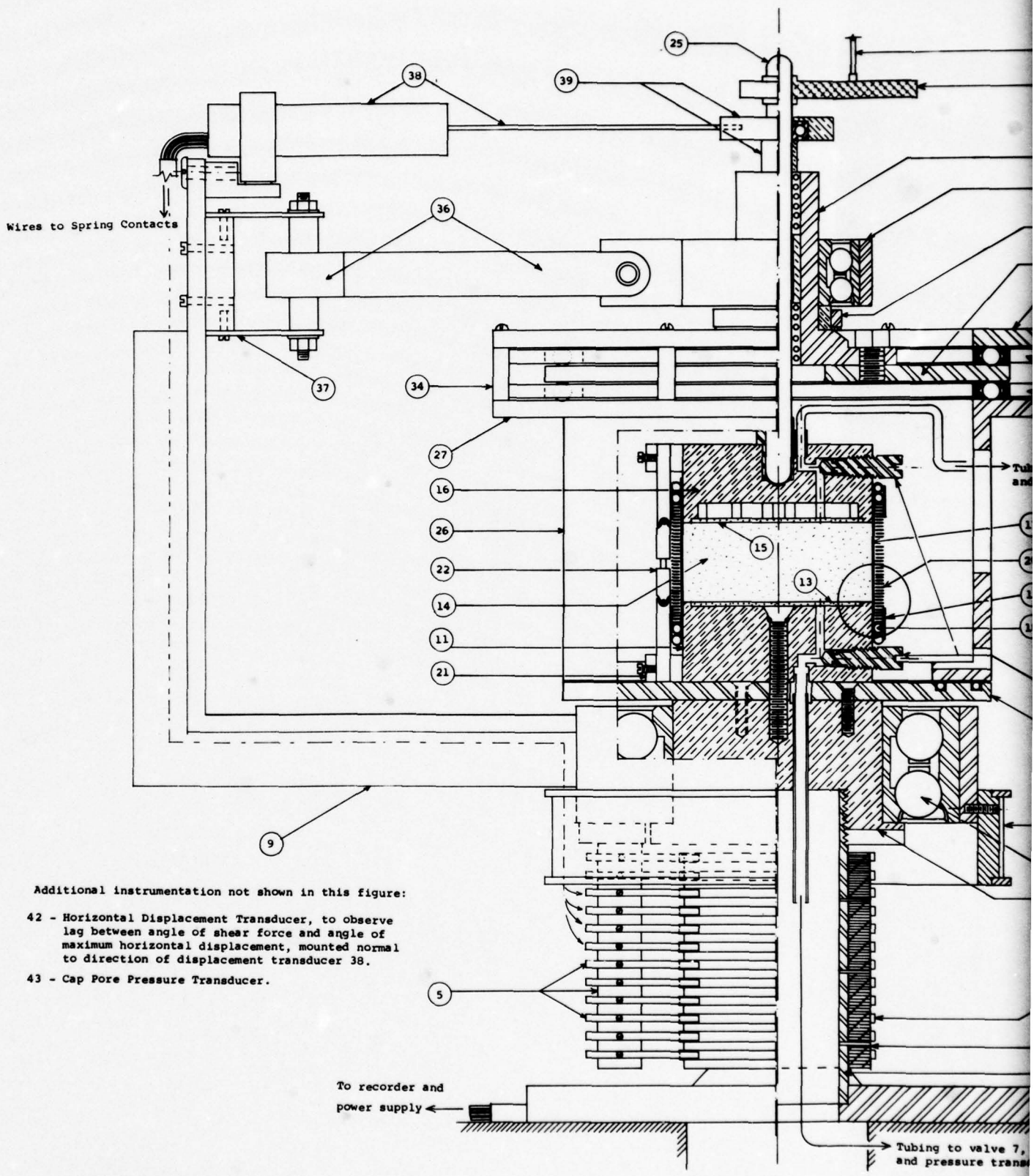


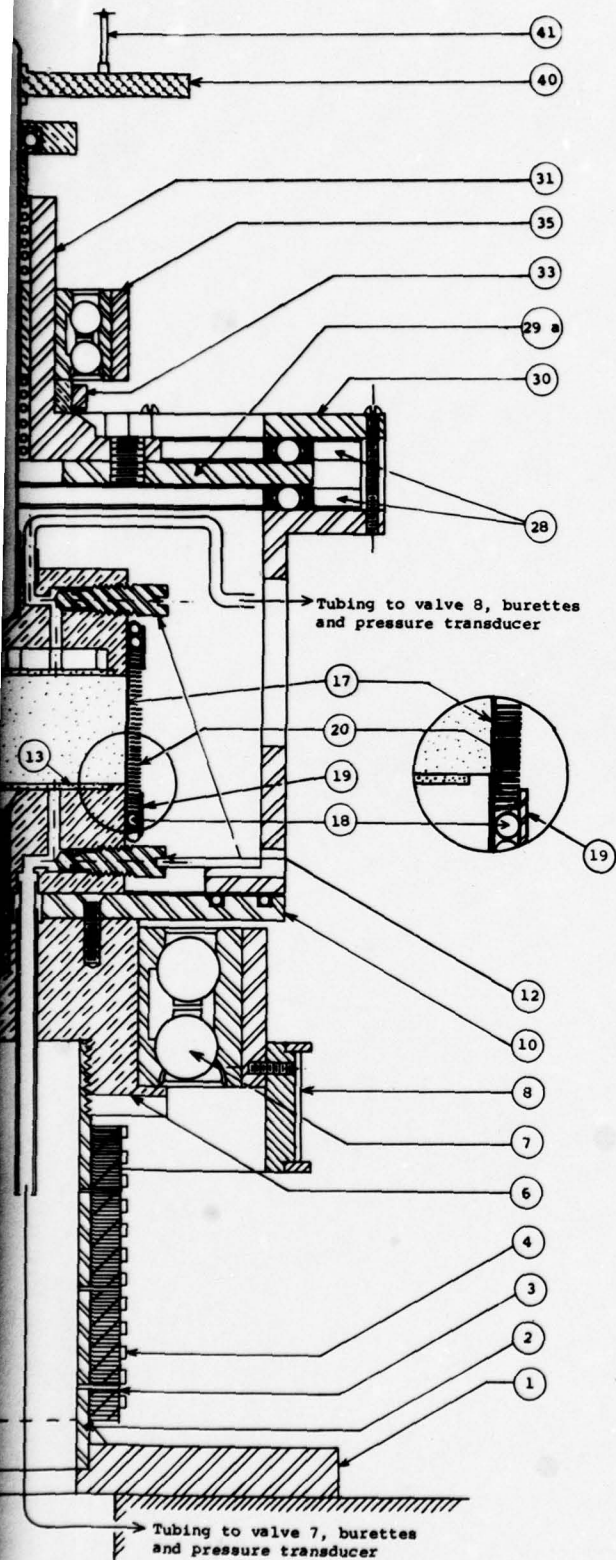
Fig. 3. Assembled gyrotory shear apparatus with Negator springs attached to gyrotory arm and before removing centering screws



Additional instrumentation not shown in this figure:

- 42 - Horizontal Displacement Transducer, to observe lag between angle of shear force and angle of maximum horizontal displacement, mounted normal to direction of displacement transducer 38.
- 43 - Cap Pore Pressure Transducer.

Fig. 4. Front view and section of gyroscope



## LEGEND

No.	Item
1	Base of Apparatus Support Column (Steel).
2	Apparatus Support Column (Steel).
3	Insulating Cylinder (Bakelite).
4	Slip Rings (Brass).
5	Spring Contacts and Support of Spring Contacts.
6	Top of Apparatus Support Column.
7	Gyratory Arm Bearing.
8	Flanged Pulley.
9	Gyratory Arm (Steel).
10	Base Plate for Chamber.
11	Base of Specimen.
12	Conical Valve.
13	Porous Plate of the Base.
14	Test Specimen.
15	Porous Plate of the Cap.
16	Cap.
17	Rubber Membrane.
18	O-rings (Parker 2-227).
19	Hose Clamp (Aero Seal QM 200 40).
20	Flat-coil Spring, "Slinky".
21	Column Holders.
22	Telescopic Slinky Columns.
[23	Rigid Slinky Columns, not shown in this figure].
[24	Slinky Coil Spreaders, not shown in this figure].
25	Loading Piston (Stainless Steel).
26	Apparatus Chamber (Stainless Steel).
27	Lower Guide Ring (Stainless Steel).
28	Gyratory Bearing.
29 a	Gyratory Sliding Plate (Stainless Steel).
[29 b	Reciprocating Sliding Plate with Vertical Guide Bearings not shown in this figure].
30	Upper Guide Ring (Stainless Steel).
31	Piston Bushing.
[32	Lateral Guide Bearings, not shown in this figure].
33	Test Starting Plate (Stainless Steel).
34	Spacers.
35	Shear Force Ball Bearing
36	Negator Springs.
37	Negator Springs Support (Frame and Spool Assembly).
38	Horizontal Displacement Transducer.
39	Bearing into which transducers probes are screwed.
40	Platform for Probe of Vertical Displacement Transducer.
41	Probe of Vertical Displacement Transducer.

Note: For further details see figures in Appendix A

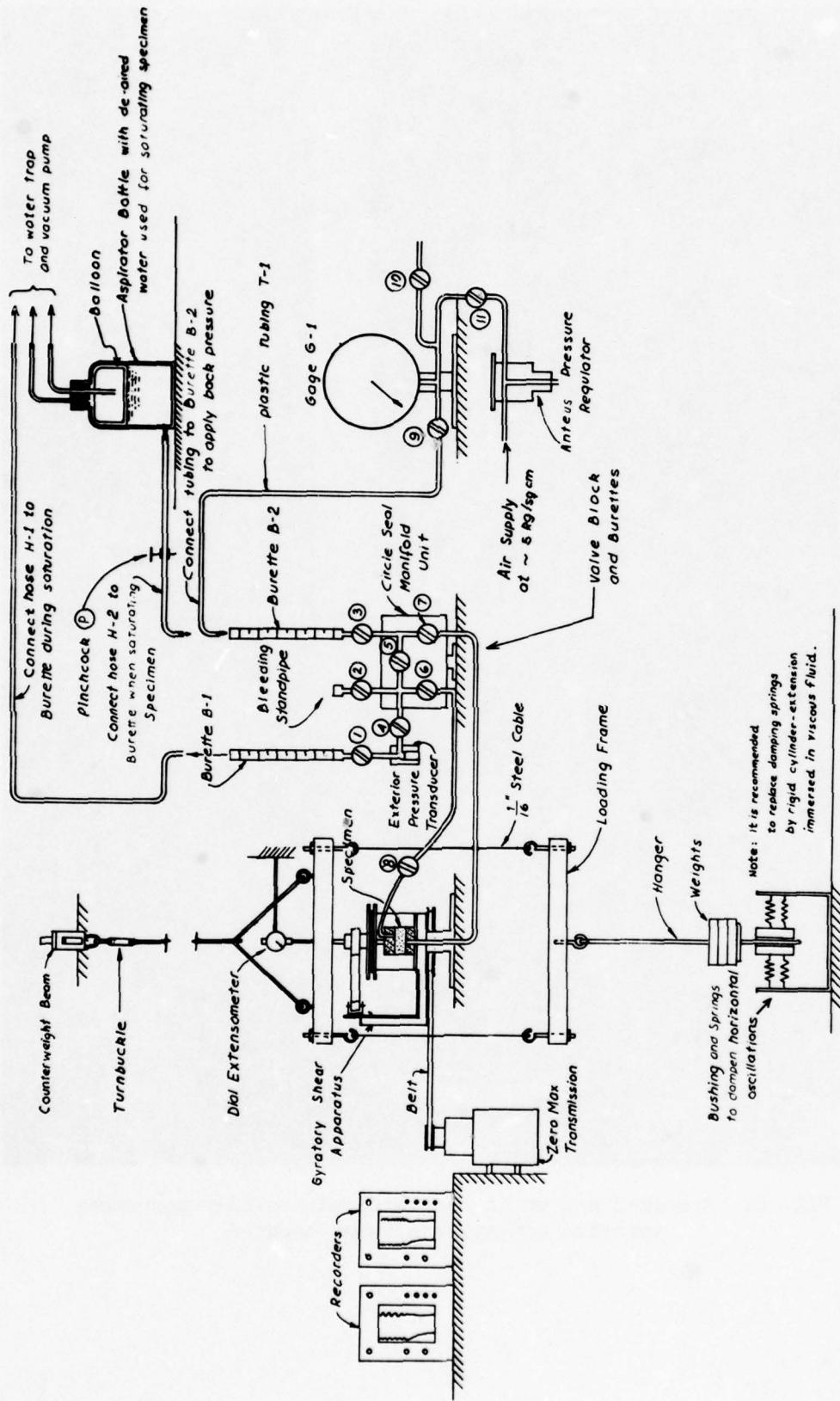


Fig. 5. Diagram of gyrotory shear apparatus and appurtenant equipment, except items for setting up a specimen and freezing it at end of test

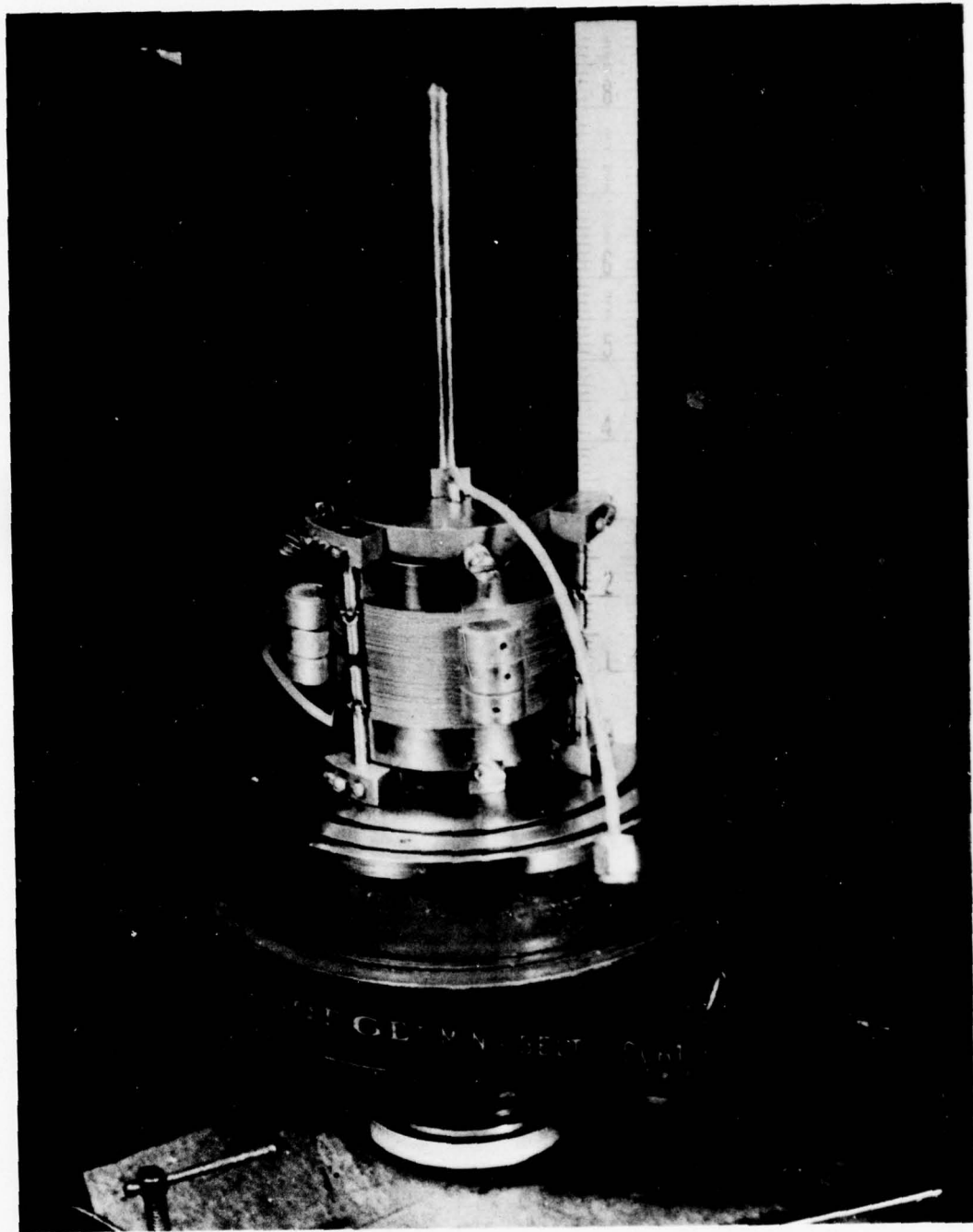


Fig. 6. Specimen set up in apparatus with slinky spreaders inserted and guide columns mounted

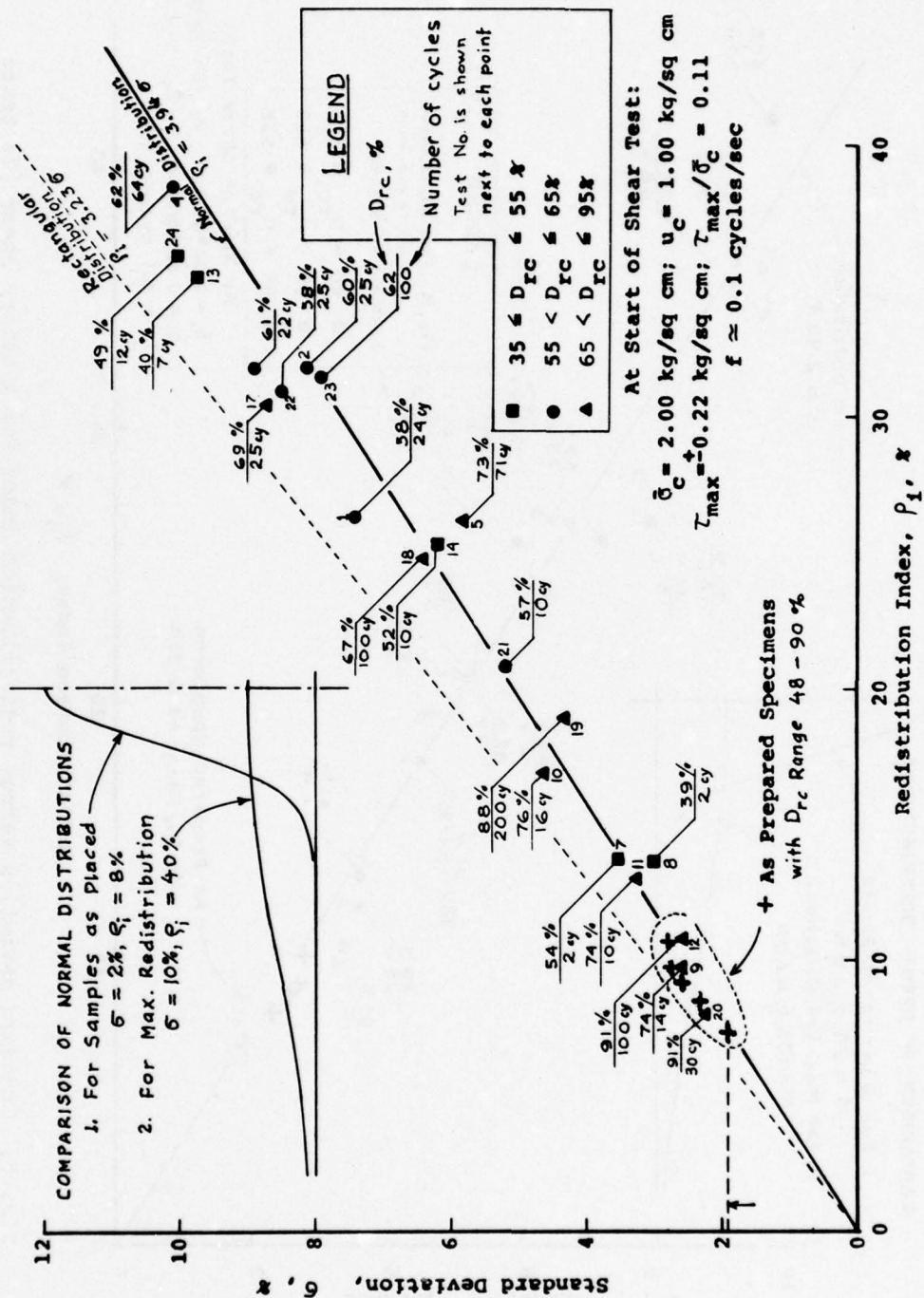


Fig. 7. Standard deviation versus redistribution index for reciprocating shear (X) tests

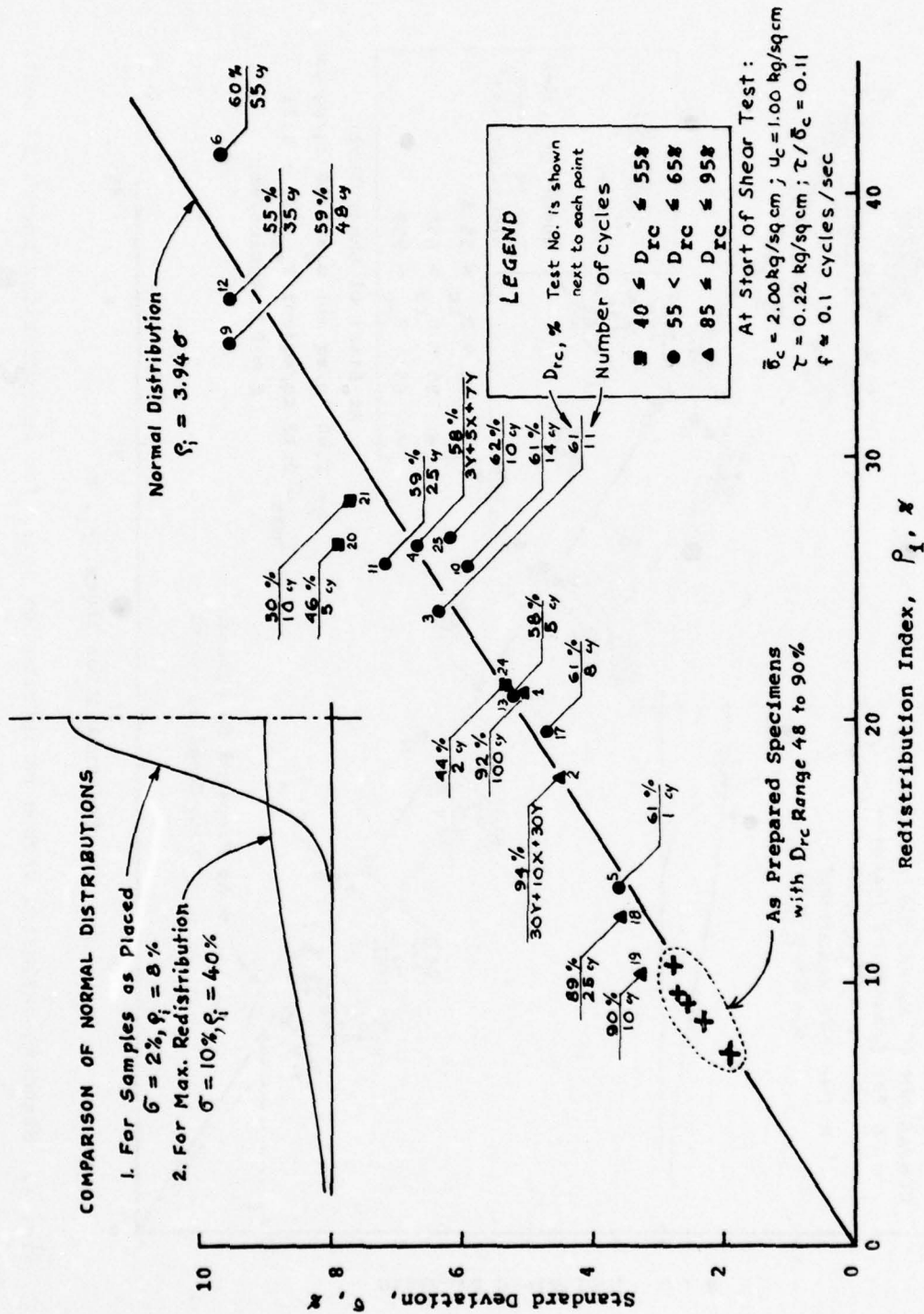
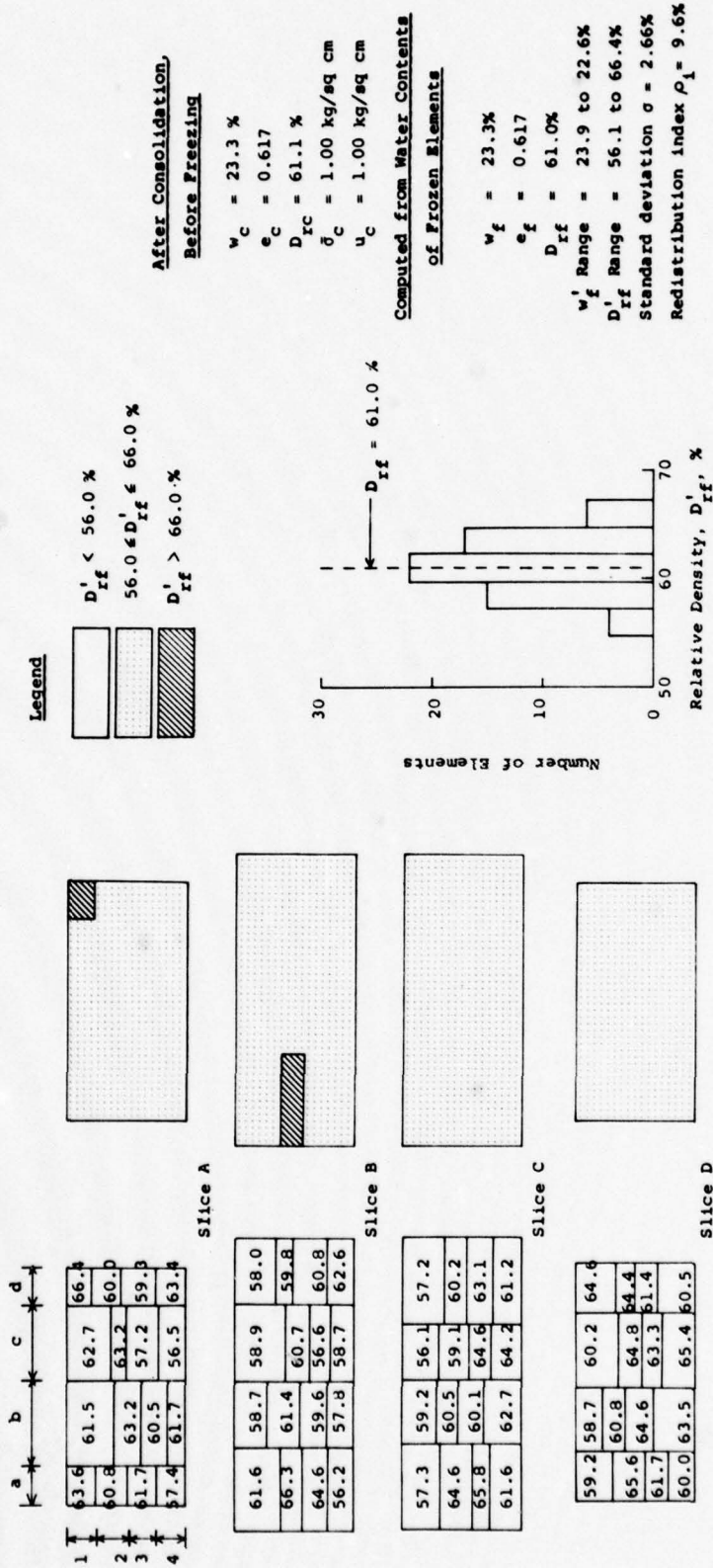
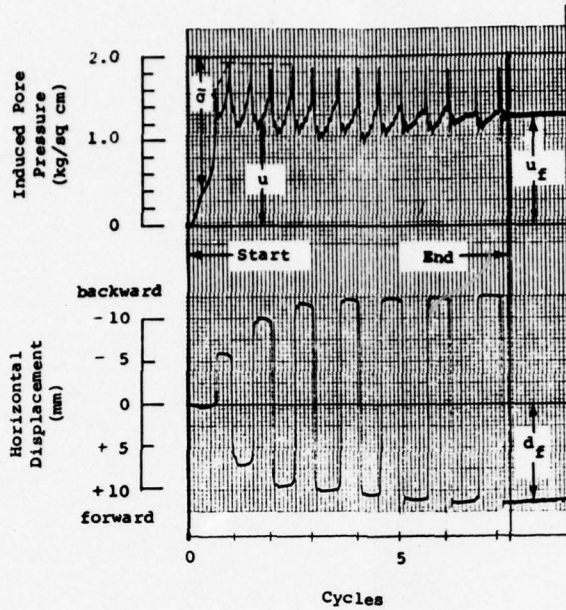


Fig. 8. Standard deviation versus redistribution index for gyratory shear (Y) tests

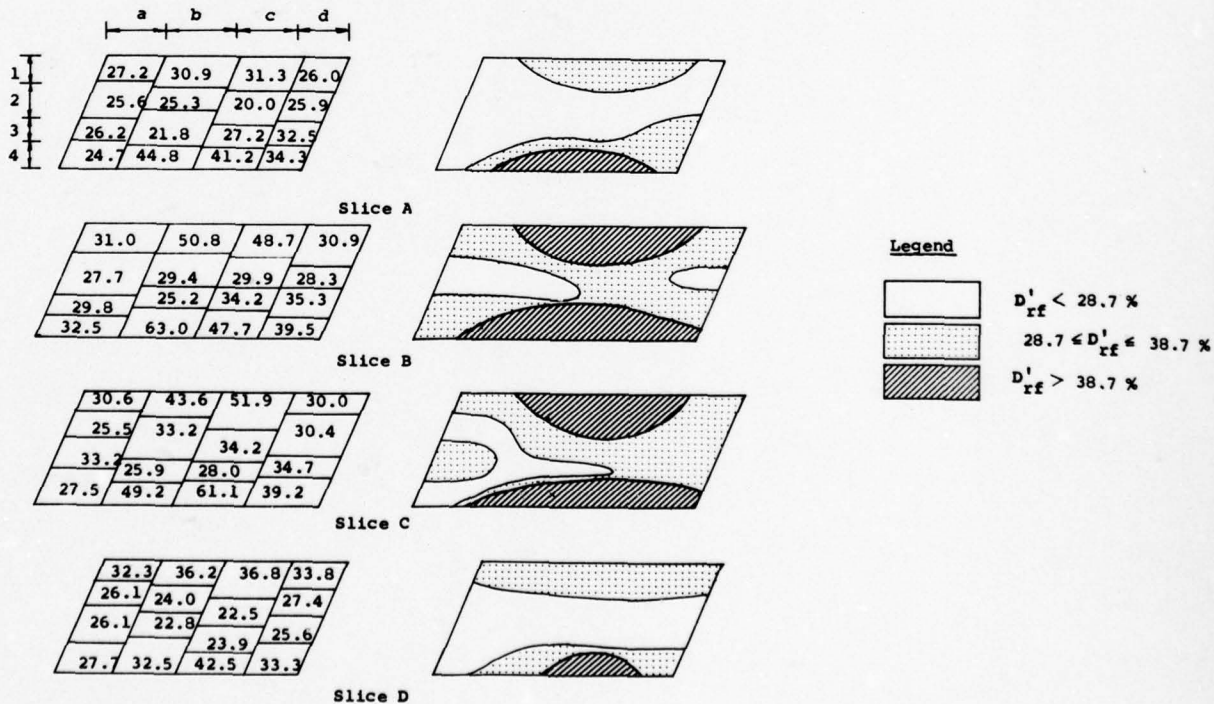


Distribution of Relative Density in Vertical Slices      Histogram of Distribution of Relative Density

Fig. 9. Distribution of relative density in specimens as prepared (test W3)

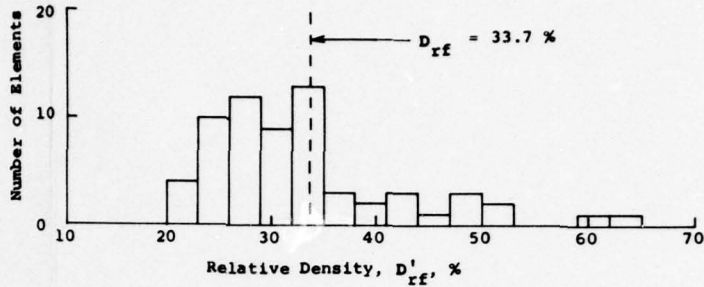
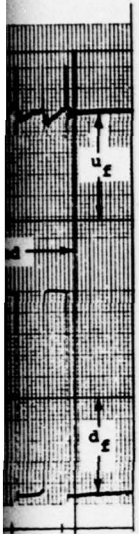


(a) Induced Pore Pressure and Horizontal Displacement versus Number of Cycles



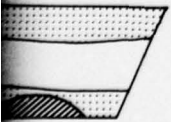
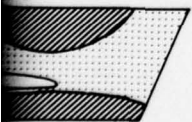
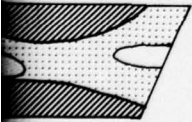
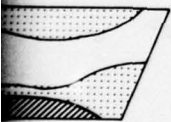
(b) Distribution of Relative Density in Vertical Slices Parallel to Direction of Motion

Fig. 10. Reciprocating test No.



(c) Histogram of Distribution of Relative Density

Displacement



ical Slices

Legend

- $D'_{rf} < 28.7 \%$
- $28.7 \leq D'_{rf} \leq 38.7 \%$
- $D'_{rf} > 38.7 \%$

After Consolidation,

At Start of Test

- $\bar{\sigma}_c = 2.00 \text{ kg/sq cm}$
- $u_c = 1.00 \text{ kg/sq cm}$
- $e_c = 0.689$
- $w_c = 26.0 \%$
- $D_{rc} = 39.8 \%$
- $\tau_{max} = \pm 0.22 \text{ kg/sq cm}$
- $\tau_{max} / \bar{\sigma}_c = 0.11$
- $f = 0.10 \text{ cycles/sec}$

At End of Test and During Freezing

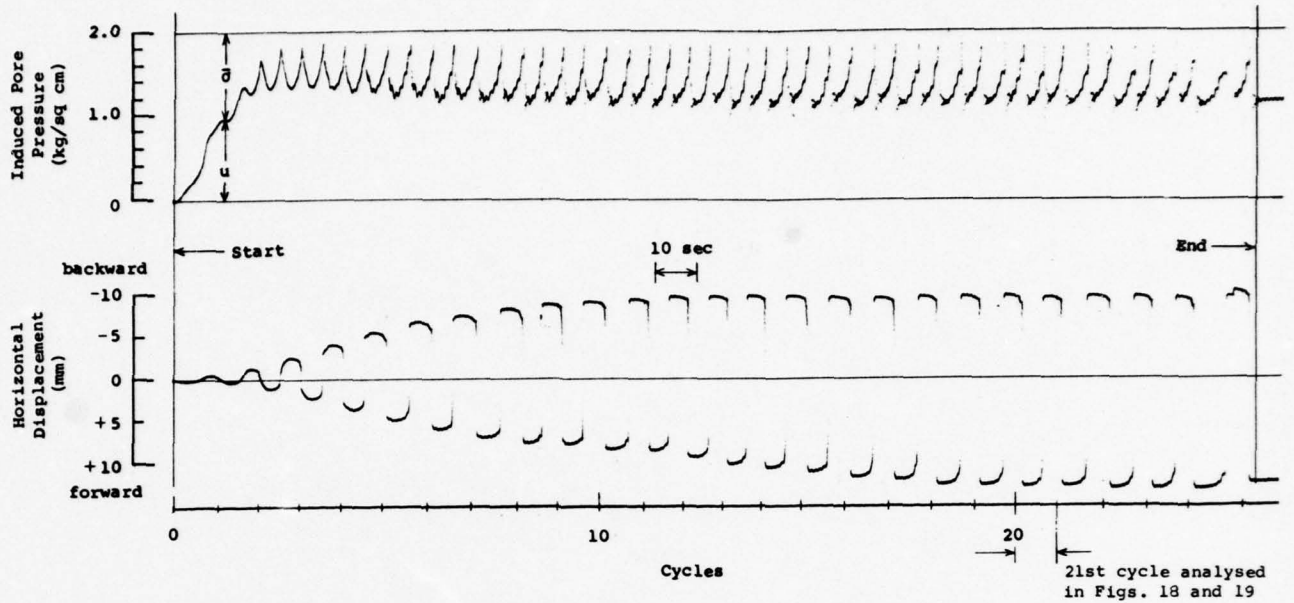
- $N_f = 7 \text{ cycles}$
- $\tau_f = 0.19 \text{ kg/sq cm}$
- $\bar{\sigma}_f = 0.71 \text{ kg/sq cm}$
- $\tau_f / \bar{\sigma}_f = 0.27$
- $u_f = 1.29 \text{ kg/sq cm}$
- $d_f = 11.5 \text{ mm}$

Computed from Water Contents

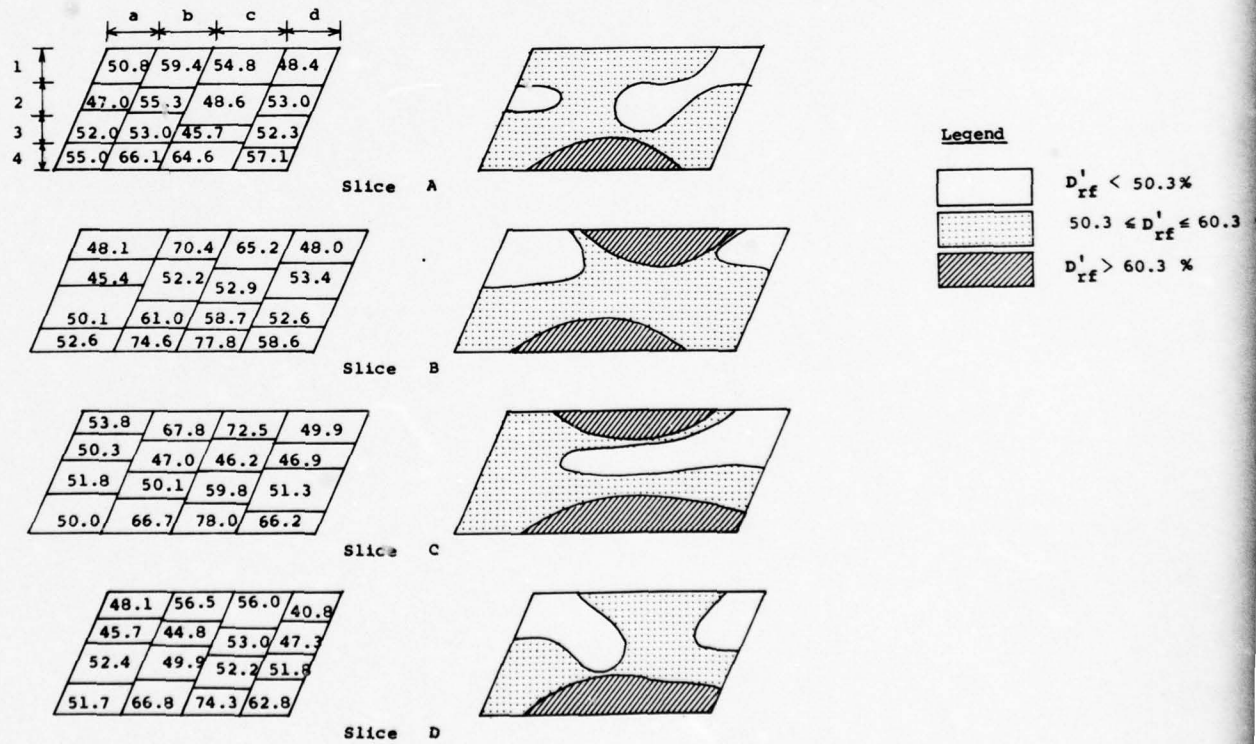
of Frozen Elements

- $w_f = 26.7 \%$
- $e_f = 0.708$
- $D_{rf} = 33.7 \%$
- $w'_f \text{ Range} = 28.5 \text{ to } 23.0\%$
- $D'_{rf} \text{ Range} = 20.0 \text{ to } 63.0 \%$
- Standard deviation  $\sigma = 9.75 \%$
- Redistribution Index  $\rho_1 = 35.2 \%$

Fig. 10. Reciprocating test No. X13

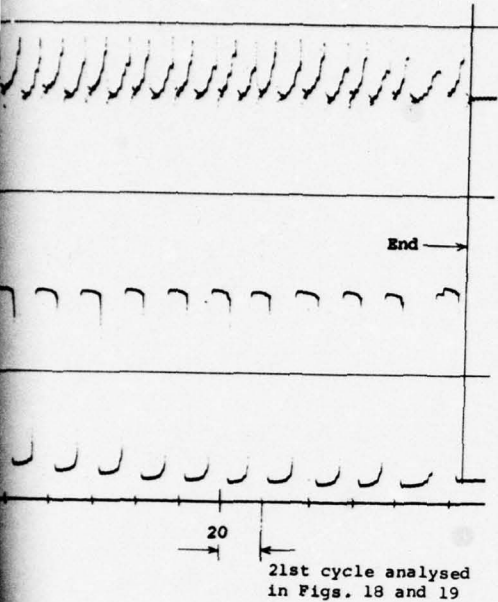


(a) Induced Pore Pressure and Horizontal Displacement versus Number of Cycles



(b) Distribution of Relative Density in Vertical Slices Parallel to Direction of Motion

Fig. 11. Reciprocating

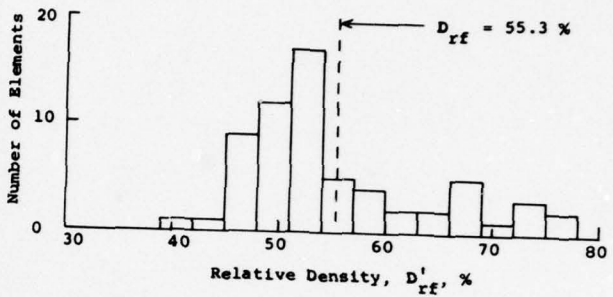


al Displacement



Legend

- $D'_{rf} < 50.3\%$
- $50.3 \leq D'_{rf} \leq 60.3\%$
- $D'_{rf} > 60.3\%$



(c) Histogram of Distribution of Relative Density

After Consolidation,

At Start of Test

- $\bar{\sigma}_c = 2.00 \text{ kg/sq cm}$
- $u_c = 1.00 \text{ kg/sq cm}$
- $e_c = 0.627$
- $w_c = 23.7\%$
- $D_{rc} = 58.1\%$
- $\tau_{max} = \pm 0.22 \text{ kg/sq cm}$
- $\tau_{max} / \bar{\sigma}_c = 0.11$
- $f = 0.10 \text{ cycles/sec}$

At End of Test and During Freezing

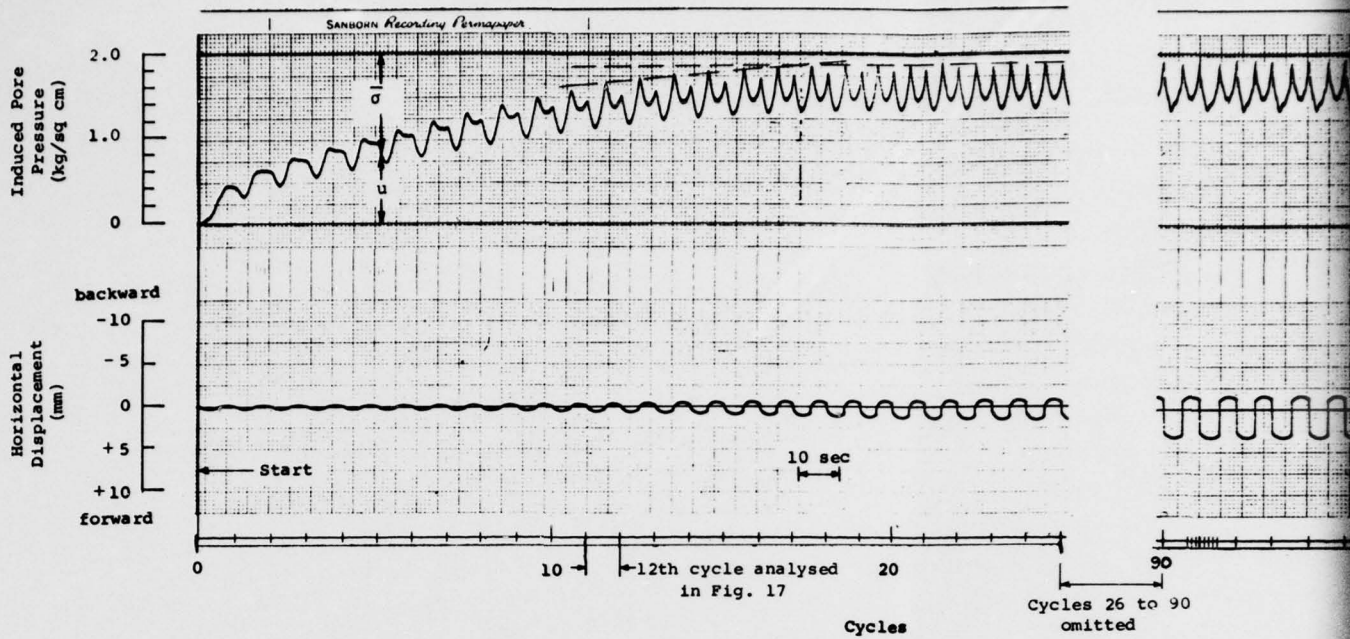
- $N_f = 25 \text{ cycles}$
- $\tau_f = 0.19 \text{ kg/sq cm}$
- $\bar{\sigma}_f = 0.82 \text{ kg/sq cm}$
- $\tau_f / \bar{\sigma}_f = 0.23$
- $u_f = 1.18 \text{ kg/sq cm}$
- $d_f = 12.5 \text{ mm}$

Computed from Water Contents

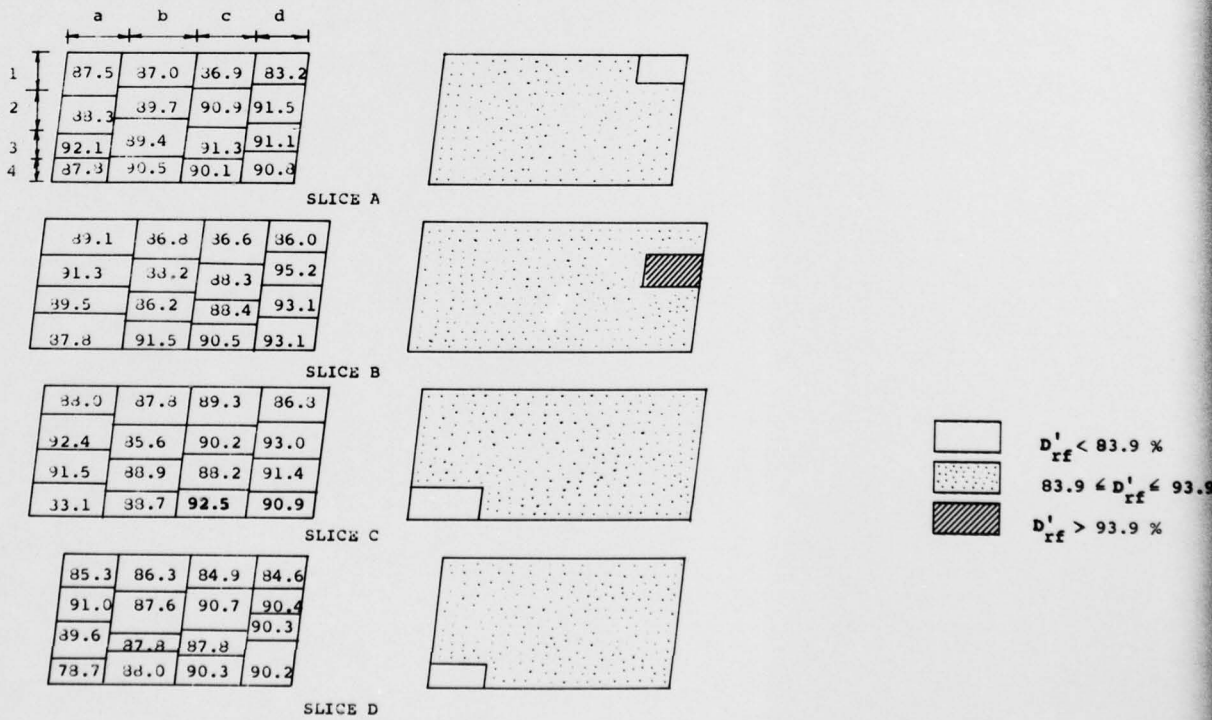
of Frozen Elements

- $w_f = 24.0\%$
- $e_f = 0.636$
- $D_{rf} = 55.3\%$
- $w'_f \text{ Range} = 23.7 \text{ to } 19.4\%$
- $D'_{rf} \text{ Range} = 40.8 \text{ to } 78.0\%$
- Standard deviation  $\sigma = 8.53\%$
- Redistribution Index  $\rho_1 = 31.0\%$

Fig. 11. Reciprocating test No. X22



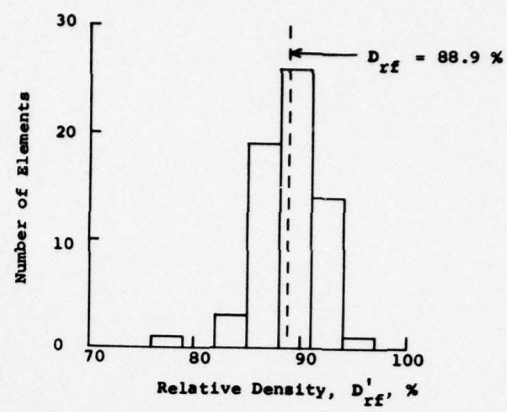
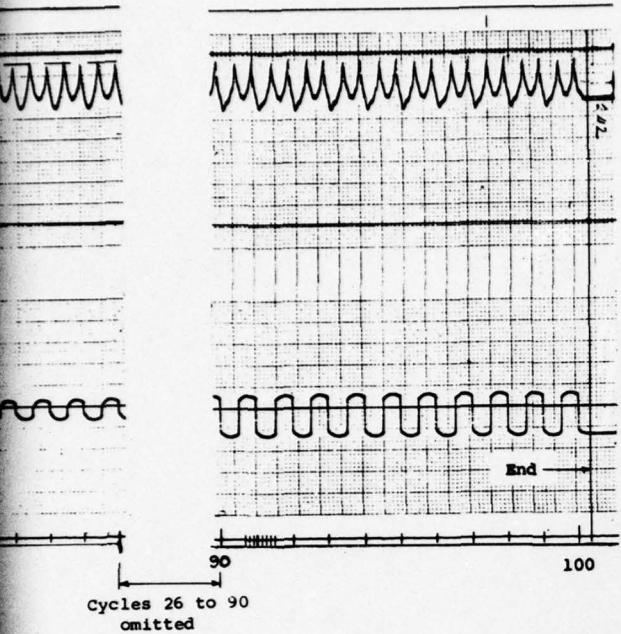
(a) Induced Pore Pressure and Horizontal Displacement versus Number of Cycles



(b) Distribution of Relative Density in Vertical Slices Parallel to Direction of Motion

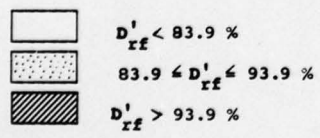
Fig. 12. Reciprocat

2



(c) Histogram of Distribution of Relative Density

Horizontal Displacement  
cycles



After Consolidation,  
At Start of Test

- $\bar{\sigma}_c = 2.00 \text{ kg/sq cm}$
- $u_c = 1.00 \text{ kg/sq cm}$
- $e_c = 0.517$
- $w_c = 19.5 \%$
- $D_{rc} = 90.9 \%$
- $\tau_{max} = \pm 0.22 \text{ kg/sq cm}$
- $\tau_{max} / \bar{\sigma}_c = 0.11$
- $f = 0.12 \text{ cycles/sec}$

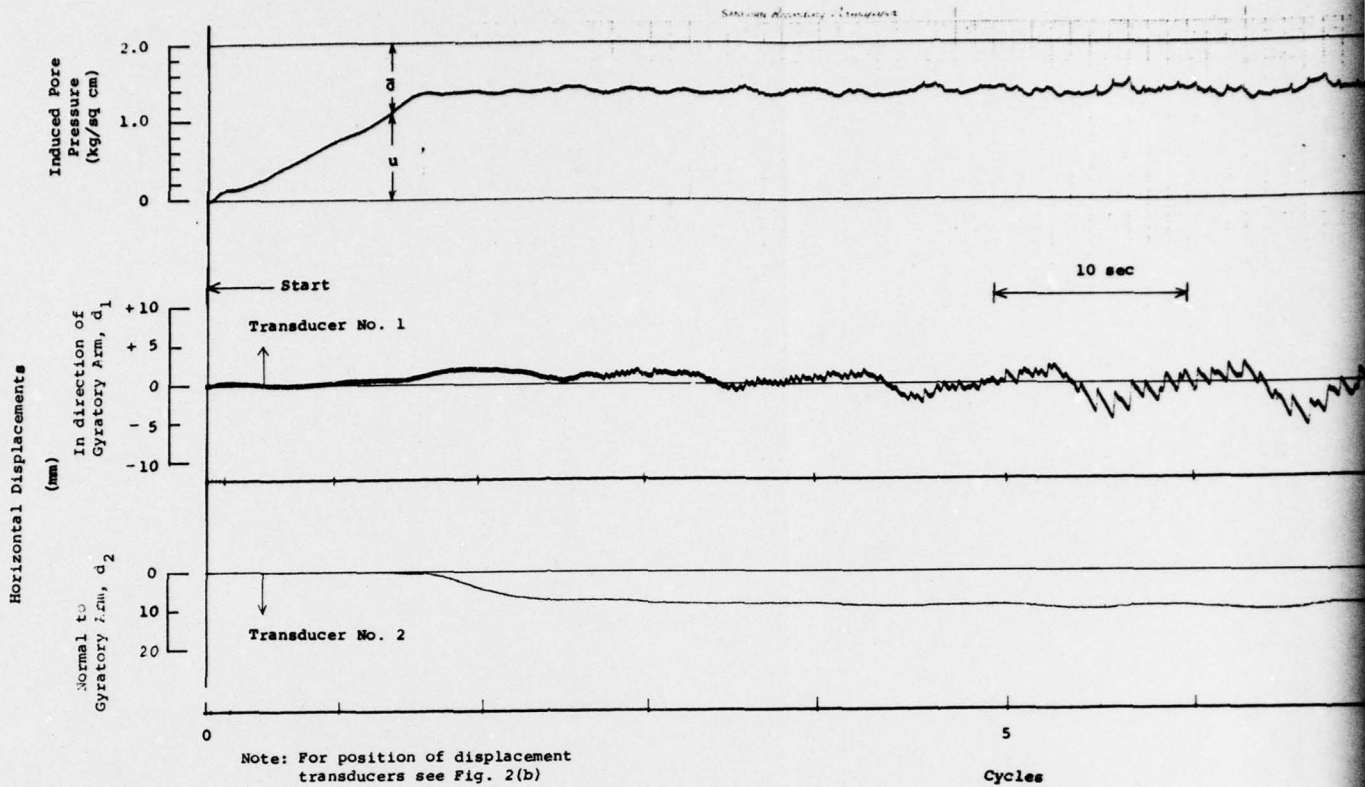
At End of Test and During Freezing

- $N_f = 100 \text{ cycles}$
- $\tau_f = 0.19 \text{ kg/sq cm}$
- $\bar{\sigma}_f = 0.58 \text{ kg/sq cm}$
- $\tau_f / \bar{\sigma}_f = 0.33$
- $u_f = 1.42 \text{ kg/sq cm}$
- $d_f = 3.5 \text{ mm}$

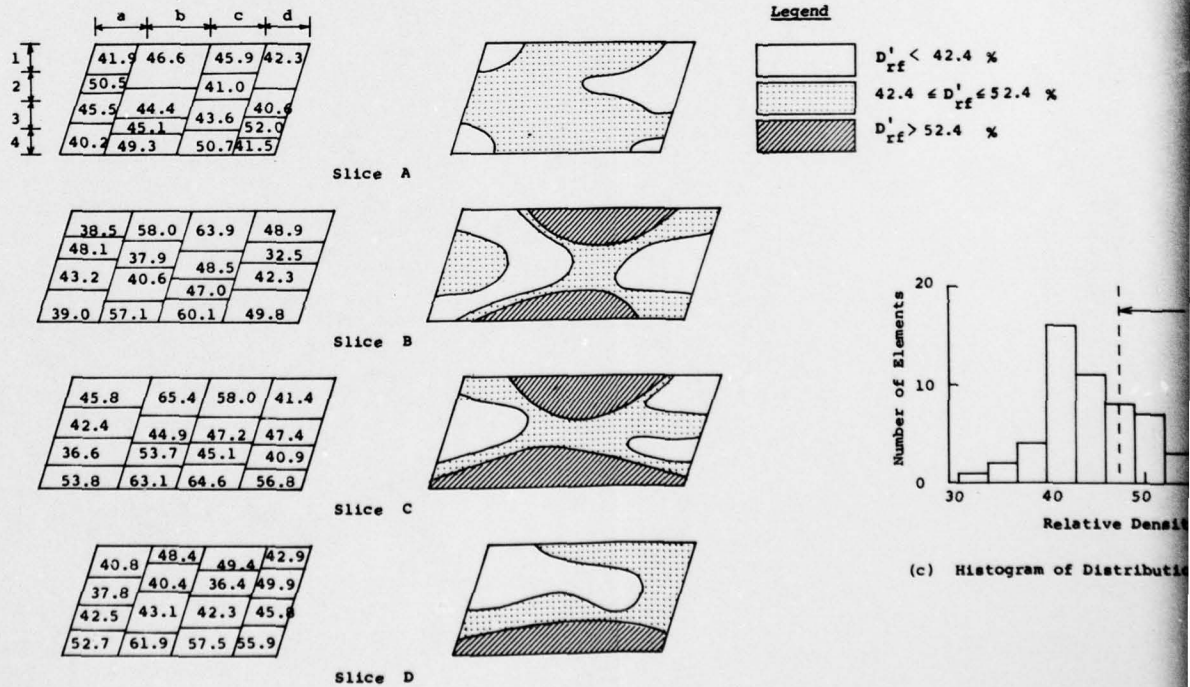
Computed from Water Contents  
of Frozen Elements

- $w_f = 19.8 \%$
- $e_f = 0.524$
- $D_{rf} = 88.9 \%$
- $w_f^i \text{ Range} = 21.0 \text{ to } 19.0 \%$
- $D_{rf}^i \text{ Range} = 78.7 \text{ to } 95.2 \%$
- Standard deviation  $\sigma = 2.55 \%$
- Redistribution Index  $\rho_1 = 10.8 \%$

Fig. 12. Reciprocating test No. X12

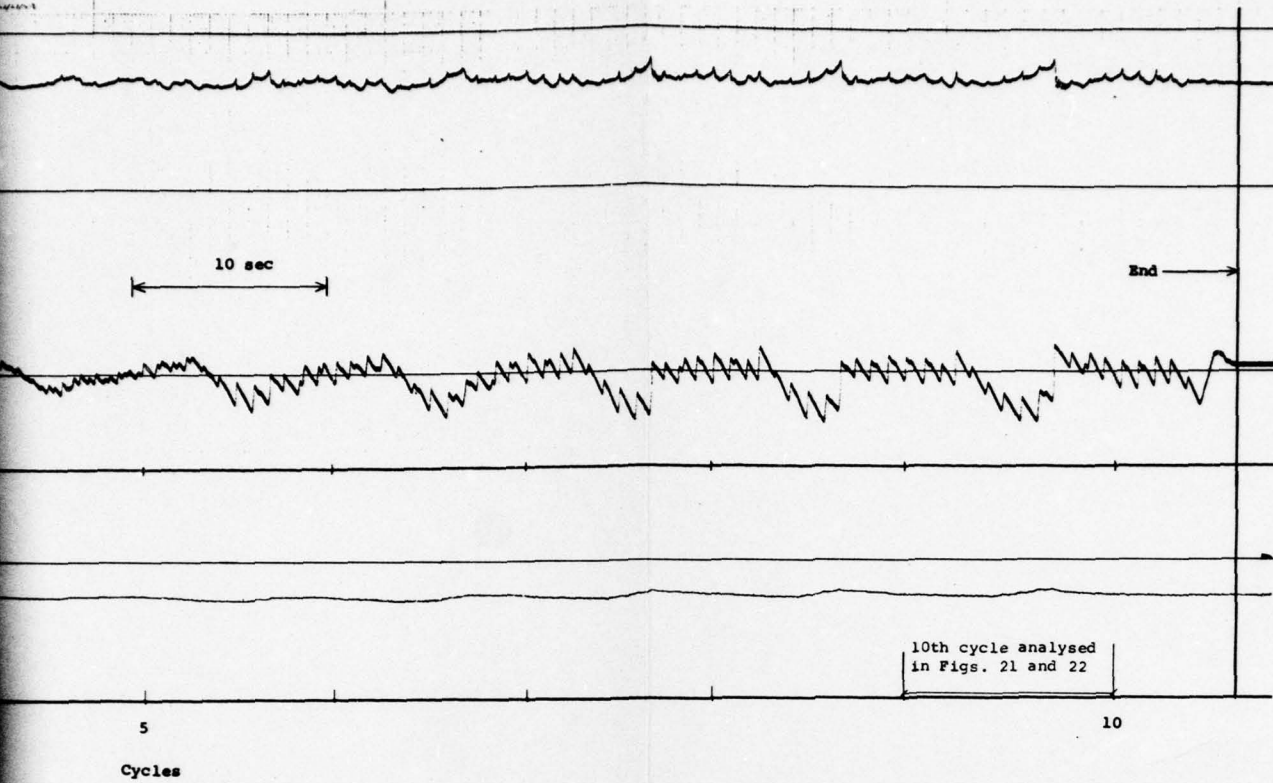


(a) Induced Pore Pressure and Horizontal Displacements versus Number of Cycles



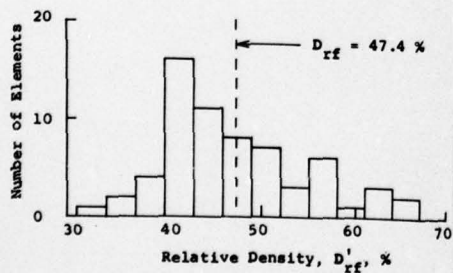
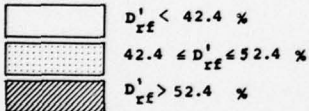
(b) Distribution of Relative Density in Vertical Slices in Direction of Final Deflection

Fig. 13. Gy



ed Pore Pressure and Horizontal Displacements  
versus Number of Cycles

**Legend**



(c) Histogram of Distribution of Relative Density

After Consolidation,

At Start of Test

- $\bar{\sigma}_c = 2.00$  kg/sq cm
- $u_c = 1.00$  kg/sq cm
- $e_c = 0.654$
- $w_c = 24.7$  %
- $D_{rc} = 50.1$  %
- $\tau = 0.22$  kg/sq cm
- $\tau / \bar{\sigma}_c = 0.11$
- $f = 0.10$  cycles/sec

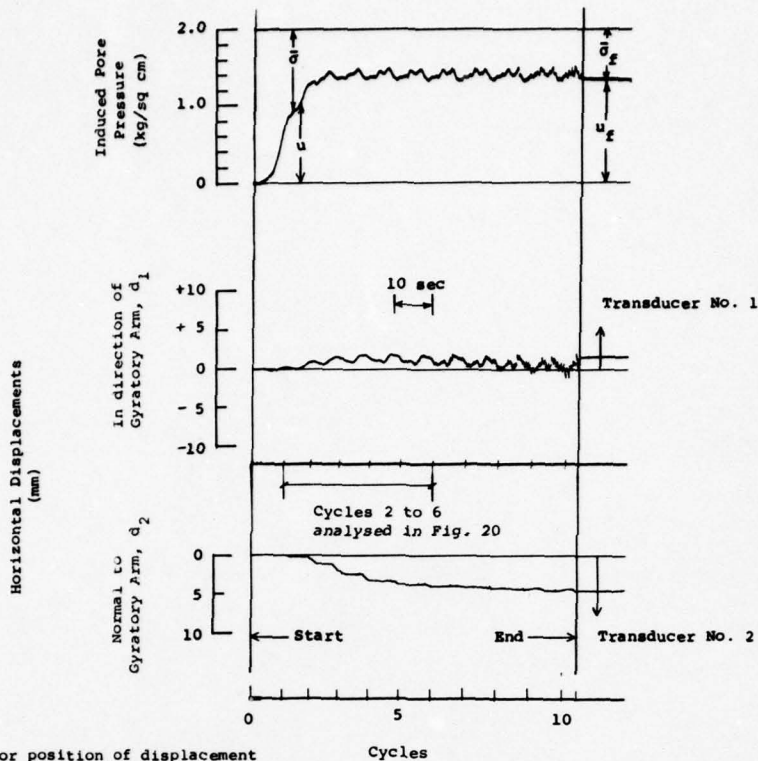
At End of Test and During Freezing

- $N_f = 10$  cycles
- $\tau_f = 0.22$  kg/sq cm
- $\bar{\sigma}_f = 0.69$  kg/sq cm
- $\tau_f / \bar{\sigma}_f = 0.32$
- $u_f = 1.31$  kg/sq cm
- $\bar{d}_f = 9.5$  mm

Computed from Water Contents  
of Frozen Elements

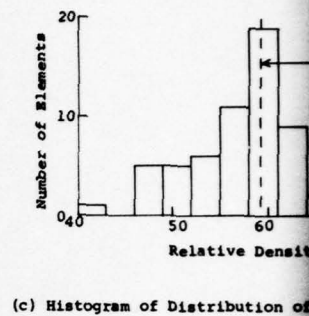
- $w_f = 25.0$  %
- $e_f = 0.663$
- $D_{rf} = 47.4$  %
- $w_f^i$  Range = 26.9 to 22.8 %
- $D_{rf}^i$  Range = 32.5 to 65.4 %
- Standard deviation  $\sigma = 7.72$  %
- Redistribution Index  $\rho_1 = 28.4$  %

Fig. 13. Gyrotory test No. Y21



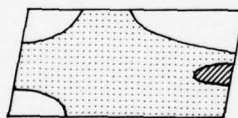
Note: For position of displacement transducers see Fig. 2(b)

(a) Induced Pore Pressure and Horizontal Displacements versus Number of Cycles



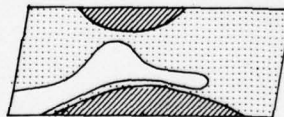
	a	b	c	d
1	49.2	57.7	53.2	42.3
2	58.2	58.0		54.6
3	57.7	59.4	60.5	69.7
4	50.1	59.7	63.5	55.3

Slice A



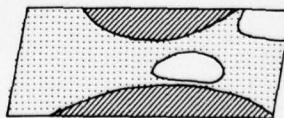
56.1	67.9	62.4	62.0
59.4	53.0	61.3	60.6
58.8	47.1	50.4	61.5
53.9	68.6	73.7	61.1

Slice B



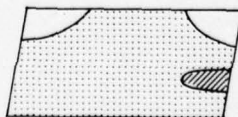
58.3	66.2	67.5	50.6
58.7	59.9	55.9	62.0
55.9	59.1	48.7	60.1
59.4	74.9	75.6	64.7

Slice C

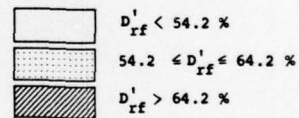


48.6	56.0	56.3	48.7
60.6	58.6	57.1	62.1
55.0	59.9	61.5	72.7
56.7	59.3	58.9	59.5

Slice D

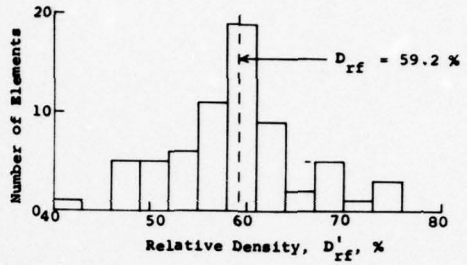
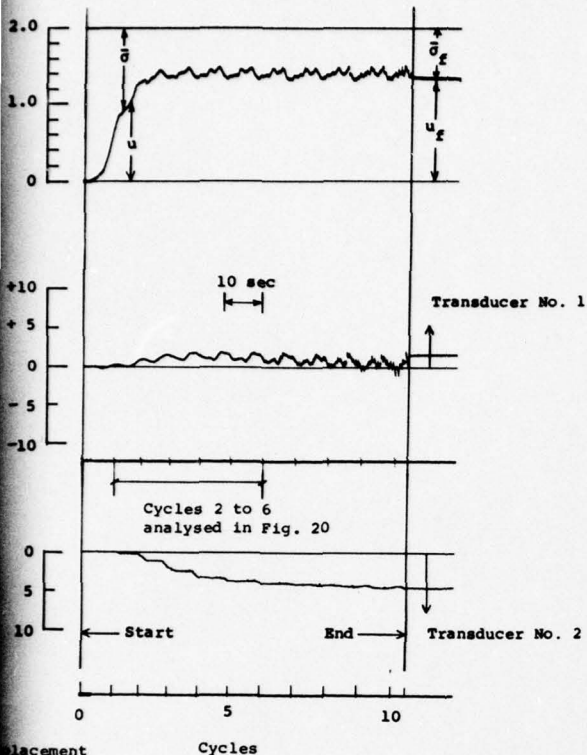


Legend



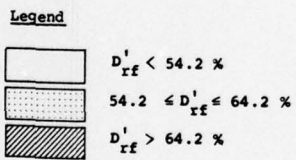
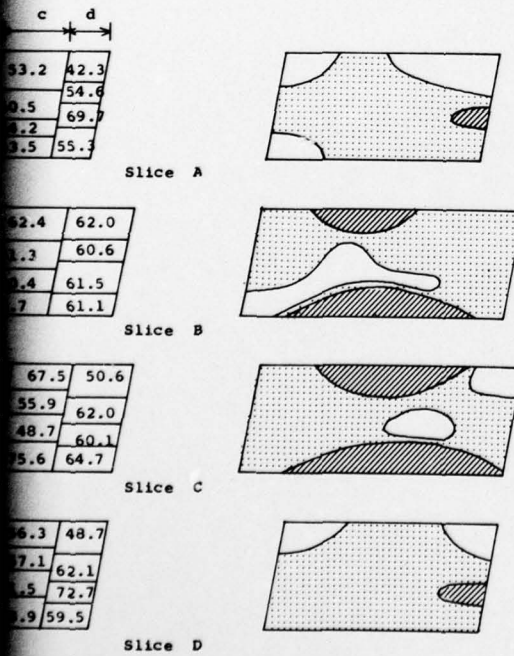
(b) Distribution of Relative Density in Vertical Slices in Direction of Final Deflection

Fig. 14. Gyrotory test No. Y25



(c) Histogram of Distribution of Relative Density

Fore Pressure and Horizontal Displacements versus Number of Cycles



After Consolidation, At Start of Test

- $\bar{\sigma}_c = 2.00$  kg/sq cm
- $u_c = 1.00$  kg/sq cm
- $e_c = 0.615$
- $w_c = 23.2\%$
- $D_{rc} = 61.7\%$
- $\tau = 0.22$  kg/sq cm
- $\tau/\bar{\sigma}_c = 0.11$
- $f = 0.13$  cycles/sec

At End of Test and During Freezing

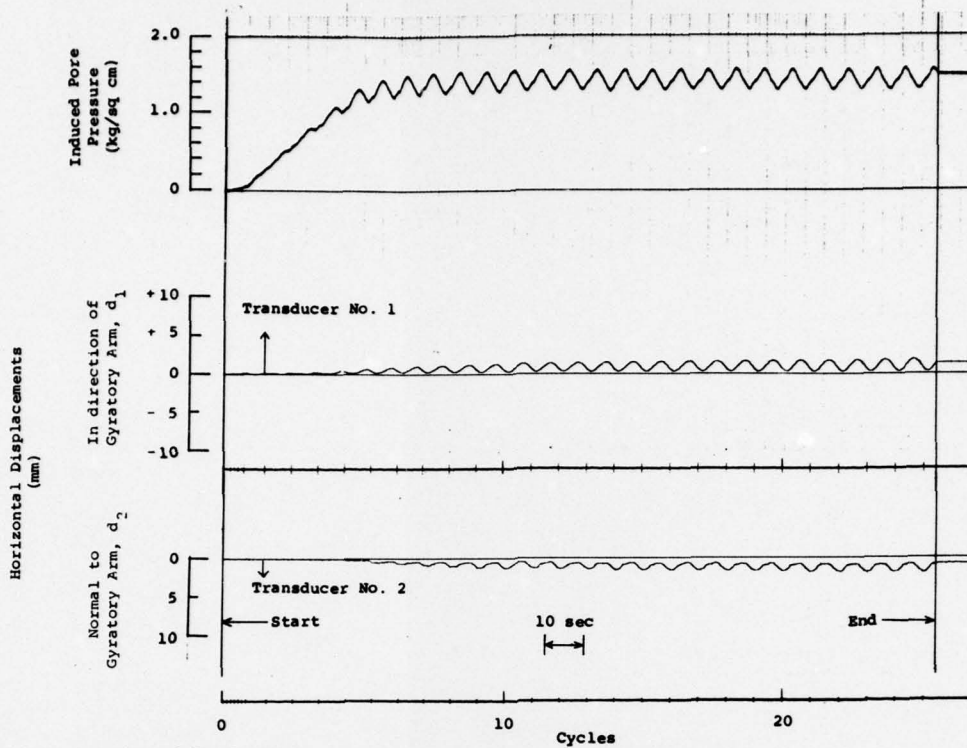
- $N_f = 10$  cycles
- $\tau_f = 0.22$  kg/sq cm
- $\bar{\sigma}_f = 0.66$  kg/sq cm
- $\tau_f/\bar{\sigma}_f = 0.33$
- $u_f = 1.34$  kg/sq cm
- $\bar{d}_f = 5.2$  mm

Computed from Water Contents of Frozen Elements

- $w_f = 23.5\%$
- $e_f = 0.623$
- $D_{rf} = 59.2\%$
- $w'_f$  Range = 25.6 to 21.4 %
- $D'_{rf}$  Range = 42.3 to 75.6 %
- Standard deviation  $\sigma = 6.17\%$
- Redistribution Index  $\rho_1 = 27.0\%$

Distribution of Relative Density in Vertical Slices in Direction of Final Deflection

Fig. 14. Gyrotory test No. Y25



Note: For position of displacement transducers see Fig. 2(b)

(a) Induced Pore Pressure and Horizontal Displacements versus Number of Cycles

	a	b	c	d
1	81.4	78.4	81.7	81.4
2	89.4	89.2	89.9	86.8
3	88.0	86.0	89.9	90.3
4	83.3	88.1	90.5	87.4

Slice A

84.1	76.9	89.5	89.3
88.4	82.1	86.5	89.2
90.5	84.8	84.9	88.0
84.9	89.3	91.0	88.1

Slice B

83.6	83.9	90.2	90.3
87.3	82.2	87.1	89.2
89.0	86.9	86.5	87.9
80.5	88.0	90.3	87.3

Slice C

81.9	79.3	81.3	76.9
89.0	86.6	90.4	86.4
89.5	88.6	88.0	90.1
81.4	86.6	86.9	87.8

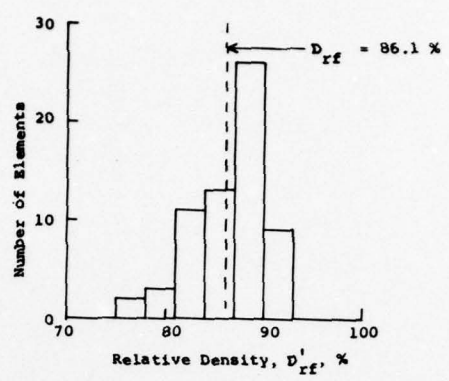
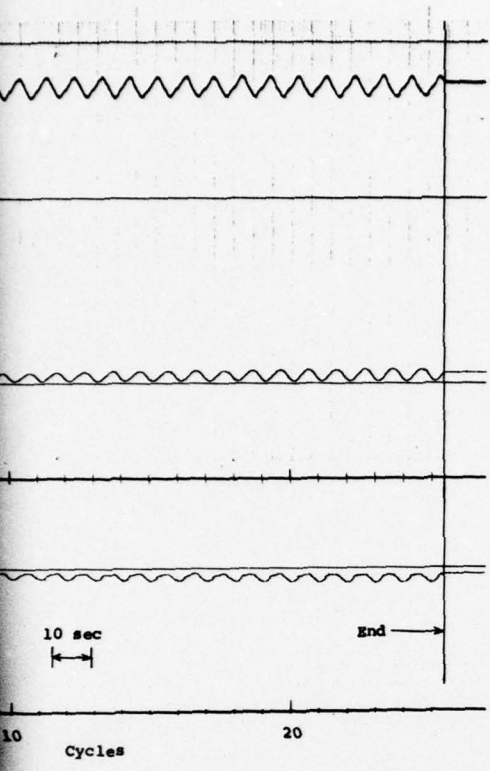
Slice D

Legend

	$D_{rf}^i < 80.5 \%$
	$80.5 \leq D_{rf}^i \leq 90.5 \%$
	$D_{rf}^i > 90.5 \%$

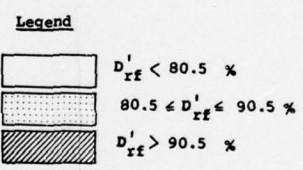
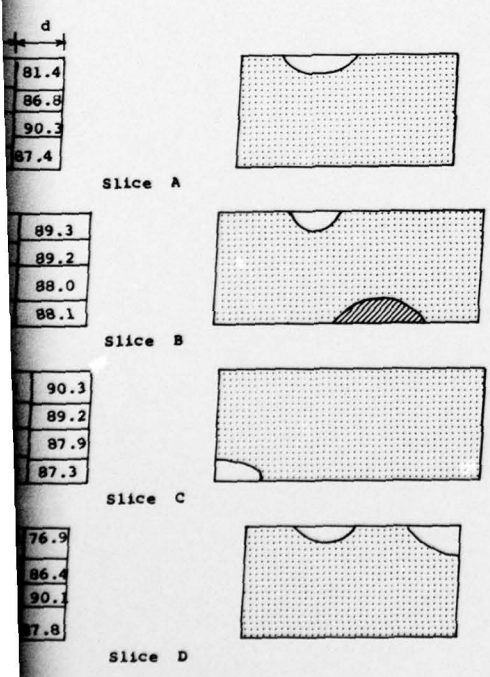
(b) Distribution of Relative Density in Vertical Slices in Direction of Final Deflection

Fig. 15. Gyratory test No.



(c) Histogram of Distribution of Relative Density

Pressure and Horizontal Displacements versus Number of Cycles



After Consolidation.

At Start of Test

- $\bar{\sigma}_c = 2.00 \text{ kg/sq cm}$
- $u_c = 1.00 \text{ kg/sq cm}$
- $e_c = 0.525$
- $w_c = 19.8 \%$
- $D_{rc} = 88.6 \%$
- $\tau = 0.22 \text{ kg/sq cm}$
- $\tau / \bar{\sigma}_c = 0.11$
- $f = 0.14 \text{ cycles/sec}$

At End of Test and During Freezing

- $N_f = 25 \text{ cycles}$
- $\tau_f = 0.22 \text{ kg/sq cm}$
- $\bar{\sigma}_f = 0.52 \text{ kg/sq cm}$
- $\tau_f / \bar{\sigma}_f = 0.42$
- $u_f = 1.48 \text{ kg/sq cm}$
- $\bar{d}_f = 1.5 \text{ mm}$

Computed from Water Contents of Frozen Elements

- $w_f = 20.1 \%$
- $e_f = 0.533$
- $D_{rf} = 86.1 \%$
- $w_f^1 \text{ Range} = 21.3 \text{ to } 19.5 \%$
- $D_{rf}^1 \text{ Range} = 76.9 \text{ to } 91.0 \%$
- Standard deviation  $\sigma = 3.57 \%$
- Redistribution Index  $\rho_1 = 12.6 \%$

of Relative Density in Vertical Slices in Direction of Final Deflection

Fig. 15. Gyrotory test No. Y18

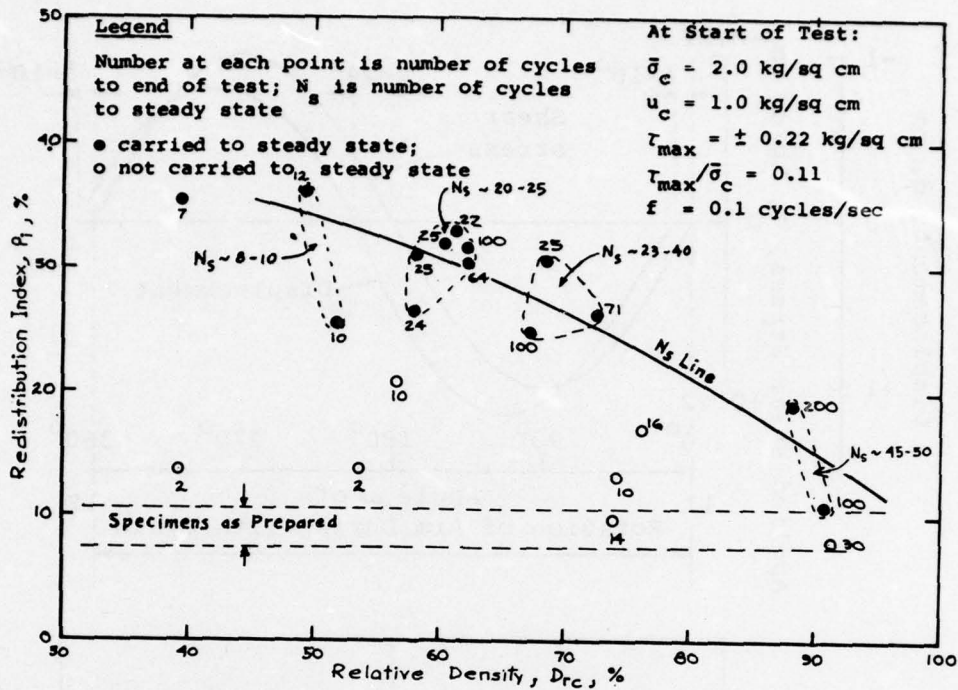


Fig. 16. Redistribution index versus relation density for reciprocating shear (S) tests

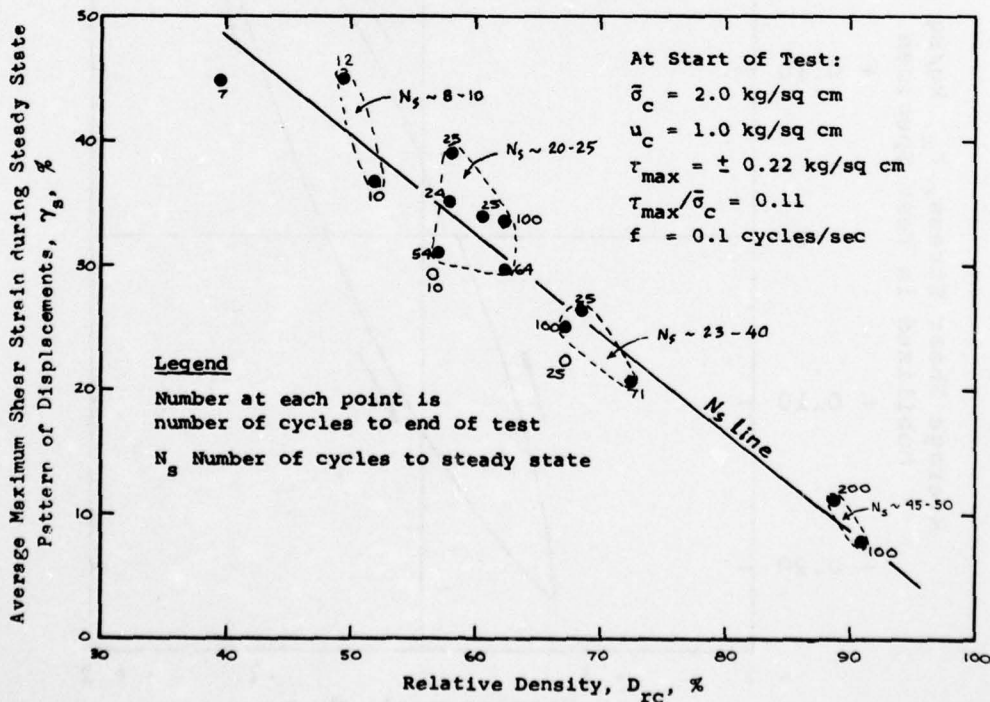


Fig. 17. X tests - shear strain versus relative density during steady state

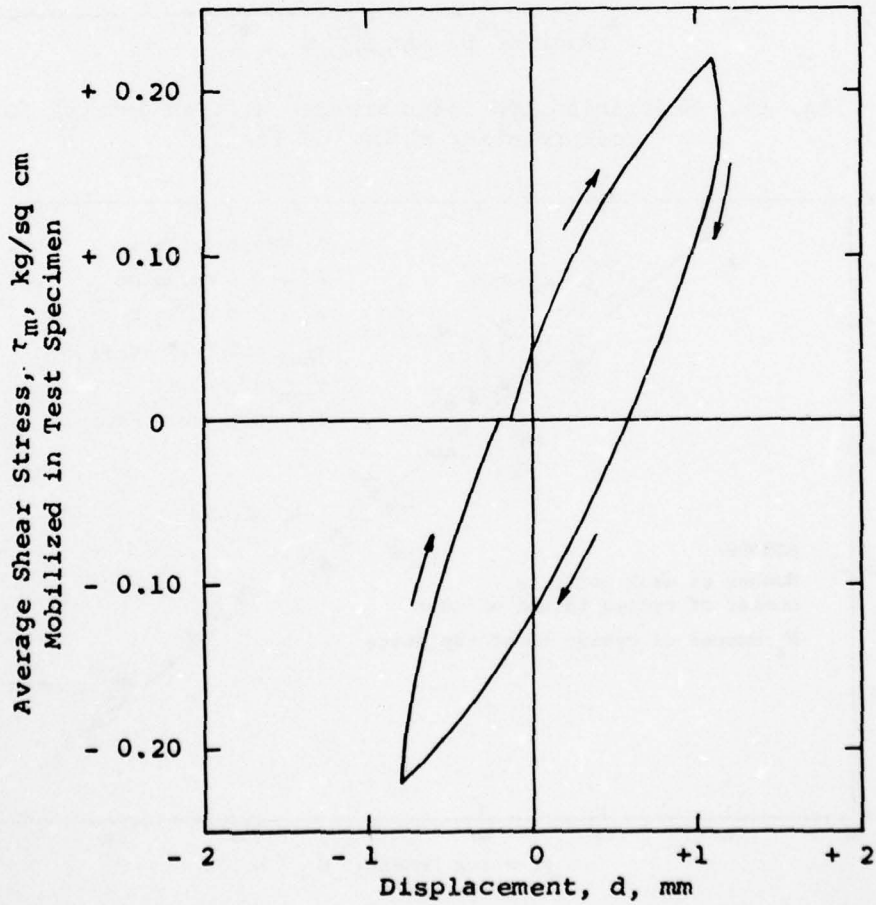
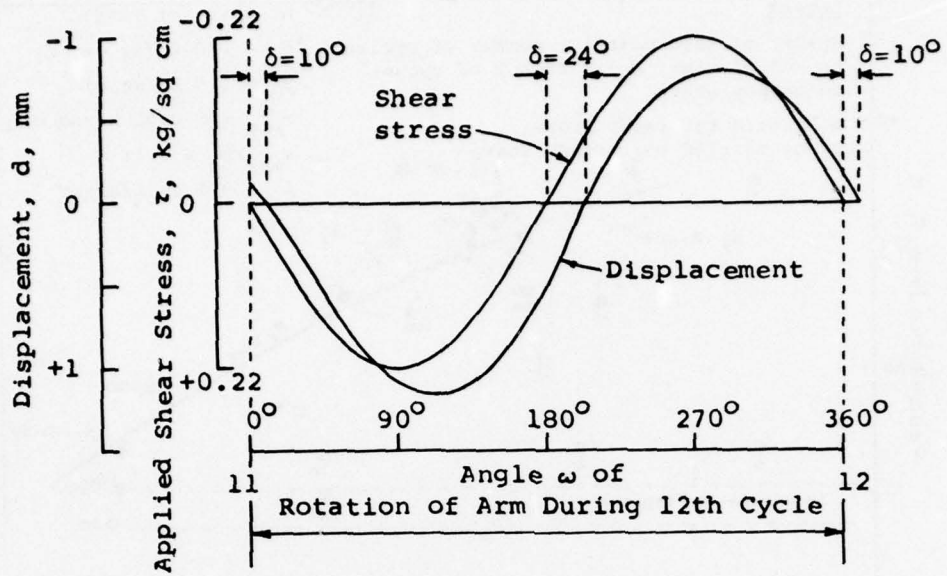


Fig. 18 Displacements and shear stresses during 12th cycle of reciprocating test X12

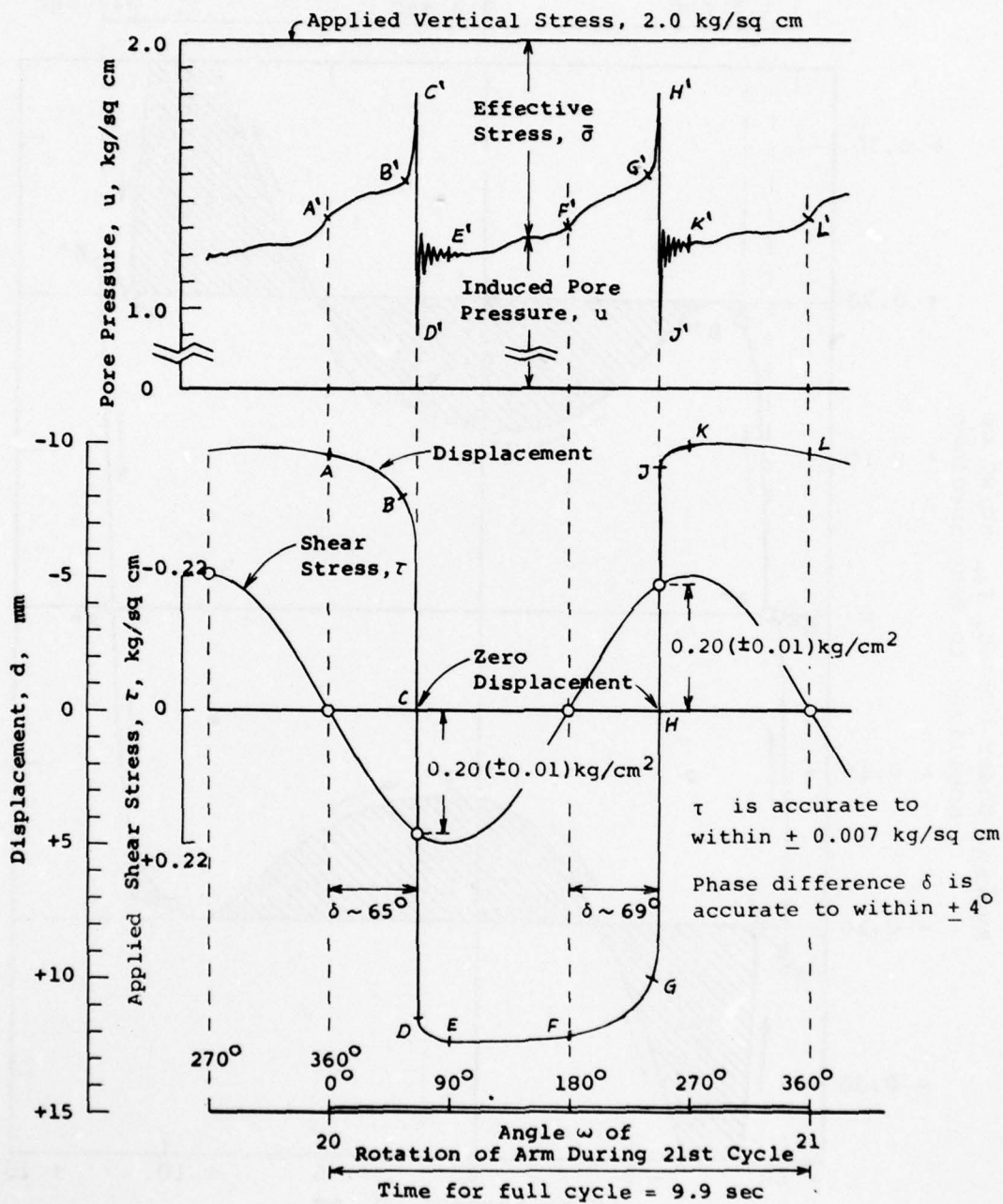


Fig. 19. Pore pressures, shear stresses, and displacements during 21st cycle of reciprocating test X22

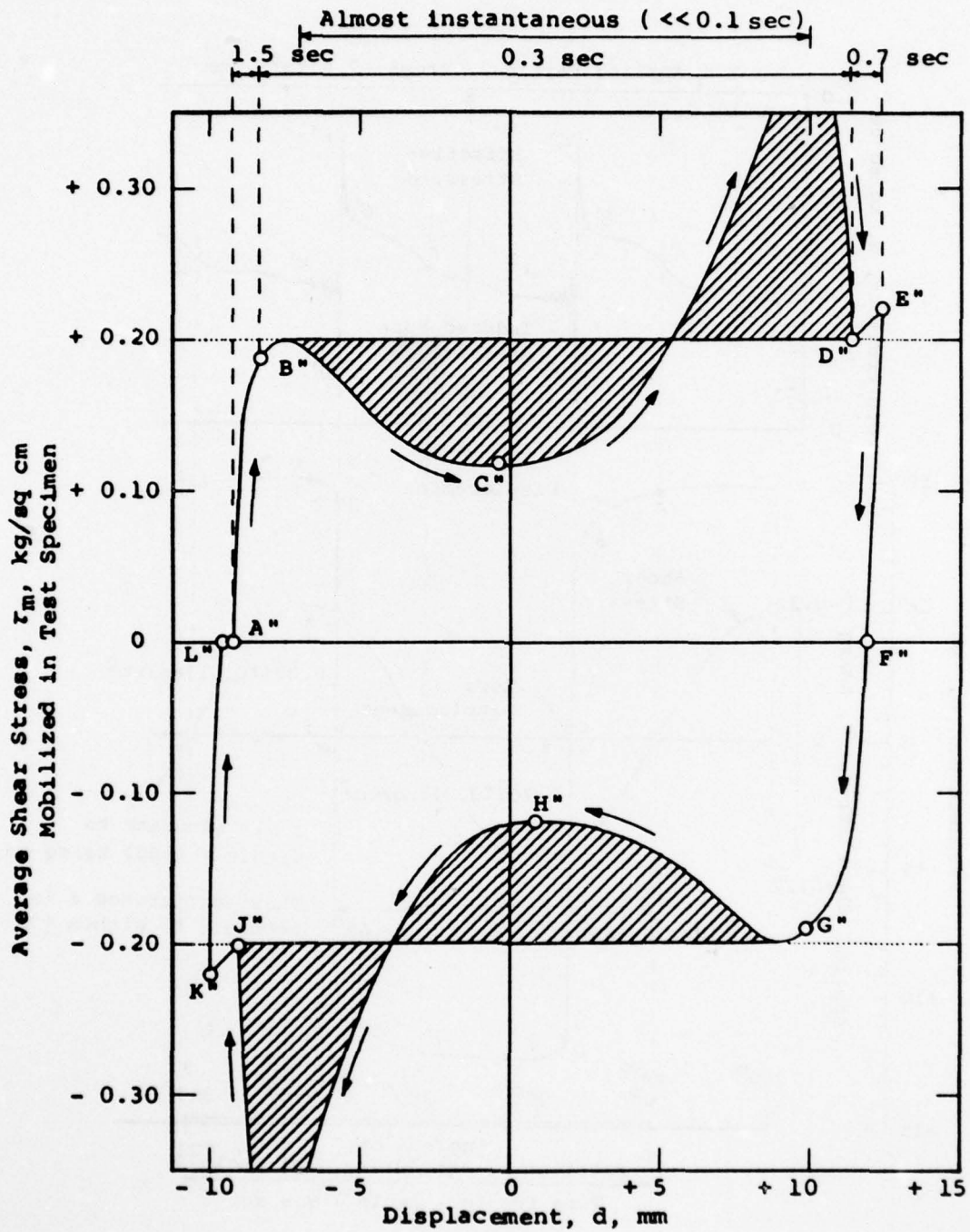
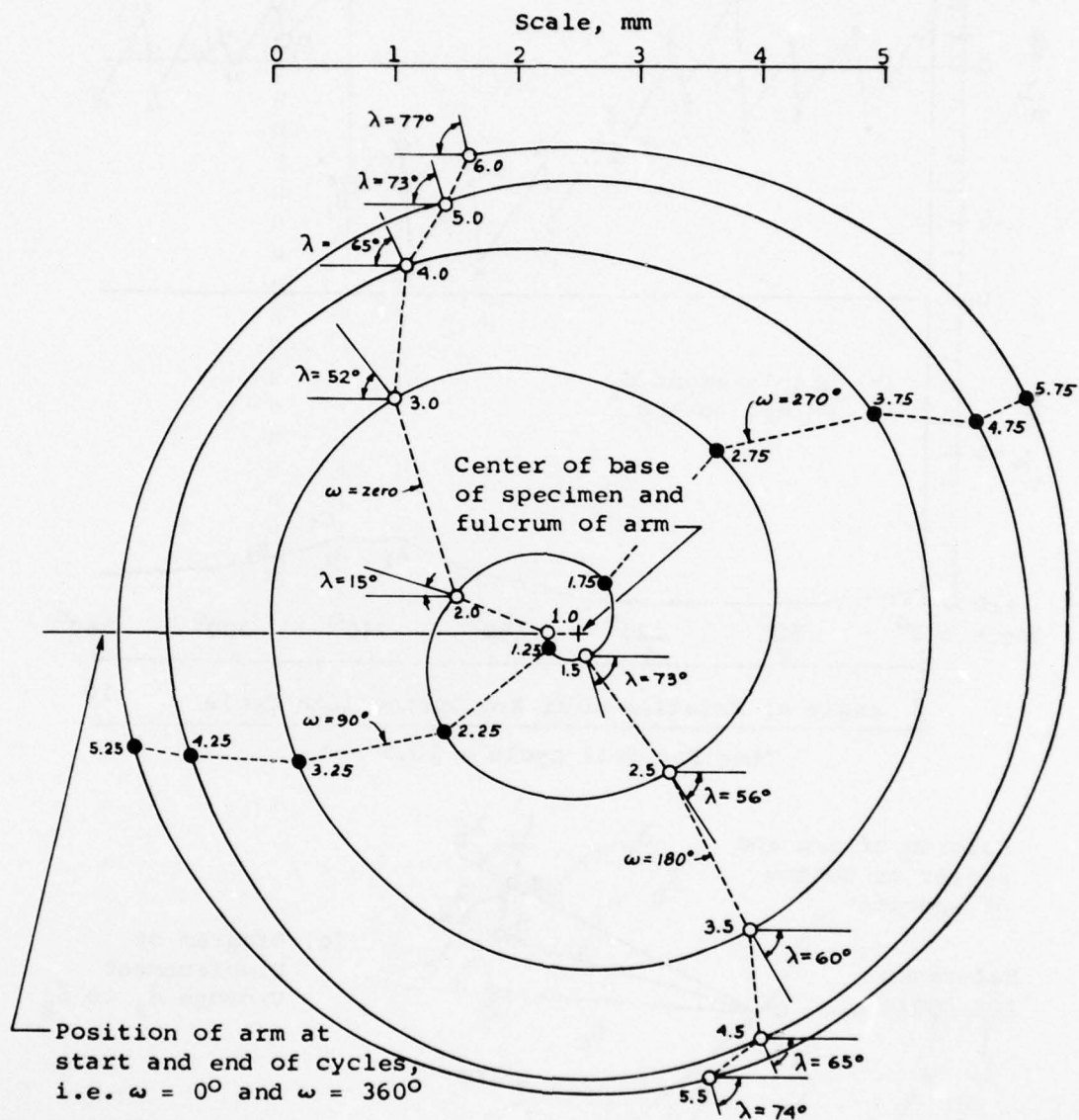


Fig. 20. Mobilized shear stresses versus displacements during 21st cycle of reciprocating test X22



For points shown, displacement vectors were computed from transducer records. Next to each point is shown cycle No., including fraction.

Fig. 21. Path of displacement vector  $\bar{d}$  during 2nd to 6th cycles in gyratory test Y25

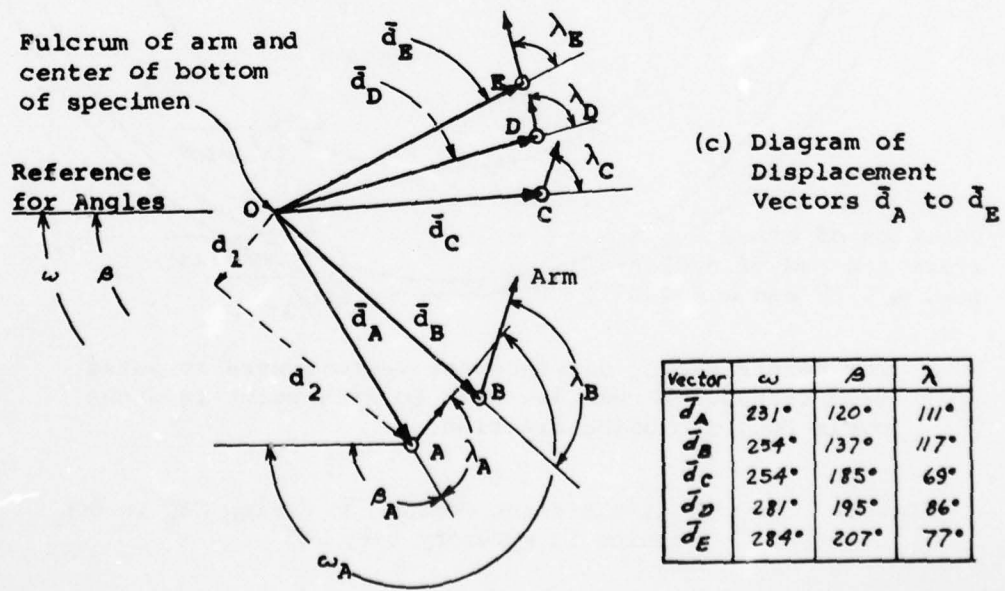
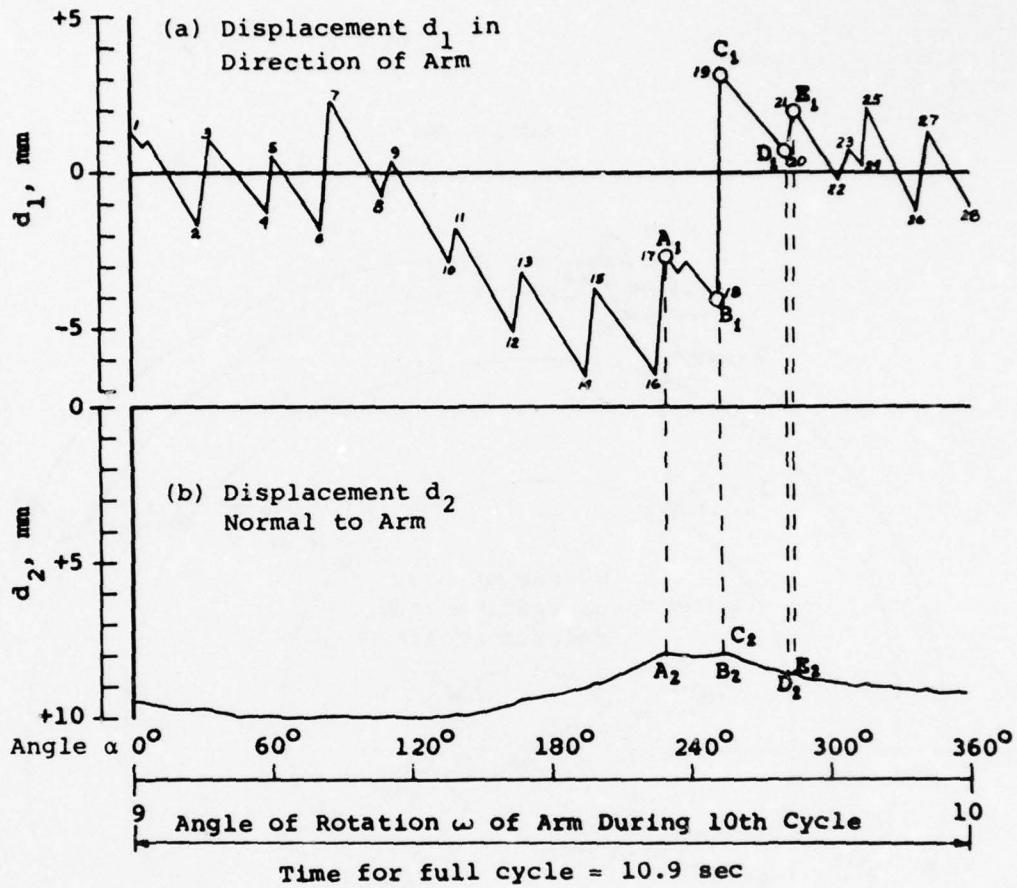


Fig. 22. Displacements during 10th cycle of gyratory test Y21

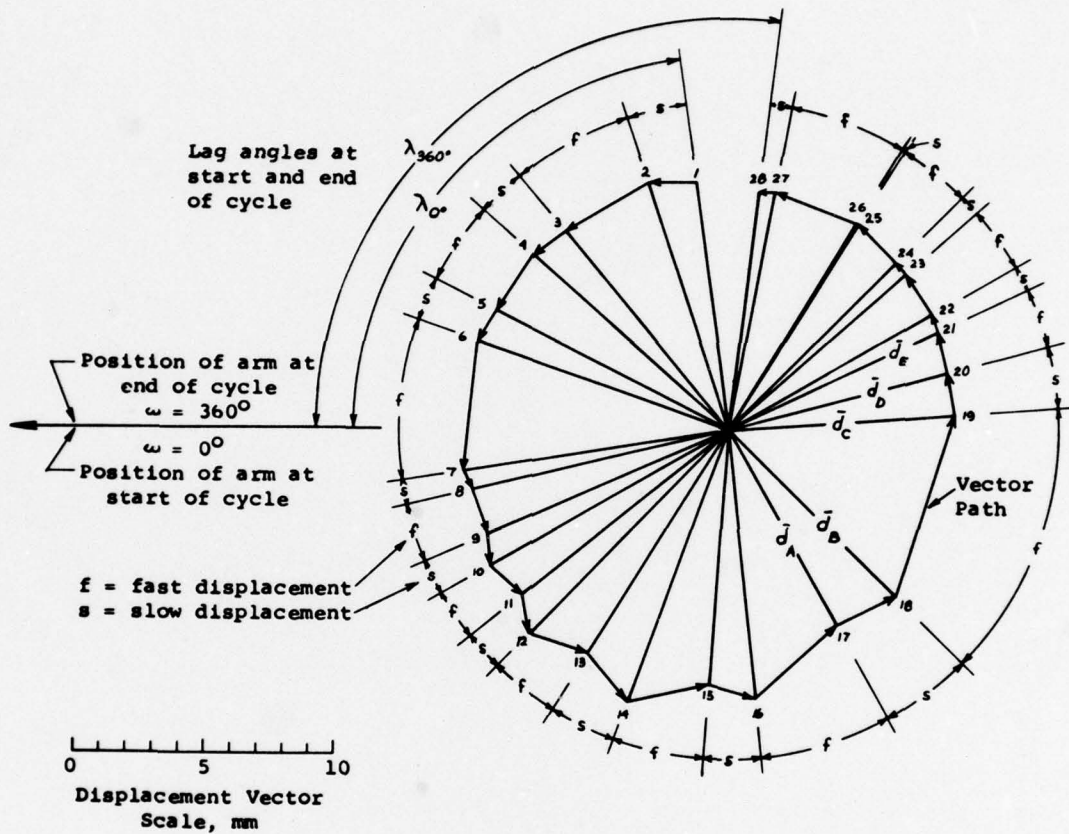


Fig. 23. Path of displacement vector  $\bar{d}$  during 10th cycle of gyratory test Y21

APPENDIX A  
DETAILED DESCRIPTION OF GYRATORY APPARATUS  
AND SHOP DRAWINGS

A.1 Lateral Confinement of Specimen by Slinky (Flat Coil Spring) and Rubber Membrane (Fig. 4)

A flat coil spring, of the type sold for children's play under the trade name "Slinky," supports a cylindrical rubber membrane, which in turn confines the specimen. The membrane is sealed to the base and to the cap by means of O-rings and hose clamps. To prevent development of friction in the slinky, the flat coils are separated by "coil spreaders" during consolidation of the specimen. These coil spreaders are removed before application of cyclic shear stresses.

The slinky springs used in this investigation were obtained from James Industries (Hollidaysburg, Pennsylvania) with the following dimensions: I.D. =  $2.700 \pm 0.005$  in. and O.D. =  $2.913 \pm 0.005$  in. For the size of the specimens used they were cut to a length of 4.3 cm. The surfaces of these springs were treated by spraying with Molykote 523 Bonded Coating Lubricant, manufactured by Dow Corning Corp.

The rubber membranes were obtained from the Testlab Division of GOI (Chicago, Illinois) with the following dimensions: diameter = 2.8 in. and thickness = 0.012 in. For this investigation they were cut to a length of 6.5 cm. They fit easily inside the slinky.

Nine coil spreaders are required to separate the slinky over the full height of the specimen. They are inserted, as shown in Fig. 6, in sets of three, one above the other, 120 deg apart. Each coil spreader consists of 12 circular, stainless steel shims, 0.003 in. thick, with a diameter of 0.5 in., which are mounted in an aluminum cylinder as shown in Fig. A-1. The shims are glued to and held in place by 0.025-in. stainless steel plates. Each coil spreader is 0.36 in. long.

The membrane is sealed by two O-rings to the base and two O-rings to the cap as shown in the detail in Fig. 4. To apply or to develop pore water pressures up to 4.0 kg/sq cm above atmospheric pressure,

the O-rings (Parker 2-227) are confined by two commercial hose clamps (Aero Seal QS 200 M 40).

#### A.2 Slinky Guide Columns (Fig. A-1)

To achieve simple shear deformation of the specimen, three stainless steel guide columns, with universal joints top and bottom, are mounted 120 deg apart around the slinky. Each column consists of two telescopic cylinders to allow changes in thickness of the specimen. They are attached to the base and to the cap by means of column holders. Two universal joints (Stainless Steel Mini-joint No. 1BS, Falcon Machine and Tool Company, North Wilmington, Massachusetts) in each column allow horizontal displacement of the cap in any direction while maintaining a straight-sided cylindrical shape of the slinky and specimen. (Note: Tests made without these guide columns resulted in C- or S-shaped deformations of the specimen.) Fig. A-1 shows the guide columns with the universal joints and the column holders.

#### A.3 Base, Cap, and Valves (Figs. A-2, A-3)

The base and the cap, including valves, are shown in Figs. A-2 and A-3 and are described below:

- (1) The base is permanently attached to the support by a flathead screw which is sealed with a Parker O-ring No. 2-9.
- (2) The open spaces in the bottom of the base allow rapid cooling of the base during the freezing operation after these spaces are filled with the freezing mixture.
- (3) The grooves in the cap above the porous plate are so designed that they allow the water, which is expelled by freezing, to escape without being trapped.
- (4) A pore pressure transducer, placed above the porous plate of the cap, permits measurement of pore pressures in the top of the specimen. This pore pressure transducer is described in Section A.11.
- (5) Conical stainless steel valves in the base and the cap permit performance of gyratory and reciprocating shear tests without drainage; see detail "B" in Fig. A-2.
- (6) Before the piston is inserted into the cap, the cap must be centered by the three horizontal screws, which are shown in Figs. A-11 and A-12. They are screwed through the cylinder wall of the apparatus chamber as indicated in Fig. A-11 and shown in the photograph, Fig. 3. These screws are removed after consolidation of the specimen is completed and immediately before the start of cyclic load application.

The base and the cap are connected to the valve block and burettes, Fig. 5, by means of 0.125-in.-diam plastic tubing. The essential parts of the valve block are:

- (1) A manifold unit (Circle Seal P-727); valves 5, 6, and 7.
- (2) Attached to the manifold unit is valve 4 (Hoke R310 A), which connects to the exterior pressure transducer holder and through valve 1 (Whitney R316) to burette B-1.
- (3) A bleeding standpipe and valve 2 connect to the left instrument port of the manifold unit.
- (4) Burette B-2 connects through valve 3 to the right instrument port of the manifold unit.

Valves 2 and 3 are 9559-B Circle Seal Plug Shutoff valves. The burettes are graduated in 0.10-cu-cm divisions and have a capacity of 5.00 cu cm.

#### A.4 Application of Vertical Load (Figs. A-3 and A-4)

The vertical load is applied by means of a loading yoke and hanger, shown schematically in Fig. 5. The weight of the loading yoke (consisting of the hanger and the upper and lower loading beams connected by steel cables) is balanced by adjusting the position of a counterweight that can be moved along a beam overhead. By means of a turnbuckle, the elevation of the loading yoke can be adjusted in reference to the loading frame that supports the apparatus. To dampen horizontal oscillations of the hanger, its lower extension is guided by a bushing which is supported laterally by three pairs of springs spaced 120 deg. Springs of somewhat different stiffness were paired. Pads of viscoelastic rubber (Norton Company) were inserted between a few of the coils in each spring and also in the joints of yoke and hanger for additional control of horizontal and vertical vibrations.

The upper loading beam of the yoke transmits the load to the loading piston (3/8-in. diameter, Thomson Shaft 60 Case), which is guided by two sets of Thomson ball bushings mounted in the piston bushing, Fig. A-4. The loading piston fits tightly into a steel cylinder set in the cap, Fig. A-3, and transmits the load by a line contact on a conical hardened steel seat in the bottom of this cylinder. Because this cylinder was added after all holes in the cap had been made, it

became necessary to make a cut on one side. In a new design, the adjacent fitting would be located differently to permit use of a cylinder of uniform thickness.

#### A.5 Equipment for Saturation and Application of Back Pressure

A specimen is saturated with de-aired water, which is forced from bottom to top into the evacuated specimen with the arrangement schematically illustrated in Fig. 5. The de-aired water is stored in an aspirator bottle, under vacuum, at an elevation approximately 1 m above the elevation of the test specimen. The aspirator bottle is connected to burette B-2 by a rubber hose, and the flow of water is controlled by laboratory pinchcocks.

Vacuum in the specimen is produced with a Cenco-Megavac pump, which is capable of producing a vacuum of  $0.99 \pm 0.01$  kg/sq cm.

The desired back pressure, to achieve at least 98 percent degree saturation of the test specimens, is maintained by means of an Anteus Pressure Regulator into which air is fed at about 5-kg/sq cm pressure. This regulator is connected to a Heise Test Bourdon gage, G-1, graduated in 0.02-kg/sq cm divisions, with a capacity from zero to 20 kg/sq cm. The test gage G-1 is connected with a plastic tubing to burette B-2 from which it is led to the bottom of the sample.

#### A.6 Application of Horizontal Force (Figs. A-8 and A-9)

A constant horizontal force is applied to the top of the specimen by means of two Negator springs which are attached to the gyratory arm and to the piston bushing, as shown in Fig. 4. The springs are wound on spools turning on ball bearings, as shown in Fig. A-8. The characteristics of the Negator springs used in this investigation (AMETEK/Hunter, Hatfield, Pennsylvania) are tabulated in Fig. A-8.

Motorized rotation of the gyratory arm is accomplished by means of an E3-M2 Zero-Max Power Block Assembly with a 600 H 100 Timing Belt and flanged pulleys. This permits a wide range of speeds that can be further extended by changing the ratio of the pulleys. The driven pulley is attached to the gyratory arm bearing, as shown in Fig. A-9. The Zero-Max Power Block is mounted on a support independent of the loading frame to avoid transmission of vibrations to the specimen.

#### A.7 Gyratory Sliding Plate and Gyratory Test Starting Plate

The design and the assembly of the sliding plate for gyratory shear tests are shown in Figs. A-4 and A-5. The sliding plate consists of a circular, 6.50-in.-diam by 0.225-in.-thick, stainless steel plate (lapped and polished) to which the piston bushing is bolted. The sliding plate has slots, as shown in Fig. A-4, to allow access to the interior of the apparatus chamber, Fig. A-11.

The sliding plate moves between two gyratory bearings, which are guided by the upper and lower guide rings, Figs. A-5 and A-6. Thus, the gyratory bearings allow horizontal motion of the sliding plate in any direction. Each bearing includes a set of forty-eight, 1/4-in.-diam, hard vinyl acetate balls (purchased from Graeco Maptack Inc., Somerville, Massachusetts). The balls are loosely held within a three-layer retaining "sandwich." They protrude approximately 0.03 in. above and below the sandwich. Plastic balls are used instead of steel balls to avoid damage to the surfaces of the sliding plate and the guide rings. The bearings are lubricated with light machine oil to minimize sliding friction between the plastic balls and the retaining sandwich. The separation between the lower and upper guide rings is fixed by the height of the column spacers shown in Fig. A-12(c). The magnitude of the friction developed in this arrangement was found by tests to be negligible.

The lower guide ring is welded to the apparatus chamber, as shown in Fig. A-11. The apparatus chamber has windows and slots which permit access to the specimen (1) for tightening column holders and hose clamp on the cap, (2) for removing the slinky coil spreaders, and (3) for filling and removing the freezing mixture.

The motion of the cap and the top of the specimen in gyratory shear is illustrated in Fig. 1(b). The cap is displaced and the specimen is deformed in the direction of the shear force. The motion of the sliding plate and the cap is also illustrated in Fig. A-13 where, for the sake of clarity, the test starting plate is omitted.

The gyratory test starting plate, as shown in Fig. A-10, is placed over the piston bushing to apply the horizontal force before starting

the motor of the Zero-Max Power Block. The plate is laterally guided by two New Departure ball bearings, type R2 (Fig. A-10), which are mounted on top of the upper guide ring at the left of the plate, Fig. A-11. With the gyratory arm in the X-direction to the left of the operator, Fig. 2, the Negator springs are stretched and attached to the arm. Then the gyratory arm is rotated by hand 90 deg, and gradually the force of the springs is applied to the specimen. Then the lateral guide bearings are removed, freeing the sliding plate and the cap.

#### A.8 Reciprocating Sliding Plate

The design and the assembly of the sliding plate for reciprocating shear tests are shown in Fig. A-14. To the rectangular stainless steel plate, 0.25 in. thick, the piston bushing is bolted. The plate is guided by six horizontal ball bearings (New Departure R2), which roll between the upper and lower guide rings of which only two corner and the opposite middle bearings are engaged at one time for controlling motion of the plate between the guide rings. The position of the four corner ball bearings are adjusted by rotating the mounting pins and by tightening the corresponding set screws (detail "A" in Fig. A-14) to create a gap of 0.0015 in. between the top of the middle ball bearings and the lower surface of the upper guide ring. The separation between the upper and lower guide rings is fixed by the height of the column spacers shown in Fig. A-12b.

The sliding plate is guided laterally by four vertical ball bearings (New Departure R2) which are mounted on the lower guide ring, Figs. A-11 and A-14.

Calibration tests showed that friction developed by the horizontal and vertical ball bearings is negligible for practical purposes.

#### A.9 Measurement of Horizontal Displacements

For gyratory shear tests, the horizontal displacements are measured by two displacement transducers mounted on the gyratory arm, Figs. 2(b), 4, and A-13. Transducer D-1 measures the displacements in the direction of the gyratory arm. Transducer D-2 measures the displacements normal to the direction of the gyratory arm. The probes of both transducers are connected to a ring mounted on a ball bearing

which rotates around the loading piston, Fig. 4. The wires from both transducers lead to spring contacts that in turn transfer the signal to slip rings surrounding the apparatus support column, Fig. A-7, from which wires lead to the power supply and the recorders, Fig. 4.

The displacement transducers (Sanborn Co., Waltham, Massachusetts, Model 7 DCDT-500) have a displacement range of 1 in. They work with an excitation voltage of 6 V DC and have an output of 6.8 V/in.

For reciprocating shear tests, the displacement transducers are removed from the gyratory arm. One is mounted in a fixed position to measure the linear motion of the cap, as schematically shown in Fig. A-15, with details in Fig. A-17, and the other one can be used to measure vertical displacements as explained in Section A-10.

A DC power supply (Power Designs, Westbury, New York, Model 2005) was used to provide a stable excitation voltage for the transducers. The output voltage of this power supply may be selected from 0 to 20 volts, and it changes a maximum of 100 microvolts when the input voltage is doubled. The calibration of the power supply is guaranteed to be better than 0.1 percent of the selected voltage  $\pm 1$  mv.

The ideal arrangement would be to use one 4-channel recorder for the two displacement transducers and the two pore pressure transducers. However, two different models of 2-channel recorders were available and were used as follows. The output of transducer D-1 is recorded by one channel of a 2-channel DC amplifier recorder (Sanborn Co., Waltham, Massachusetts, Model 320), which will be referred to as Recorder No. 1. The output of transducer D-2 is recorded by one channel of a second 2-channel DC amplifier recorder (Sanborn Co., Model 60-1300), which will be referred to as Recorder No. 2. Both recorders have the following characteristics: The channels are 50 mm wide, and the recording is made with hot wire writing arms on heat-sensitive paper. The recording speed can be selected from 1 to 100 mm/sec. For the great majority of tests the speed of 1 mm/sec was used. The response time for full displacement of the writing pen is 5 msec.

The recorders were adjusted so that 1-mm displacement measured by means of a dial extensometer, with 0.01-mm divisions, will correspond

to a width of 20 mm on the strip chart. For this purpose, the transducer probe was screwed into the dial extensometer in lieu of the tip of the dial stem, with both instruments mounted on a suitable support. This adjustment was checked after every four or five tests. At the start of each test, the amplification dial on each recorder was so set that the maximum anticipated deflection would not exceed the width of the strip chart.

#### A.10 Measurement of Vertical Displacements

Before the transmission of the Zero-Max Power Block is engaged, the vertical displacements are measured with a dial extensometer with 0.01-mm divisions and a travel of 25 mm. It is mounted on the instrument supporting frame and measures the displacement of the upper loading beam of the loading yoke with respect to a fixed reference frame, Fig. 5 and Fig. A-17.

If desired, vertical displacements can be measured in reciprocating shear tests with one of the two displacement transducers described in Section A.9. For such measurements, the transducer probe rests on an aluminum plate which is attached to the loading piston, Fig. 4. To reduce sliding friction, the probe is provided with a tip made of Teflon. A weak spring maintains continuous contact between the probe and the plate as shown in Fig. A-17. The transducer is mounted on the instrument supporting frame.

#### A.11 Pore Pressure Measurements

For most of the tests made in this investigation, the pore pressures were measured at the bottom of the test specimen by means of the pore pressure transducer mounted outside the apparatus below burette B-1, Fig. 5. This transducer (General Transducer Co., Santa Clara, California, Model GT-20) has a range of 0 to 250 psi and a natural frequency of 50,000 cps. It measures the difference between the pore pressure applied to a diaphragm and the atmospheric pressure. It is used with an excitation voltage of 10 V DC and has an output of 1.75 mv/kg per sq cm.

To check the pore pressures, a second pressure transducer (Entram Devices, New York, New York, Model EPA-125-50D) was installed in the

cap, immediately above the porous plate, Fig. A-3. It measures the difference between the pore pressure applied to a diaphragm and the atmospheric pressure with a range of  $\pm 50$  psi. It is used with an excitation voltage of 6 V DC and has an output of 1.97 mv/psi.

The pore pressure transducer in the cap was used only in a few tests to demonstrate that there is no phase difference in the pore pressure fluctuations between top and bottom of a specimen. Both pore pressure transducers are excited by a second power supply of the same type as that used for the displacement transducers.

Because the two available recorders did not have sufficient amplification, rather than to acquire another recorder, the necessary amplification was achieved by amplifying the signal first in one channel of Recorder No. 2, then feeding it into one channel of Recorder No. 1 where it was again amplified.

The amplification of Recorder No. 2 was set at its maximum, and the amplification of Recorder No. 1 was adjusted to obtain a width of 20 mm on the strip chart for 1-kg/sq cm pore pressure, as measured on the Heise Test Bourdon Gage (Gage G-1, Fig. 5).

#### A.12 Auxiliary Devices for Placement and Compaction of Specimens

During placement and compaction of a specimen, the slinky is supported by the "rigid columns," which are shown in Fig. A-1.

For placing sand layers of uniform thickness, the device called "sand placer" is used, which is shown in Fig. A-16(b). This device consists of a levelling vane which is turned by means of a solid brass stem. The vane is inclined at 60 deg, such that its bottom edge is ahead of the top edge in the direction of clockwise movement. The stem is guided by a brass bushing to which are attached four brackets that support a thinwall brass cylinder which fits with a small clearance inside the rubber membrane. To the bottom edge of this cylinder is soldered a No. 16 mesh screen. Experience with the use of this spreader demonstrated the need of the cutouts from the bottom of the thin wall cylinder as shown in Fig. A-16(b). Different layer thicknesses can be achieved by changing the position of the stop collar which limits the downward travel of the stem. The upward travel of the

stem is limited by the radial brackets. The sand placer is lifted and lowered by means of a thread fastened to the stem and suspended from a turnbuckle, as shown in Fig. A-16(a). To effect smooth vertical movement of the spreader, the thread is passed one turn around a guide pulley which is attached to an overhead beam.

Placement of a sand layer is performed as follows:

- (1) The position of the collar is adjusted for the desired layer thickness.
- (2) With a teaspoon, a prepared quantity of sand is placed in the spreader. Then the stem is rotated clockwise until the sand surface is level. The spreader is then lifted slowly by turning the turnbuckle until all sand has dropped through and slightly below the screen. The turnbuckle is then turned in opposite direction, until the screen rests on the surface of the sand. The turnbuckle is then turned further until the stop collar rests on the bushing.
- (3) To achieve a relative density of about 40 percent, the spreader is lifted and lowered, as described before, two or three times. For relative densities of 45 percent to 55 percent, the total weight of stem, stop collar, and levelling arm is used to tamp the layer by raising and dropping the stem a specified height and transmitting the tamping force through the bushing, brass cylinder, and screen to the sand. To achieve relative densities between 55 percent and 75 percent, a 20-g weight is added to the stem on top of the stop collar, and appropriate variations are used in the number of tamps. For relative densities greater than 75 percent, compaction is performed by dropping a tamping weight onto an anvil, i.e. the device shown in Fig. A-16(c). The weight is lifted by hand to the desired height, which is marked on the stem, and then dropped by free fall.

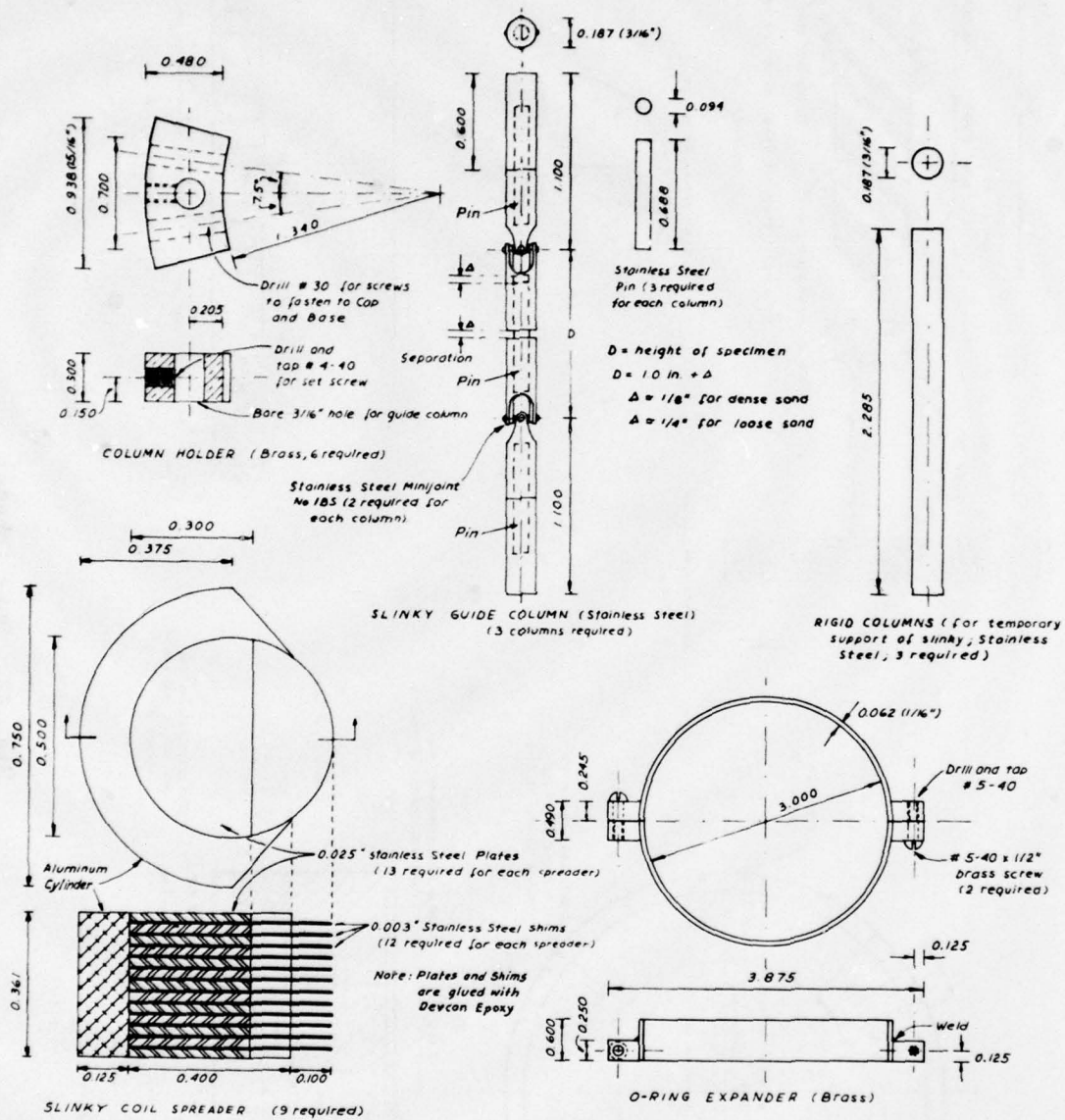


Fig. A1. Slinky guide columns, O-ring expander and slinky coil spreader

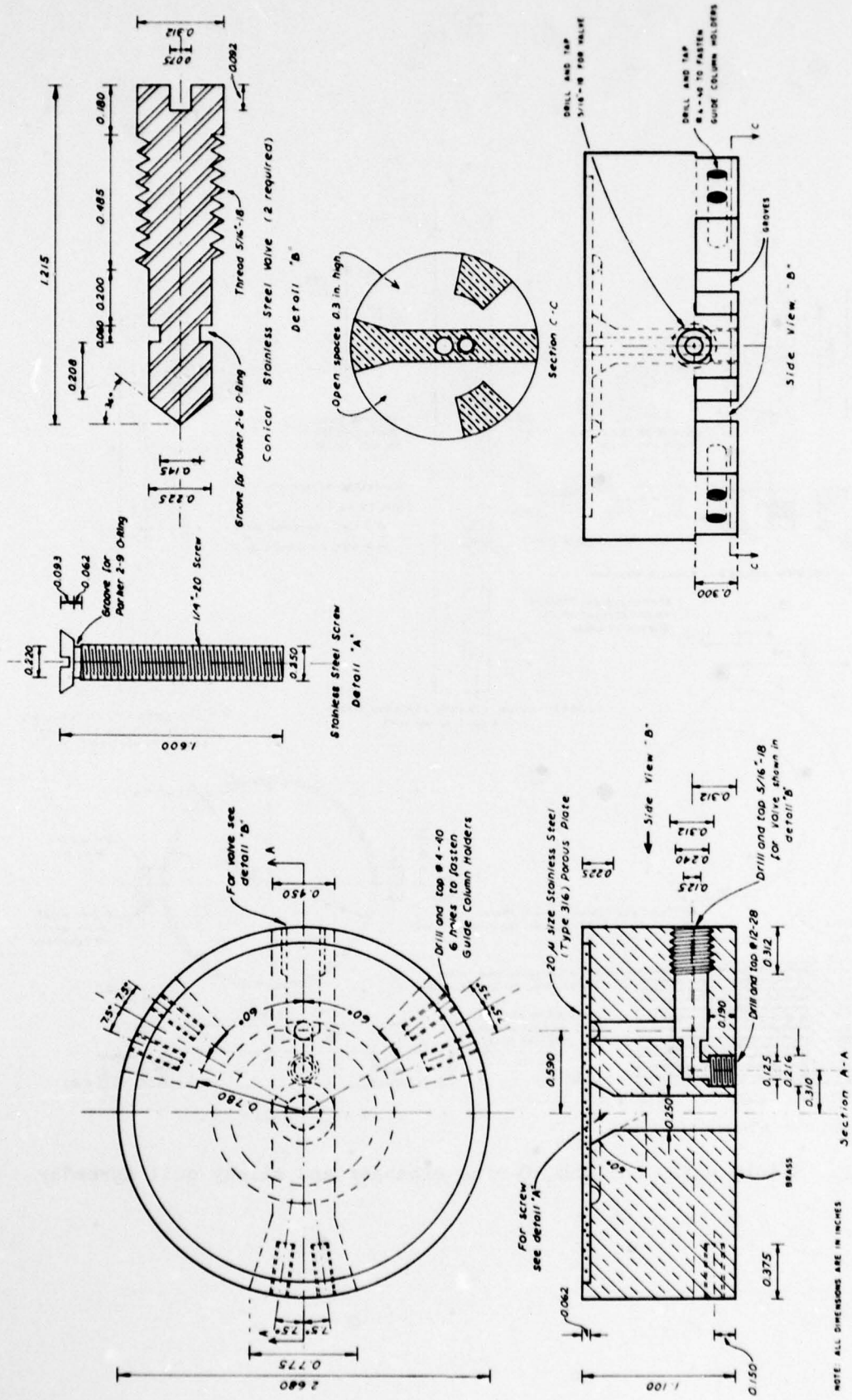
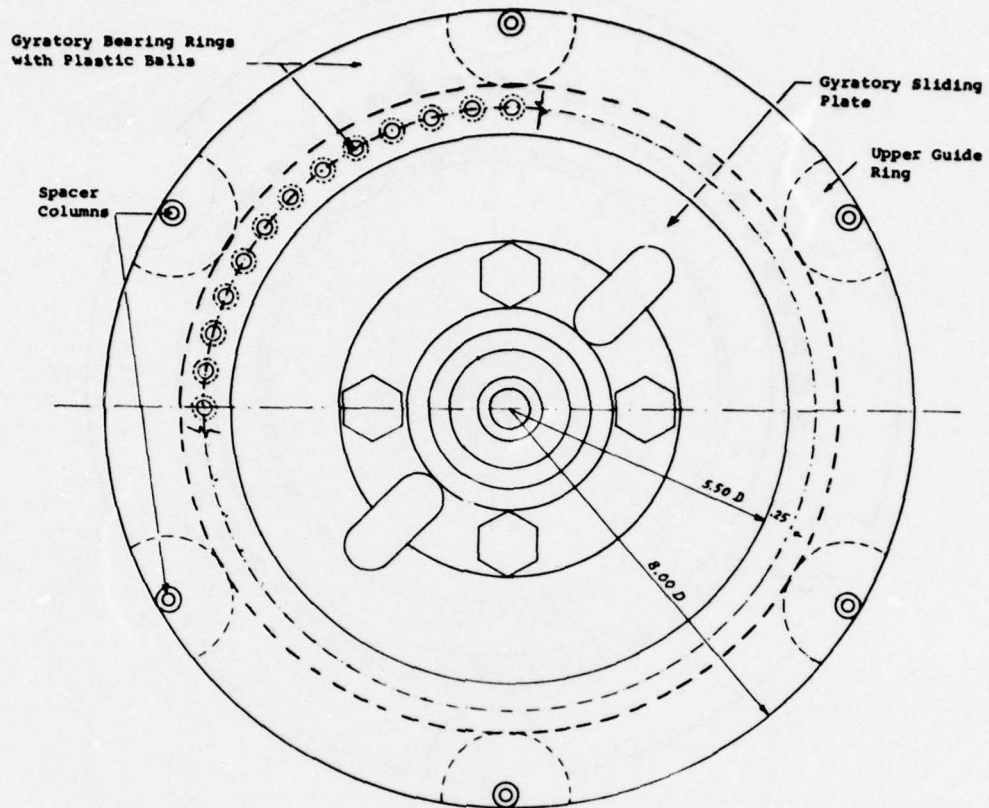


Fig. A2. Base (brass)







- Notes: 1. See Fig. A-6 for details of gyratory bearing rings.  
 2. All dimensions are in inches.

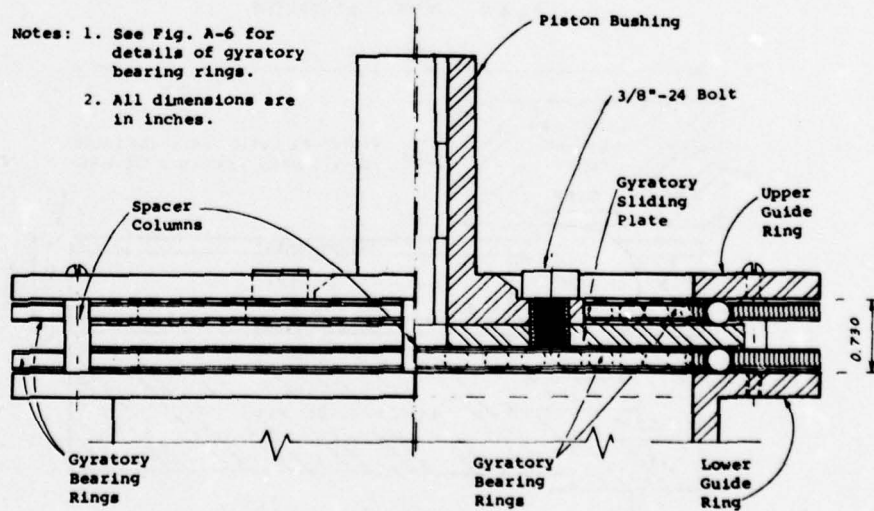


Fig. A5. Assembly of gyratory sliding plate, gyratory bearings and piston bushing

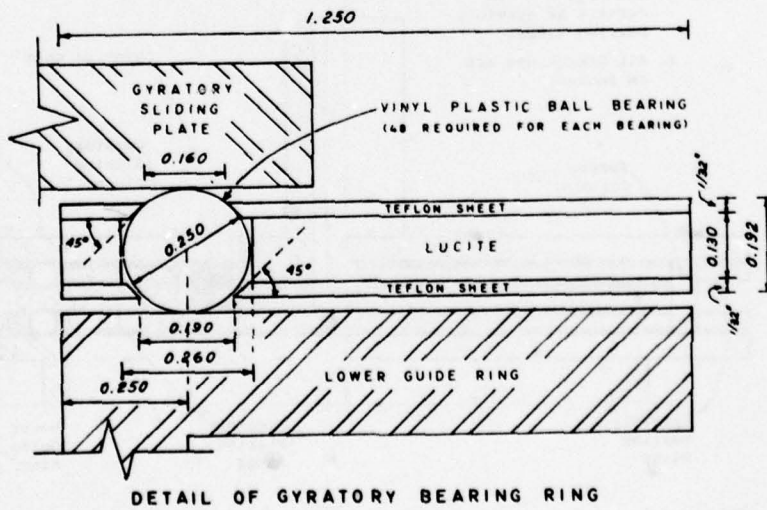
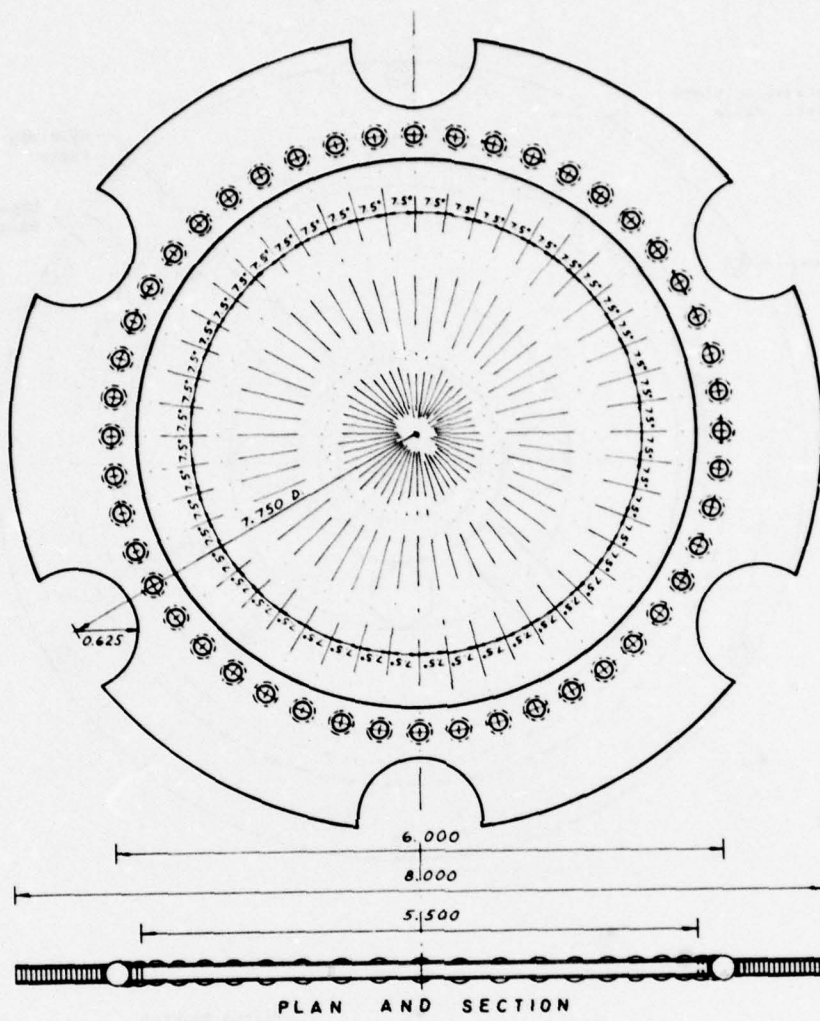
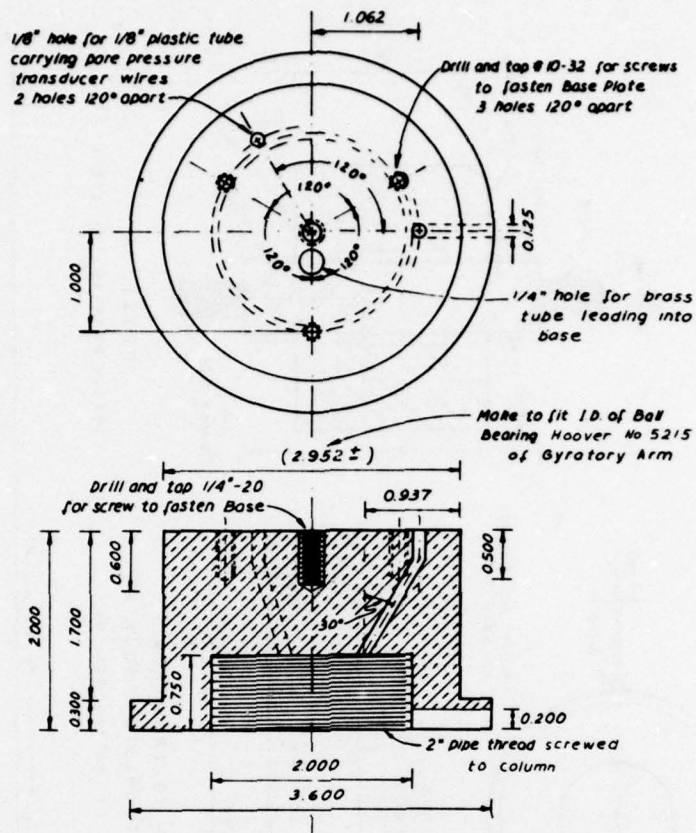
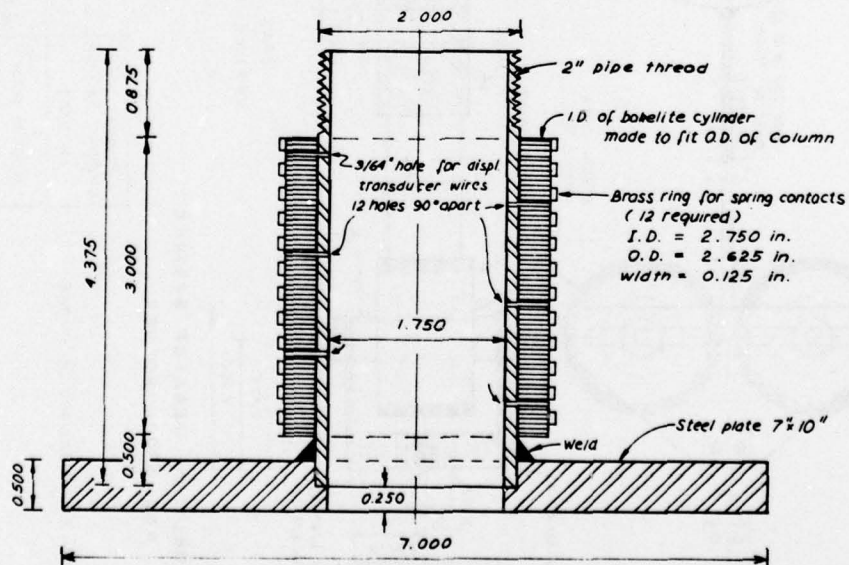


Fig. A6. Gyrotary bearing (2 required)



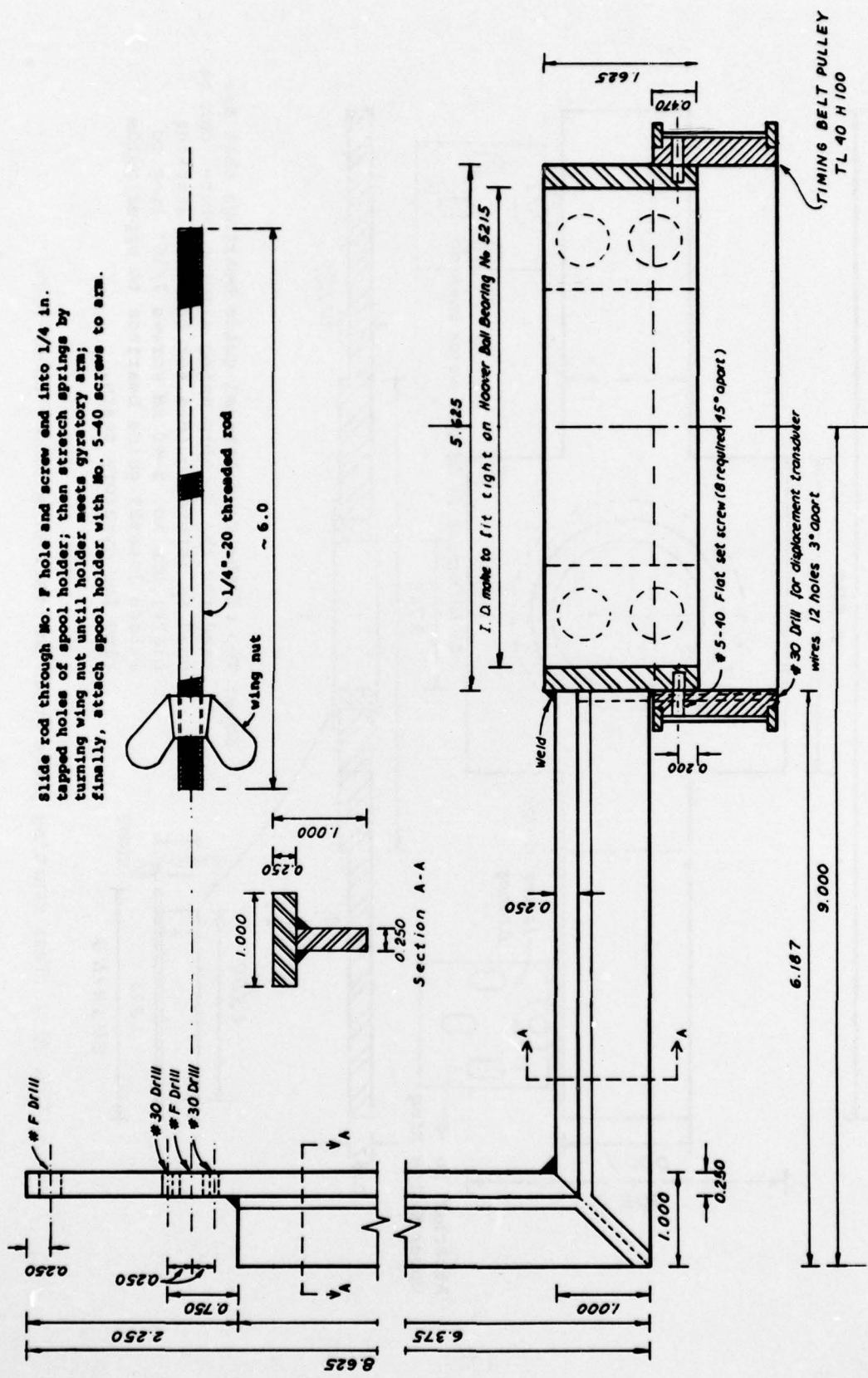
(B) TOP OF SUPPORT (BRASS)



(A) BASE AND COLUMN OF SUPPORT

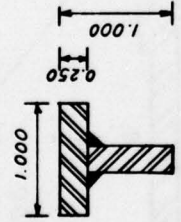
Fig. A7. Apparatus support column





Slide rod through No. F hole and screw end into 1/4 in. tapped holes of spool holder; then stretch springs by turning wing nut until holder meets gyrotory arm; finally, attach spool holder with No. 5-40 screws to arm.

1/4"-20 threaded rod  
wing nut



Section A-A

Fig. A9. Gyrotory arm (steel)

TIMING BELT PULLEY  
TL 40 H100

#5-40 Flat set screw (8 required 45° apart)

#30 Drill for displacement transducer  
wires 12 holes 3° apart

weld

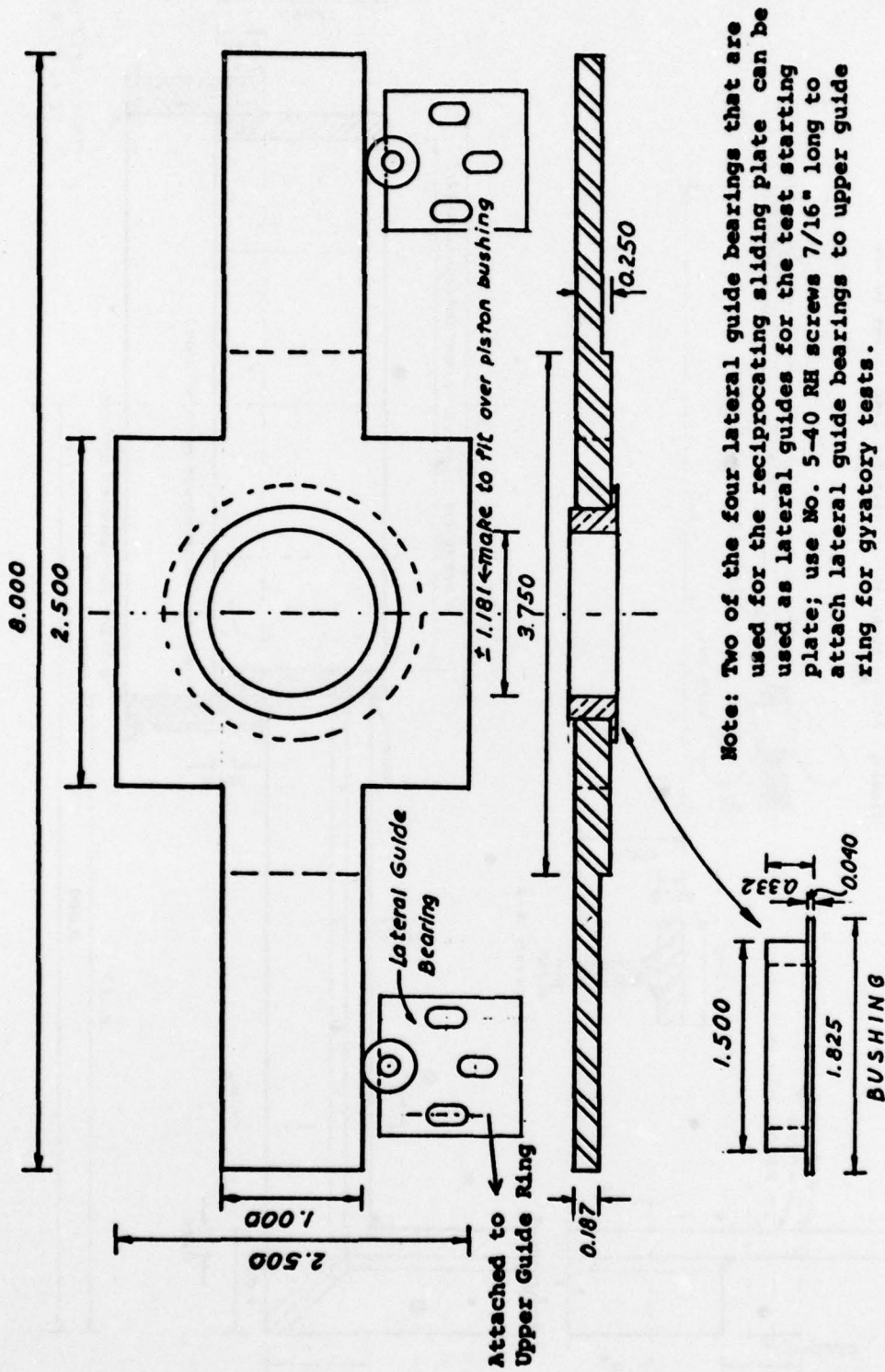
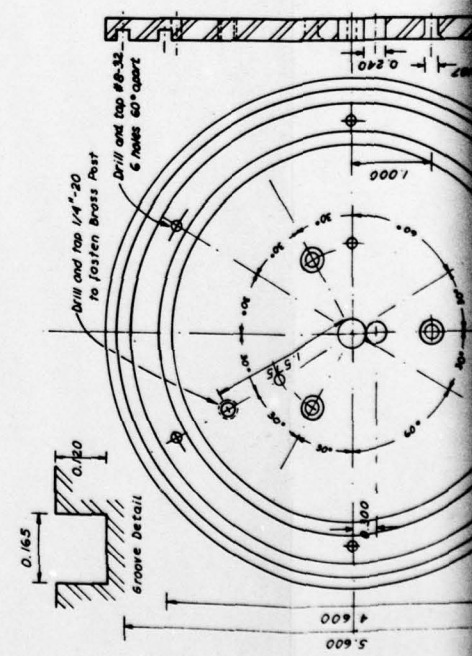
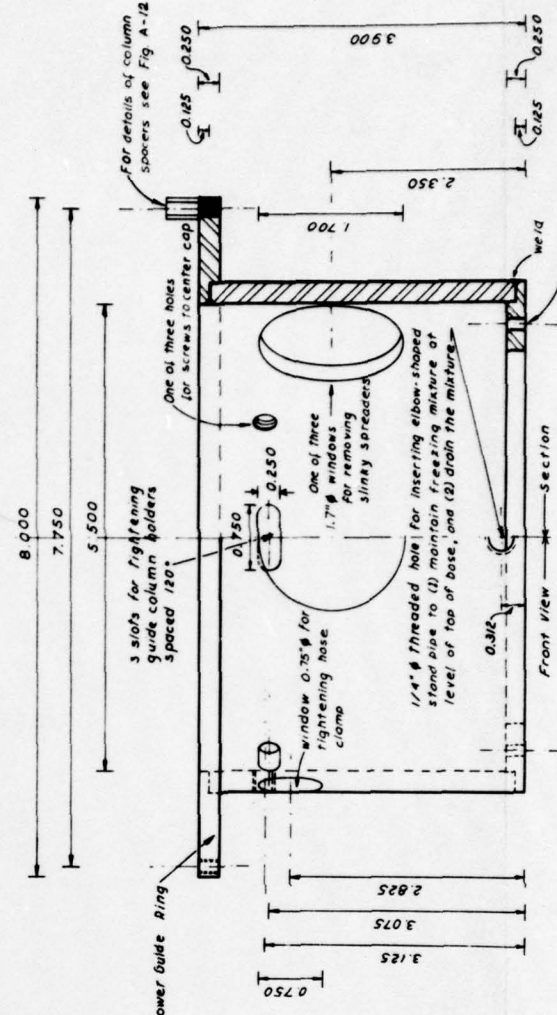
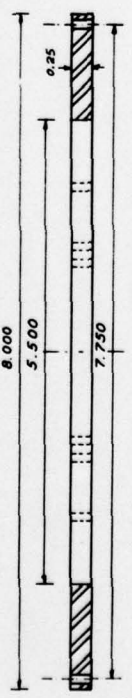
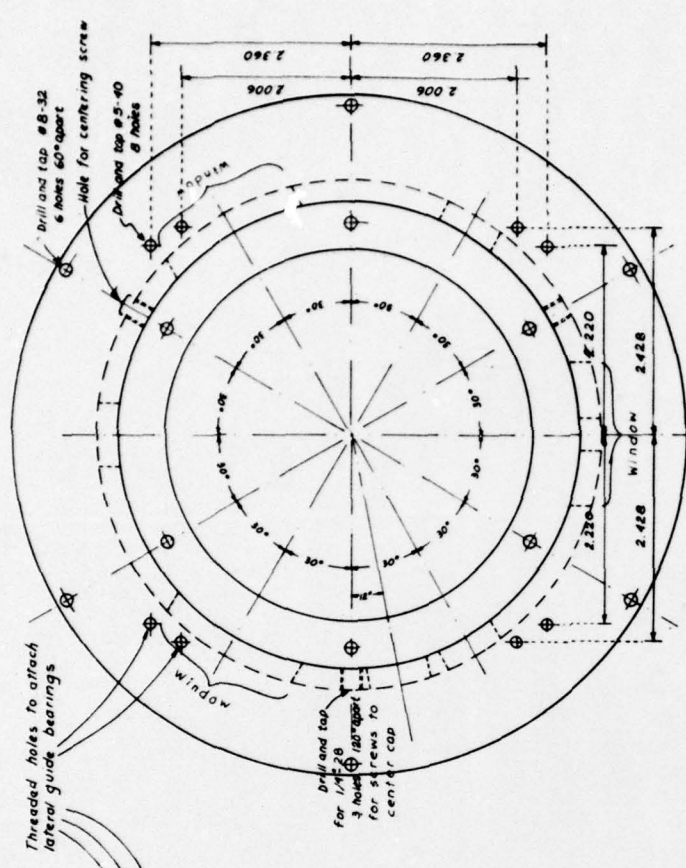
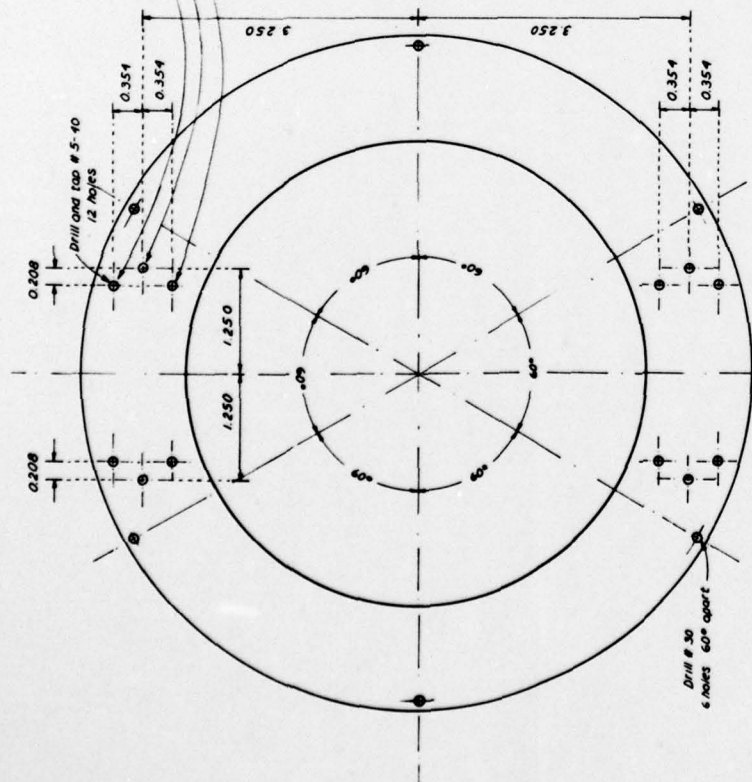
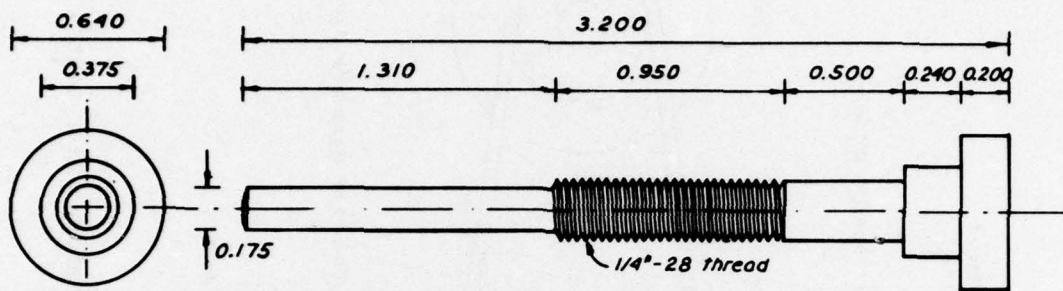


Fig. A10. Test starting plate (used at start of gyrotory shear test)

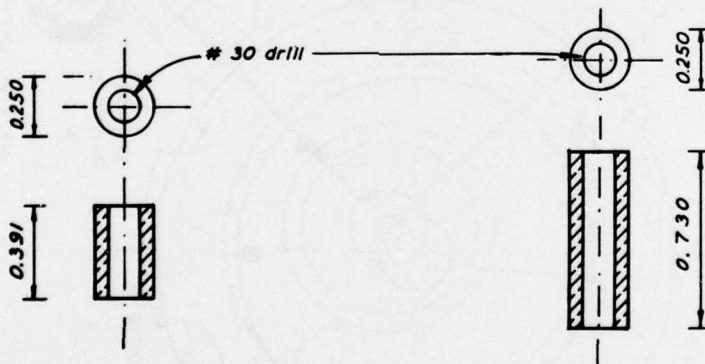






Two lock nuts on each screw are so adjusted that the end of the screw defines the correct position of the cap. The screws and the holes in the chamber wall are numbered 1 - 2 - 3, and each screw must be used only in the hole with the same number for which the lock nuts are properly adjusted.

a) SCREW FOR CENTERING CAP (stainless steel, 3 required)



b) GUIDE RING SPACERS FOR USE WITH RECIPROCATING SLIDING PLATE

c) GUIDE RING SPACERS FOR USE WITH GYRATORY SLIDING PLATE

Fig. A12. Guide ring spacers and horizontal screws to center cap

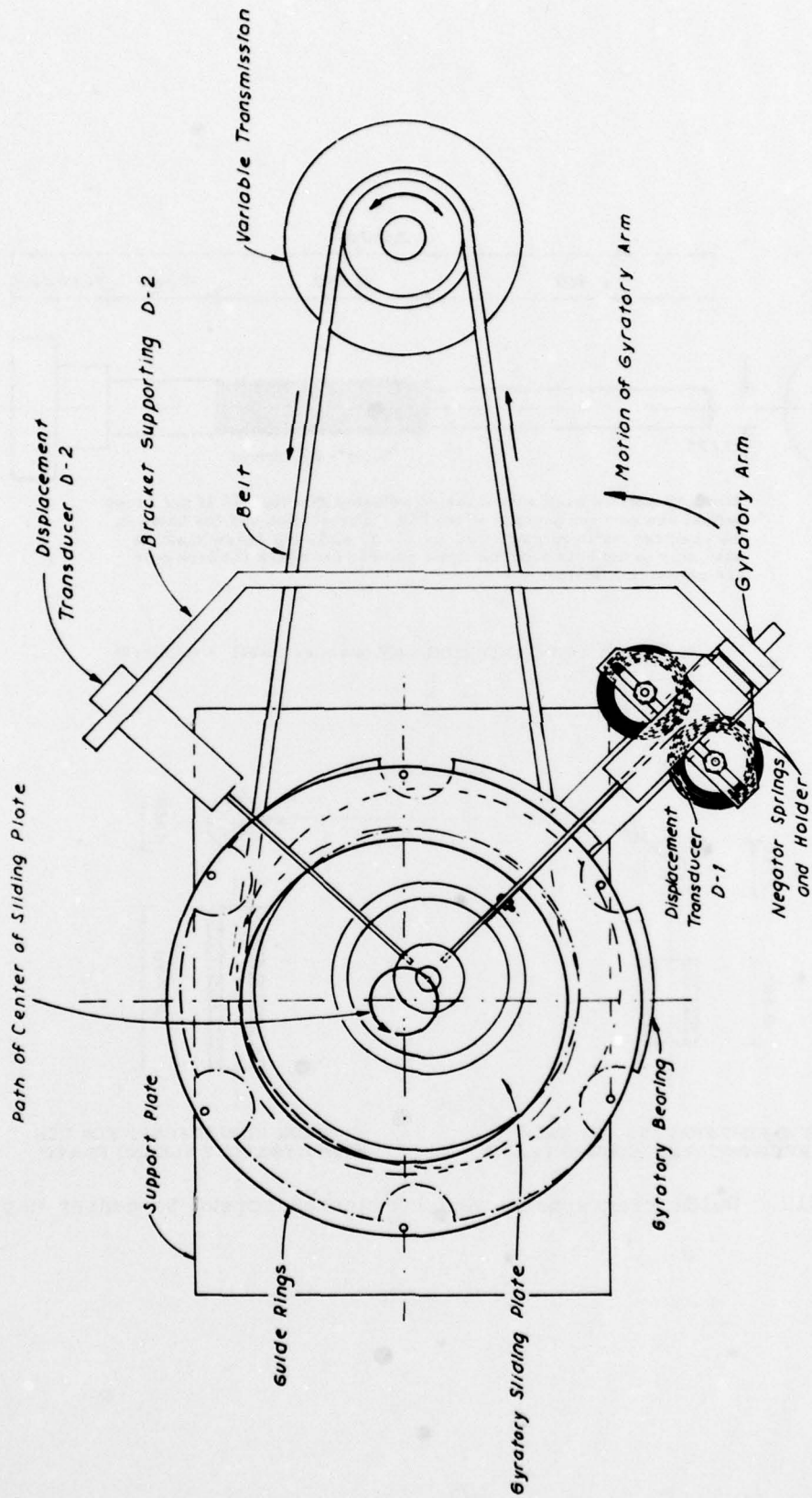
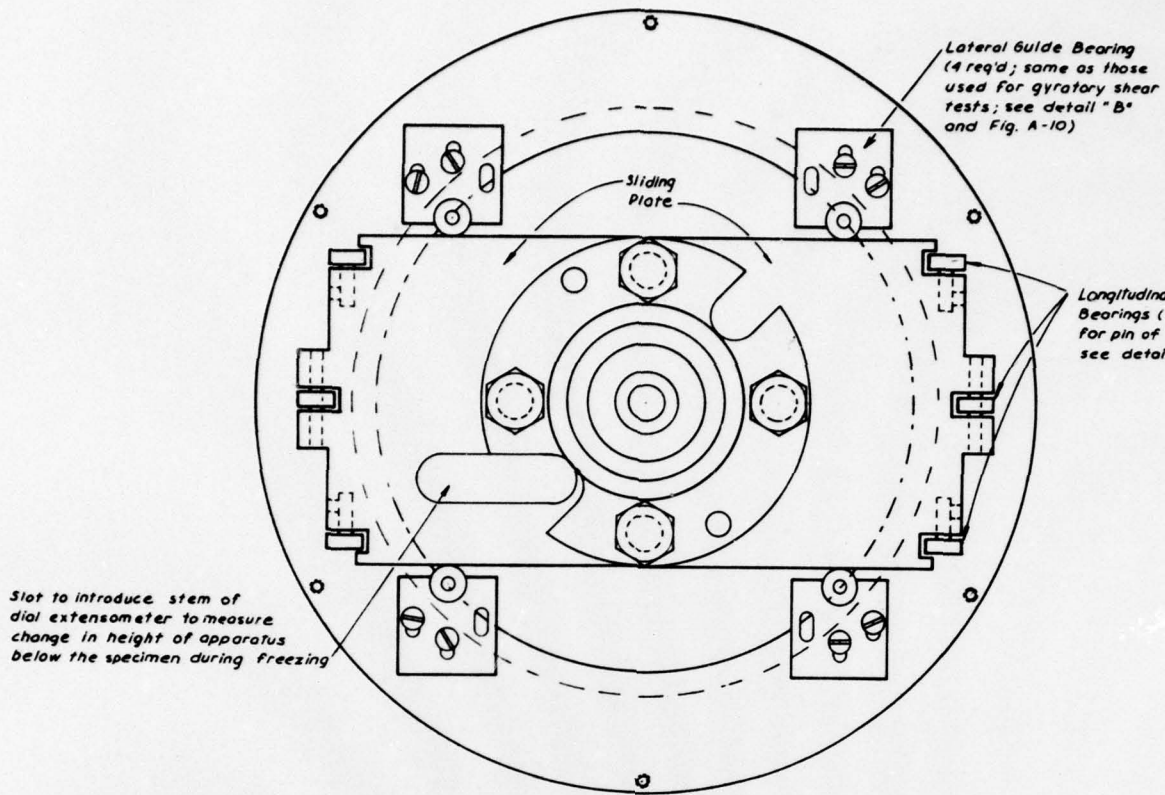
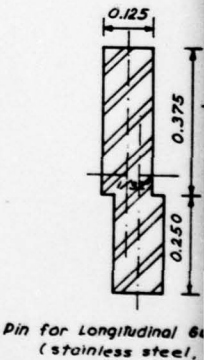
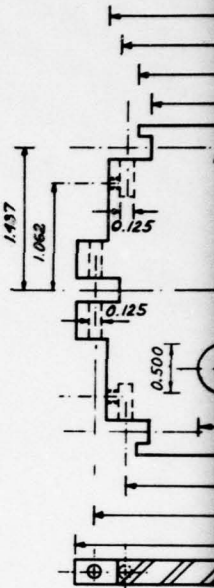
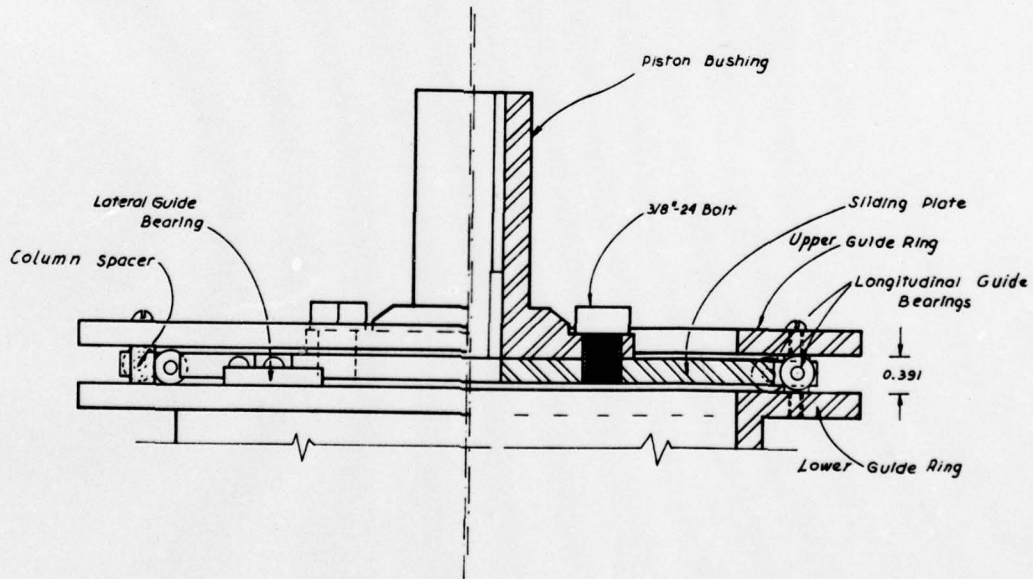


Fig. A13. Arrangement for measuring displacements in gyrotary shear tests



ASSEMBLY WITH UPPER GUIDE RING REMOVED



DETAIL

Fig. A14. Assembly of reciprocating sliding plate, lateral



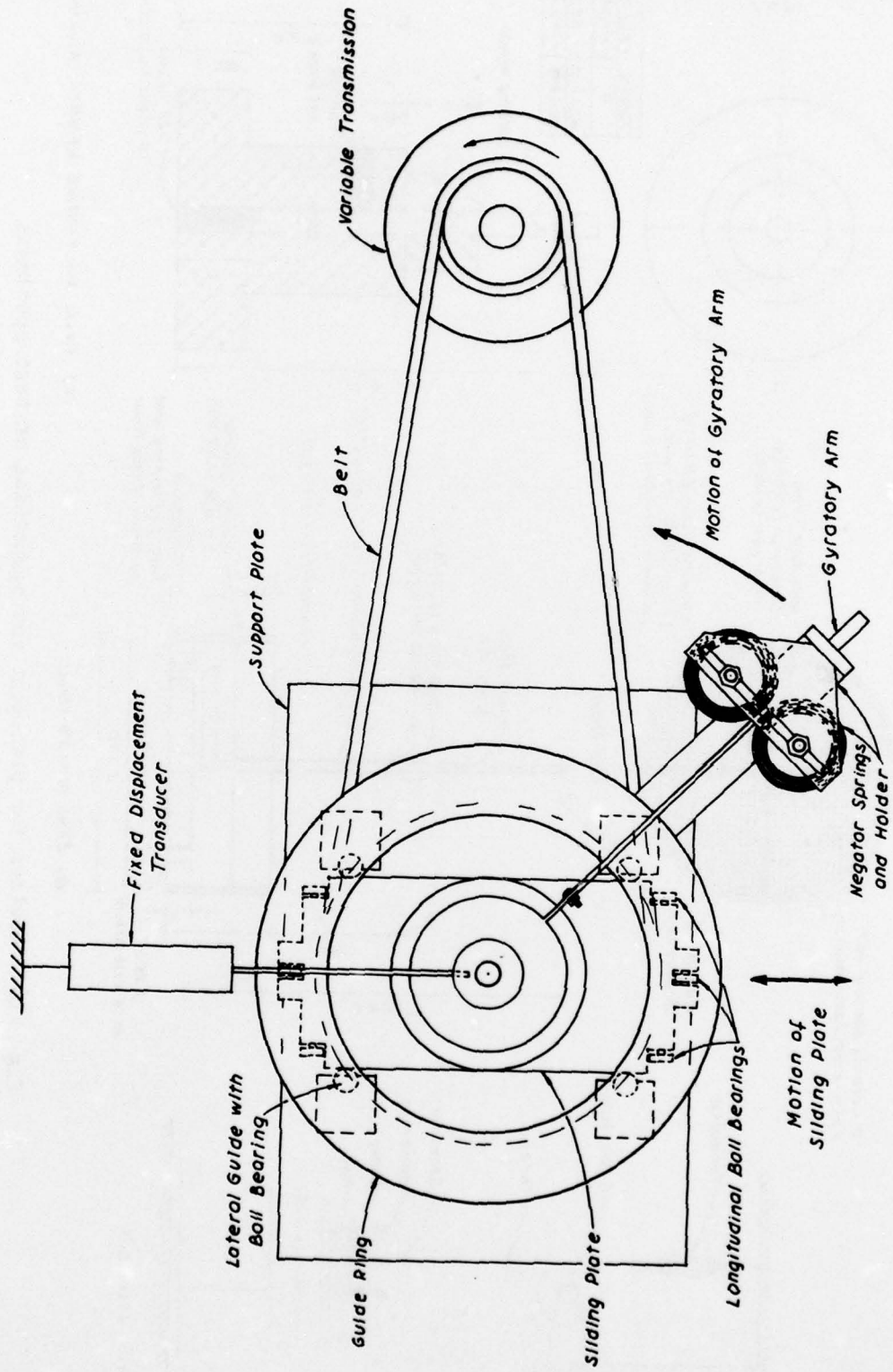


Fig. A15. Arrangement for measuring displacements in reciprocating shear tests

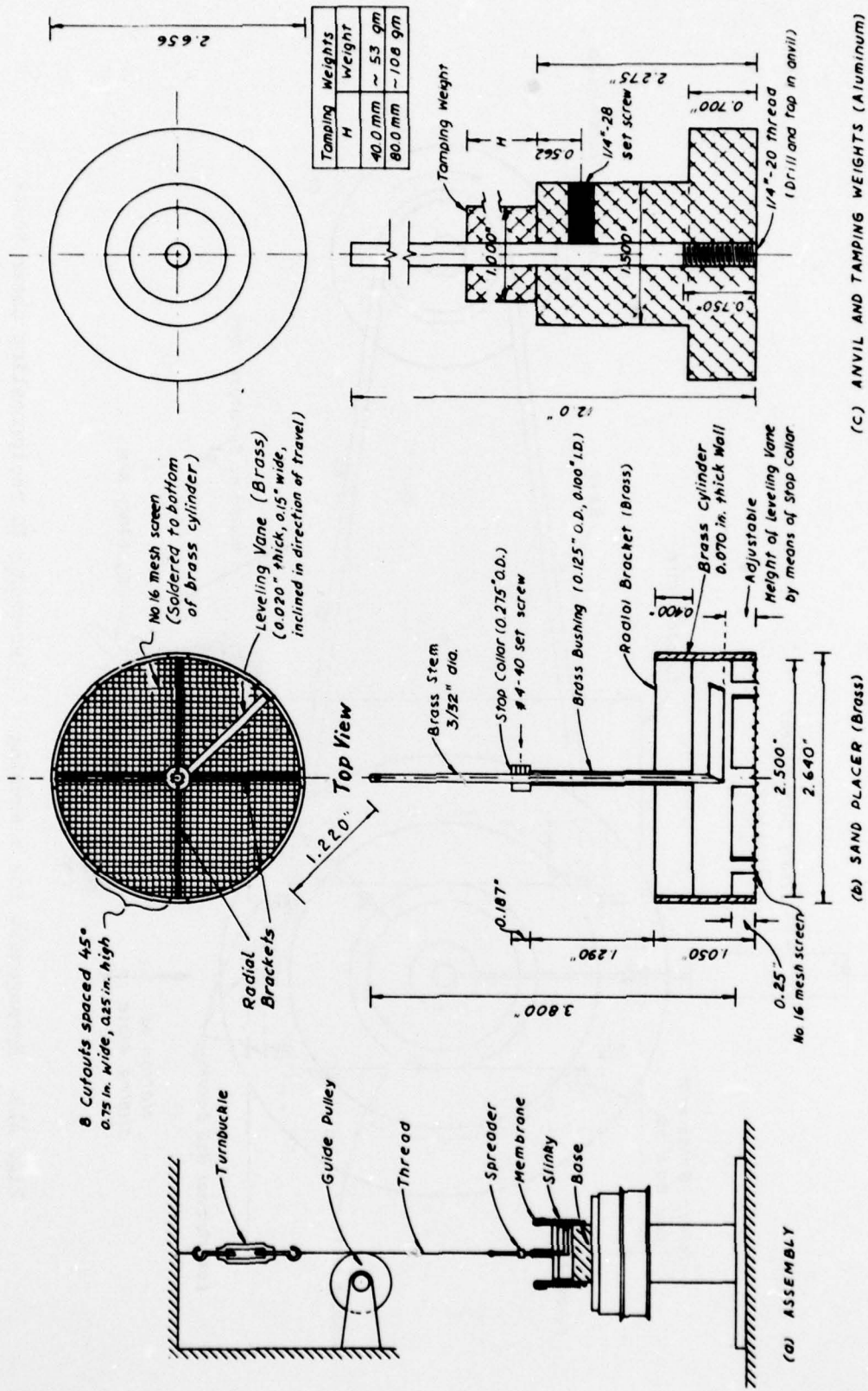


Fig. A16. Devices for placement and compaction of test specimens

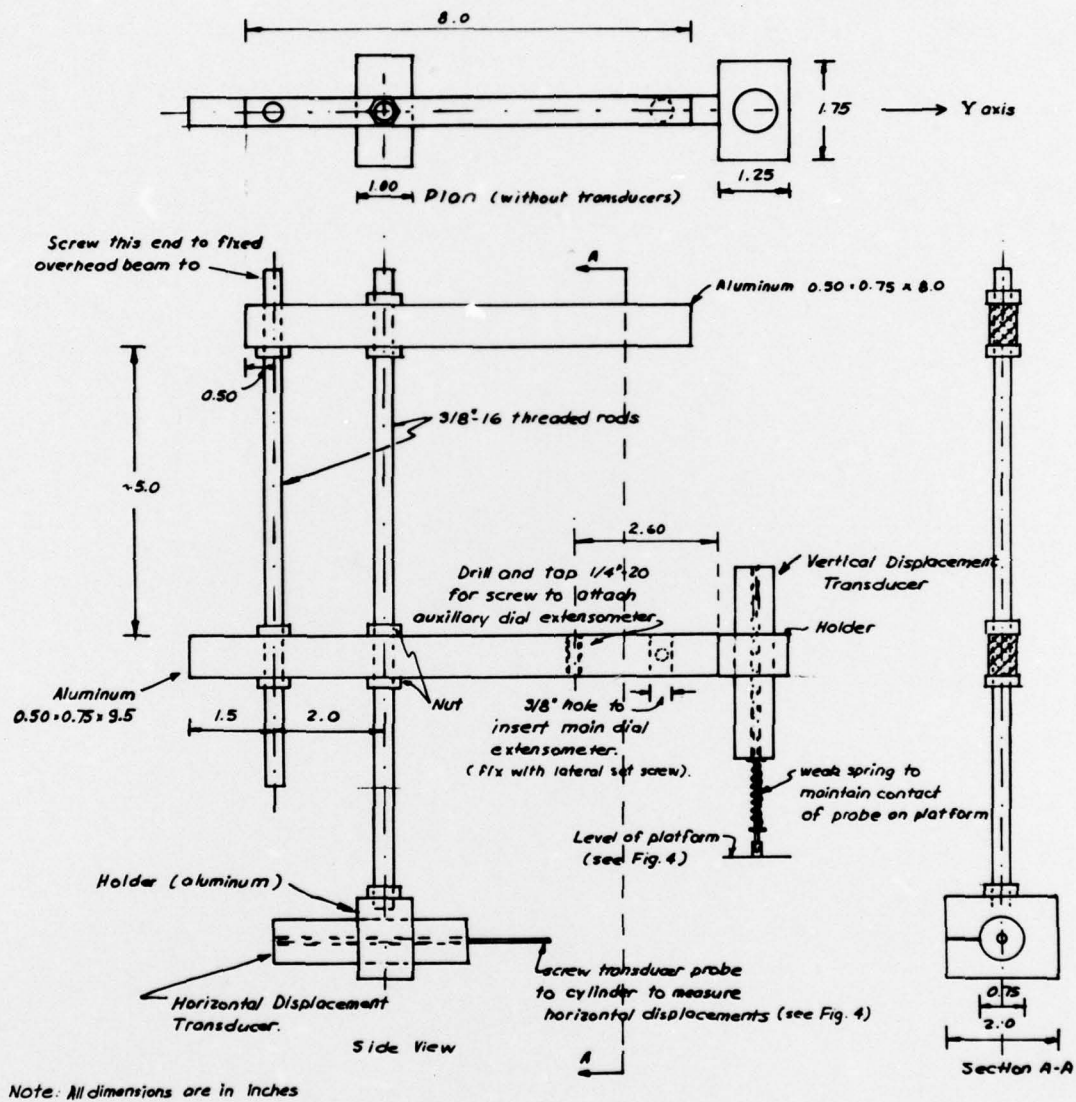


Fig. A17. Supporting frame for (1) dial extensometers and (2) for displacement transducers when used

In accordance with letter from DAEN-RDC, DAEN-ASI dated 22 July 1977, Subject: Facsimile Catalog Cards for Laboratory Technical Publications, a facsimile catalog card in Library of Congress MARC format is reproduced below.

Casagrande, Arthur

Gyratory shear apparatus design, testing procedures, and test results on undrained sand / by Arthur Casagrande and Franklin Rendon, Harvard University, Cambridge, Massachusetts. Vicksburg, Miss. : U. S. Waterways Experiment Station ; Springfield, Va. : available from National Technical Information Service, 1978.

xiii, 111 p. : ill. ; 27 cm. (Technical report - U. S. Army Engineer Waterways Experiment Station ; S-78-15)

Prepared for Office, Chief of Engineers, U. S. Army, Washington, D. C., under Contract No. DACW39-74-C-0026. Harvard Soil Mechanics Series No. 89.

References: p. 50.

1. Cyclic load tests. 2. Gyratory testing machines. 3. Sands.  
4. Undrained shear tests. I. Rendon, Franklin, joint author.  
II. Harvard University. III. United States. Army. Corps of Engineers. IV. Series: United States. Waterways Experiment Station, Vicksburg, Miss. Technical report ; S-78-15.  
TA7.W34 no.S-78-15